

Quantum-critical theory of the spin-fermion model and its application to cuprates. Normal state analysis.

Ar. Abanov¹, Andrey V. Chubukov¹, and J. Schmalian²

¹ *Department of Physics, University of Wisconsin, Madison, WI 53706*

² *Department of Physics and Ames Laboratory, Iowa State University, Ames, IA 50011*

(November 26, 2024)

We present the full analysis of the normal state of the spin-fermion model near the antiferromagnetic instability in two dimensions. This model describes low-energy fermions interacting with their own collective spin fluctuations, which soften at the antiferromagnetic transition. We argue that in 2D, the system has two typical energies - an effective spin-fermion interaction \bar{g} and an energy ω_{sf} below which the system behaves as a Fermi liquid. The ratio of the two determines the dimensionless coupling constant for spin-fermion interaction $\lambda^2 \propto \bar{g}/\omega_{sf}$. We show that λ scales with the spin correlation length and diverges at criticality. This divergence implies that the conventional perturbative expansion breaks down. We developed a novel approach to the problem - the expansion in either the inverse number of hot spots in the Brillouin zone, or the inverse number of fermionic flavors - which allowed us to explicitly account for all terms which diverge as powers of λ , and treat the remaining, $O(\lambda)$ terms in the RG formalism. We applied this technique to study the properties of the spin-fermion model in various frequency and temperature regimes. We present the results for the fermionic spectral function, spin susceptibility, optical conductivity and other observables. We compare our results in detail with the normal state data for cuprates, and argue that the spin-fermion model is capable to explain the anomalous normal state properties of high T_c materials. We also discuss the non-applicability of the conventional ϕ^4 theory of the quantum-critical behavior in 2D.

I. INTRODUCTION

The 15 years after the discovery of superconductivity in cuprate oxides [1] witnessed a large number of efforts to understand the mechanism of superconductivity and numerous unusual normal state properties of cuprates. Parent compounds of cuprates (e.g., $YB_2C_3O_6$) are insulators and also best examples of 2D Heisenberg antiferromagnets [2]. Upon hole doping, the antiferromagnetism disappears, and the system instead becomes a superconductor. Above optimal doping (which is defined such that superconducting T_c is the largest), superconducting features, such as the gap, Δ , in the spectral function, disappear at T_c [3]. Below optimal doping, the gap survives above T_c , and disappears only at a higher temperature T^* [4]. In addition, T_c and $\Delta(T=0)$ become progressively uncorrelated with underdoping - T_c decreases as doping decreases, while $\Delta(T=0)$ gets larger [5,6]. This clearly contradicts BSC theory in which $\Delta(T=0)$ scales with T_c . The region between T_c and T^* is called the

pseudogap region.

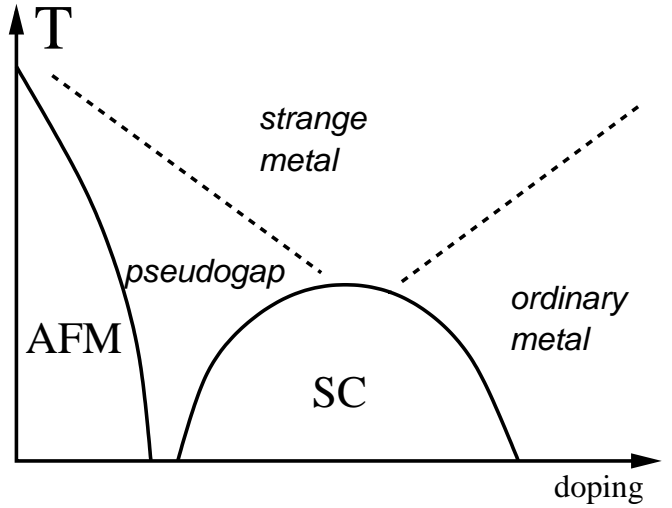


FIG. 1. A schematic phase diagram of cuprates.

A schematic phase diagram of cuprates is presented in Fig.1. There is general agreement among the researchers that the superconducting state predominantly has $d_{x^2-y^2}$ symmetry [7]. In this pairing state, the superconducting gap has nodes for diagonal directions along the Fermi surface, i.e., for $k_x = \pm k_y$. Much less, however, researchers agree at the present time about what is the origin of the pseudogap and also the anomalous normal state properties of cuprates. These two features (the pseudogap and the anomalous normal state behavior) are challenging for researchers and keep high T_c problem afloat over such large period of time.

This paper is devoted to the normal state properties of cuprates, so to keep our discussion focused we discuss only the experimental evidence for anomalous normal state behavior. The key evidence collaborated by very detailed photoemission [8,9], optical [10], transport [11] and other studies is that near optimal doping, the inverse quasiparticle lifetime is nearly linear in both temperature and frequency over a range of T between T_c and $1000K$, and at frequencies roughly between few tens and few hundred meV. The Fermi liquid theory on the other hand predicts that the inverse quasiparticle lifetime is quadratic in ω and T at the lowest energies. In overdoped cuprates, the low-frequency behavior of the

quasiparticle lifetime is more consistent with the Fermi liquid theory [12].

While there is no experimental proof at the moment that the measured non-Fermi liquid behavior at optimal doping extends down to $\omega, T = 0$ (i.e., that there is no crossover to the Fermi liquid behavior at the lowest energies), the very fact that the system behavior is markedly different from that in a Fermi liquid over a wide range of energies implies that theoretical description of cuprates should necessarily involve strong coupling effect.

From theoretical perspective, there exist two very distinct proposals about what may cause non-Fermi-liquid behavior. First proposal is that this behavior is generic to doped Mott insulators in two dimensions and is due to the fact that strong Coulomb interaction not only makes the picture of weakly interacting electrons invalid, but electron even ceases to exist as a quasiparticle (its residue is identically zero), and should instead be viewed as a convolution of two other objects one of which (spinon) carry spin but no charge, while the other (holon) carry charge but no spin [13]. The theories based on the idea that spin and charge excitations in cuprates are separated have been worked out in great detail [14] and substantially deepened our understanding of the physics of very strongly coupled electrons.

A second proposal is based on the assumption that the anomalous normal state behavior is caused by the closeness to a quantum phase transition of one type or another [15,16,18,17,20]. Near phase transitions, quantum fluctuations are generically enhanced, and this should give rise to deviations from Fermi-liquid behavior [21]. Moreover, in low D systems, the region of Fermi liquid behavior progressively shrinks to lower and lower energies as the system approaches quantum criticality. In distinction to the first approach, the idea that normal state behavior is due to a near quantum criticality necessary implies that at least on one side of a transition, the system behaves as a Fermi liquid at the lowest frequencies.

The idea of quantum criticality emerged in the early days of high T_c era as a way to justify the successful phenomenology [15] which used the linear energy dependence of the quasiparticle scattering rate as an input (the Marginal Fermi Liquid theory (MFL)). Another early idea of quantum criticality was focused on magnetic properties of cuprates, and was based on the assumption that the behavior of weakly doped antiferromagnet is close to that of undoped systems near the quantum transition between magnetically ordered and disordered states [22].

At present, there are three suggestions as to what kind of quantum criticality may cause the observed non Fermi-liquid behavior. The first is a phenomenological idea that there exists a quantum critical point somewhere around optimal doping, which separates Fermi-liquid and pseudogap phases [23]. In this phenomenology, superconducting region emerges as a dome on top of this point. The

second, also phenomenological, suggestion is that quantum criticality and pseudogap behavior may be caused by a competition between superconductivity and some other yet undiscovered ordering (specific suggestion involves d -density wave [24]). The third suggestion is that non Fermi liquid physics is due to the closeness to a magnetic quantum critical point which separates paramagnetic and antiferromagnetic phases [17,20].

In this paper we explore the third possibility and discuss what kind of critical behavior one can expect near antiferromagnetic transition. The magnetic scenario emerged from the early days of high T_c era [17,25] and was primarily based on the experimental observations that although antiferromagnetism observed in parent compounds quickly disappears upon doping, short-range antiferromagnetic correlations persist up to much larger doping concentrations as is evident from NMR [27] and neutron scattering [26,28] data, and these concentrations possibly cover the whole doping range of a superconducting behavior. Another favorable feature of a magnetic scenario, known even before high T_c , is that near half-filling, the spin fluctuation exchange gives rise to an attraction in a $d_{x^2-y^2}$ -pairing channel [25] and hence can cause d -wave superconductivity [29]. A simple way to understand this is to assume that spin-fluctuations in high- T_c materials play the same role as phonons in ordinary superconductors and create an analog of a deformation potential in the form

$$\mathcal{H}_{sf} = g \int d\vec{k}d\vec{q} c_{k,\alpha}^\dagger \vec{\sigma}_{\alpha,\beta} c_{k+q,\beta} \vec{S}_{-q}, \quad (1)$$

where $\sigma_{\alpha,\beta}^i$ are Pauli matrices and g is the coupling constant. Using this Hamiltonian, one can obtain an effective pairing interaction between fermions which amplitude is proportional to the propagator of the bosonic field S_q , i.e., to the dynamical spin susceptibility. In a weak coupling BSC theory, spin dynamics is irrelevant, and the gap equation in a spin singlet channel has the form [30]

$$\Delta_k = -\frac{3}{2}g^2 \int \chi(\mathbf{k} - \mathbf{p}) \Delta_p \frac{\tanh(\epsilon_p/2T)}{2\epsilon_p} d\vec{p} \quad (2)$$

In distinction to phonons, the r.h.s. of this equation has an extra minus sign due to a summation over spin components [29] (a projection of $\vec{\sigma}_{\alpha\beta}\vec{\sigma}_{\gamma\delta}$ onto a singlet spin channel yields $-(3/2)(\delta_{\alpha\beta}\delta_{\gamma\delta} - \delta_{\alpha\delta}\delta_{\beta\gamma})$ whereas a conventional spin-independent interaction yields no overall minus sign). Because of a sign change, an s -wave solution $\Delta_k = const$ is impossible. However, since $\chi(\mathbf{q})$ is peaked near an antiferromagnetic $\mathbf{Q} = (\pi, \pi)$, pairing interaction relates the gap at momenta \mathbf{k} and $\mathbf{k} + \mathbf{Q}$. In this situation, one can eliminate the overall minus sign by using an ansatz $\Delta_k = -\Delta_{k+Q}$. For tetragonal lattice, this ansatz implies $d_{x^2-y^2}$ symmetry of the pairing gap [31], i.e., spin fluctuation exchange gives rise to a d -wave superconductivity.

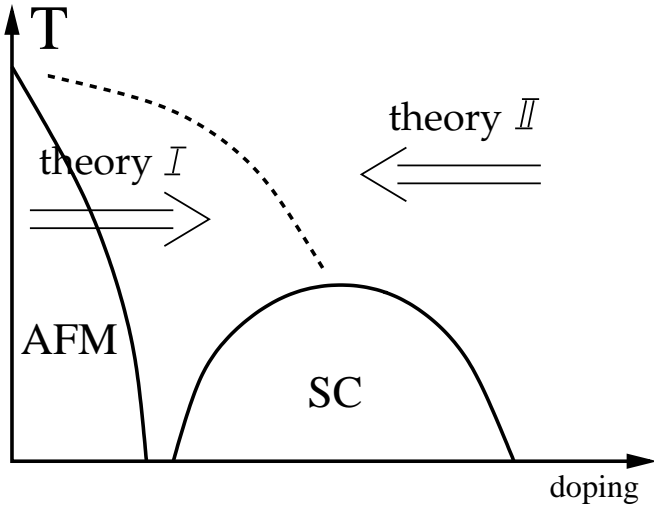


FIG. 2. Two different theoretical paths to study the physics of underdoped and optimally doped cuprates. In the first path, labeled as “theory I”, the point of departure is the antiferromagnetic state at half-filling. In the second path, labeled as “theory II” the point of departure is the conventional metallic state in the overdoped regime.

The studies of the normal state properties of cuprates within the magnetic scenario could also be divided into two subclasses (see Fig. 2). In the first class, which we labeled as “theory I”, the point of departure is Heisenberg antiferromagnetism at half-filling, and the issue addressed is how the system evolves with increasing doping [18,19,22,32,34,33,35,36]. These studies mostly consider small concentrations of electrons at which either long-range or quasi-long range magnetic order keeps majority of electrons localized, and the Fermi surface consists of separated patches (hole pockets). In the second class, labeled in Fig 2 as “theory II”, the point of departure is the Fermi liquid metallic state at large dopings, and the issue addressed is how this Fermi liquid behavior modifies and eventually disappears as the system approaches the magnetic transition. In this second approach, the physics is governed by the interaction between electrons and their collective spin bosonic excitations which become soft modes near the transition. This model is often called the spin-fermion model. Indeed, both approaches describe the same strongly interacting electronic system near magnetic instability and should yield the same results for the same regions of doping and temperatures, unless there are instabilities at large energies (comparable to e.g., fermionic bandwidth), which cannot be detected in the low-energy theory and have to be taken as inputs. From this perspective, the choice of the model is somewhat subjective and is mostly determined by which starting point is thought to be closer to real situation at a given doping. Very near half-filling, the system clearly displays Heisenberg antiferromagnetism, and the Fermi surface should consist of hole pockets. In

this limit, one has to work rather hard within the spin-fermion model to reproduce the features which are readily obtained if one departs from antiferromagnetic state at half-filling. On the other hand, we believe that the spin-fermion model is a better starting point if one wants to describe the physics at and somewhat below optimal doping mostly because at present the majority of photoemission experiments even in heavily underdoped cuprates do not show the emergence of the shadow Fermi surface (the extra piece of the Fermi surface shifted from the original one by antiferromagnetic \mathbf{Q}), which is the necessary ingredient for the formation of hole pockets [38].

The present paper summarizes our analysis of the spin-fermion model in the normal state, or, more precisely, when the pairing correlations can be neglected. We argue that in $2D$, a dimensionless coupling constant for the spin-fermion interaction λ scales as inverse magnetic correlation length ξ and diverges as the system approaches a quantum-critical point (QCP) of a transition to a magnetically ordered state. We show that due to a divergence of λ , there exists a wide region in the T, λ plane where the system is in the quantum-critical regime near the magnetic transition. We will show that in this regime, the system behavior is qualitatively different from that in a Fermi liquid.

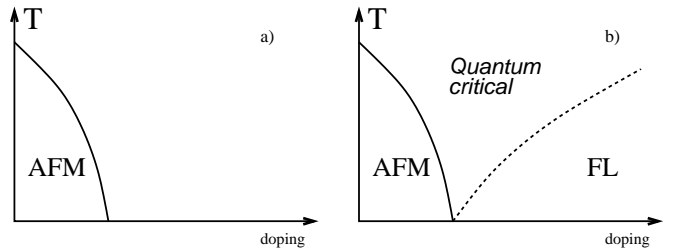


FIG. 3. A cartoon of the system behavior near antiferromagnetic quantum-critical point

Our point of departure is the “zero-order” phase diagram with antiferromagnetism included as an input (Fig.3a). The deviations from the magnetic transition are measured by the doping dependent spin correlation length $\xi(x)$. We assume that all other features on the phase diagram, such as superconductivity, pseudogap regime, and the crossover from a Fermi-liquid to not Fermi liquid behavior in the normal state are *low-energy phenomena* which should be *obtained* within the model. Alternatively speaking, we assume that antiferromagnetism is produced by fermions with energies comparable to the bandwidth, while other phenomena are produced by fermions near the Fermi surface. In cuprates, the separation of scales is not very strong (T^* for strongly underdoped materials is a fraction of an exchange integral J), i.e., to some extent high-energy fermions do contribute to pseudogap phenomenon and may also contribute to anomalous normal state behavior. This contribution is

inevitably lost in our approach. However, we believe that the fundamental physics can be understood by separating the scales perhaps more strongly than in reality, and the inclusion of fermions with energies comparable to the bandwidth will change the results quantitatively but not qualitatively.

The phase diagram which emerges from our studies is presented in Fig. 3b. We argue that the region near the QCP is divided into a Fermi liquid regime and a quantum-critical regime where the system behavior is the same as at the critical point. The upper boundary of the quantum-critical behavior is roughly located at frequencies comparable to spin-fermion coupling constant \bar{g} . The crossover from a Fermi liquid to a quantum-critical behavior on the other hand occurs at energies of order $\omega_{sf} \sim \bar{g}\lambda^2$ where λ , which we already introduced above, is the dimensionless coupling constant in the problem ($\lambda \propto \bar{g}/v_F\xi^{-1}$, where v_F is the Fermi velocity). At weak coupling, ω_{sf} exceeds \bar{g} , and the quantum-critical behavior is not realized. However, at strong coupling, $\omega_{sf} \ll \bar{g}$, and the system displays quantum-critical behavior in a wide range of frequencies. This strong coupling behavior necessary occurs very near the transition as $\lambda \propto \xi$, but it can also be reached at intermediate ξ when the spin-fermion interaction \bar{g} increases.

In the Fermi liquid regime, fermionic self-energy behaves as $\Sigma'' \propto \omega^2/\omega_{sf}$. In the opposite limit, when $\omega_{sf} = 0$, we found that it scales, up to logarithmical corrections, as $\Sigma'' \propto \sqrt{\bar{g}E}$, where $E = \max(\omega, T)$. At a finite ω_{sf} , we find that there also exists a wide intermediate region, roughly between $0.5\omega_{sf}$ and $6 - 8\omega_{sf}$, where $\Sigma'' \propto E$, i.e., it is linear in both frequency and temperature. This behavior of the self-energy causes a cascade of crossovers in the fermionic spectral function and conductivity measured as functions of temperature and frequency.

These are the key results of the paper. We derive them in Sec. III -VI below in a formal $1/N$ expansion where N can be regarded either as the number of hot spots in the Brillouin zone (crossing points between the Fermi surface and the magnetic zone boundary), or the number of electron flavors.

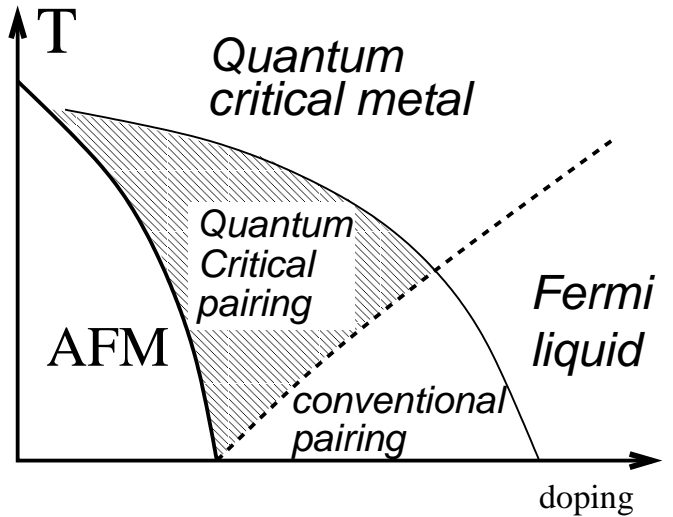


FIG. 4. A schematic phase diagram of cuprates obtained in [39] in the Eliashberg-type formalism

As we said, in this paper we focus on the normal state properties of the spin-fermion model. For completeness, we also present in Fig. 4 the phase diagram which we obtained [39] in the Eliashberg-type formalism (extended compared to that for phonons [42] to include the feedback from pairing on magnetically mediated interaction) by using the normal state results as a base and adding the interaction in the pairing channel. Our key point here is that the two scales ω_{sf} and \bar{g} which we find in the normal state are also present in the pairing problem. Namely, the pairing instability temperature T_{ins} tends to a finite value $\sim \bar{g}$ (more accurately, \bar{g}/N) at the quantum-critical point. In a conventional situation, this would imply that superconducting properties gradually evolve below T_{ins} . In our situation, this, however, is not the case as at strong coupling, when $T_{ins} \propto \bar{g} \gg \omega_{sf}$, the pairing comes from frequencies which well exceed ω_{sf} , and thus involves incoherent fermions [40]. This pairing is qualitatively different from that in the BCS theory. We found that in this situation, immediately below T_{ins} electrons form singlet pairs, but the pairs still behave incoherently and do not propagate. Only when the temperature is reduced well below T_{ins} , the feedback from superconductivity eventually “clears up” fermionic excitations, and the system behaves as a conventional superconductor. We found that the conventional superconducting behavior with e.g., a sharp quasiparticle peak in the spectral function) emerges only when the temperature becomes smaller than the fraction of $(\omega_{sf}\bar{g})^{1/2} \sim \bar{g}/\lambda \ll \bar{g}$. Physically, this second scale (modified ω_{sf}) is the gap in the spectrum collective spin excitations which become propagating, magnon-like in a d -wave superconductor [41].

The cuprates are not the only objects which motivate our study. Over the last few years, there is a growing interest in the behavior of various heavy-fermion materi-

als near the magnetic instability which can be achieved either by chemical variation (i.e., doping) or by applying external perturbation such as pressure [43,44,47]. The magnetic instability can be either ferromagnetic or antiferromagnetic, depending on material. There is a convincing experimental evidence that at least in some of heavy fermion materials, there exists a dome on top of a quantum critical point where the system is in a superconducting phase [44]. From this perspective the behavior of heavy-fermion materials may be not very different from that of cuprates. There is also a number of experimental data which show that the normal state behavior near magnetic instability likely deviates from that in a Fermi liquid down to very low energies [45,46]. These deviations have been observed in both fermionic and spin properties [47]. We caution, however, that heavy-fermion materials are mostly three-dimensional [46] while our analysis is valid in two dimensions. Still, we believe that the computational scheme we developed for $2D$ can be applied also to $3D$ materials at strong coupling.

Our approach to the spin-fermion model is an extension of the earlier detailed studies by D. Pines and co-workers [17,29,48]. The only qualitative difference is that we do not assume a priori the form of the dynamical susceptibility but rather derive it. From this perspective, our work should be regarded as an attempt to put the studies of the spin-fermion model on a solid theoretical basis and to understand whether one can attack the problem analytically, in a controllable way. Previous studies of the spin-fermion model were mostly performed numerically.

Also, our approach and computational technique are in many respects similar to the studies by B. Altshuler, A. Millis and L. Ioffe [49,50] of fermions interacting with low-energy collective modes. Our studies also agree, in most part, with numerical studies of the spin-fermion model by Benemman and co-authors [51]. Our analysis of the effective bosonic theory of the model at criticality agrees in most parts with the studies of Lercher and Wheatley [53].

Finally, our analysis bears some parallels with large D studies of fermionic systems [54]. Just as in $D \rightarrow \infty$ theories, our self-energy predominantly depends on frequency (at the lowest energies the renormalization of ϵ_k in the fermionic propagator is by $\log \lambda/\lambda$, smaller than the renormalization of ω). The difference, as we understand it, is that large D theories were chiefly applied to explain the effects, such as metal-insulator transition, for which fermions with energies comparable to the bandwidth play an important role. We, on the contrary, focus on universal features of the system behavior at the lowest frequencies, when the fermionic density of states can be approximated by a constant, i.e., the bandwidth can be set to infinity. The paper is organized as follows. In the next section, we discuss the spin-fermion model and its relation to lattice models of cuprates. In Sec III we present

the calculations at $T = 0$. We first discuss ordinary perturbation theory and then $1/N$ expansion in the strong coupling ($\lambda \gg 1$) limit. We then proceed in Sec. IV with the calculations at $N \rightarrow \infty$. In the next Sec V we discuss $1/N$ expansion at $T = 0$. In this Section we also compare our results at the QCP with the conventional ϕ^4 theory of such transition [55,56]. We argue that spin-fermion model at criticality is *not* described by a standard ϕ^4 theory because of complex momentum and frequency dependences of the effective four-boson vertex made out of fermions. In the next Sec VI we present the results of our calculations at finite temperature. Here we obtain the full form of the fermionic spectral function which can be directly compared to the photoemission data. In Sec. VII we discuss in detail the behavior of optical conductivity $\sigma = \sigma_1 + i\sigma_2$, effective scattering rate $1/\tau$ and the effective quasiparticle mass. These expressions can be directly compared with optical and transport data. In Sec VIII we present the results for other observables: fermionic density of states, dynamical spin susceptibility, and Raman intensity. Finally, in Sec IX we discuss the behavior of the pairing vertex and show that although pairing fluctuations in the normal state generally affect fermionic propagator only to order $1/N$, the ladder corrections to the pairing vertex are not small in $1/N$. We argue that the ladder series give rise to a d -wave pairing instability. The results of our analysis are summarized in Sec X. In this last section we also compare our results for the fermionic spectral function and conductivity with the photoemission and optical data for near optimally doped cuprates.

Some of the results presented in the paper have already been discussed in short communications [20,39,40,57–62].

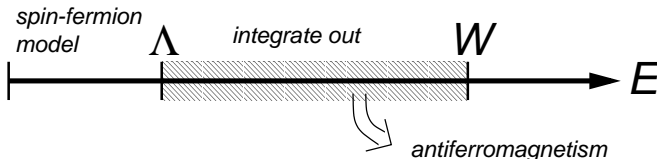
II. SPIN-FERMION MODEL

In this section, we present the microscopic justification for the spin-fermion model. We use renormalization group (RG) arguments and general considerations to obtain the effective Hamiltonian which describes the interaction between low-energy fermions and their collective spin degrees of freedom. We then develop a new method to compute the forms of the fermionic propagator and dynamical spin susceptibility for strong spin-fermion interaction.

The first-principle approach to cuprates demands that one chooses a microscopic model which describes fermions on a lattice with a short-range, Hubbard-type interaction. If the choice is correct and if one manages to solve this model and understand the result, there is no need to introduce any low-energy phenomenology. Unfortunately, this microscopic model is unknown and presumably is rather involved. The Hubbard model with on-site interaction is a undoubtedly a reasonable first

choice [63,33], but one has to have in mind that it indeed gives only an approximate description of the actual physics in cuprates. Furthermore, even for the single band Hubbard model no exact solution has been yet obtained in two dimensions, and one has to either study the model numerically [63,33], or use an approximate theoretical scheme such as small U expansion [64], or an expansion in the artificially extended number of electronic orbitals per site [65].

In the low-energy approach which we advocate, we are not interested in the behavior at high energies (comparable to the fermionic bandwidth W), and want to get only a limited information about the system, namely, how it behaves at energies smaller than some cutoff energy $\Lambda \leq W$. In the RG sense, this effective theory can be regarded as obtained by integrating out fermionic degrees of freedom with energies between W and Λ .



It is generally believed that this procedure does not take the system away from the basin of attraction of the Fermi-liquid fixed point. We are not aware of any solid calculations which would indicate the opposite. In other words, we assume that the fermionic interactions at high energies do not destroy the Fermi-liquid behavior. This, however, does not imply the throughout applicability of the conventional Landau Fermi liquid theory because of possible infrared singularities. In fact we show below that in some range of parameters the fermionic self-energy corrections are indeed singular, and give rise to a non-Fermi liquid behavior.

Strictly speaking, the RG procedure is justified only if the spin-fermion coupling does not exceed fermionic bandwidth which we assume to hold. If this condition is not satisfied, the separation between low-energy and high-energy excitations becomes problematic. We believe that our results are valid, with some minor modifications, also in the limit of very large couplings provided, indeed, that there is no destruction of the Fermi liquid due by fluctuations at lattice scales. However, universal results which we report here are only valid if the coupling are smaller than the bandwidth, and typical fermionic momenta are located near the Fermi surface, when the fermionic dispersion can be linearized.

In general, the low-energy behavior of fermionic systems is governed by degrees of freedom which have low-energy excitations. One such degree of freedom is obviously given by the fermion itself since it possesses an arbitrary low energy near the Fermi surface. Potential can-

didates for other low energy excitations are the bosonic collective modes of fermions. In a general situation, these collective modes are gaped already at energies comparable to the bandwidth. However, if the fermionic system is close to an instability of some kind, then the corresponding bosonic collective mode has a much smaller gap which vanishes at the instability point. The closeness to anti-ferromagnetism naturally makes spin excitations relevant candidates for such low-energy degrees of freedom.

Throughout this paper we assume that

1. spin fluctuations can be treated as low-energy excitations in the wide range of dopings,
2. one can neglect the effects of all other low-energy collective degrees of freedom, independent of spin excitations

These are two basic assumptions of our approach. Their applicability is solely determined by comparisons with the experimental data. We believe that the NMR and neutron scattering data in cuprates indicate that for all doping ranges (including overdoped materials), the spin susceptibility possesses a substantial momentum and frequency dependence near the antiferromagnetic momentum (π, π) , and the typical energies associated with these dependencies are at least by order of magnitude smaller than the fermionic bandwidth. We also believe that there is no clear experimental indication of the presence of the low-energy excitations in other interaction channels. In principle, this does not preclude moderately strong effects from other channels which can account for moderate values of the Landau parameters [66]. These effects may change numbers but certainly do not change the basics physics. Note also that our approach does not rule out the effects in other channels which are secondary in the sense that they emerge within the spin-fermion model. For example, charge excitations may acquire a low-energy dynamics due to a coupling with spin fluctuations. This coupling may eventually lead to phase separation [67,68] and, potentially, (when lattice effects are included) to the formation of stripes [69].

The treatment of spin fluctuations as separate bosonic degrees of freedom requires some extra clarifications. The point is that in distinction to heavy-fermion materials, there is only one species of fermions in cuprates, and spin fluctuations just result from a multiple interactions between particles and holes, i.e., are collective modes of the fermions. From this perspective, the introduction of spin excitations as an extra low-energy degree of freedom is just a convenient way to separate the energy scales: we assume that there exists a single dominant channel for fermion-fermion interaction at energies smaller than Λ , and introduce a (spin) collective mode which mediates this interaction. At the same time, the static propagator of this collective mode (and, in particular, the value of the spin correlation length) is obviously determined by high

energy fermions about which we have little information. We only expect, as we already said, that the integration over high fermionic energies does not give rise to any singularity in the bare spin susceptibility. The latter then should have a regular Ornstein-Zernike form

$$\chi_0(\mathbf{q}, \omega) = \frac{\chi_0}{\xi^{-2} + (\mathbf{q} - \mathbf{Q})^2 - (\omega/v_s)^2}. \quad (3)$$

The input parameters in Eq. (3) are the spin correlation length, ξ and the spin velocity v_s which is obviously of order v_F as spins are made out of fermions. The overall factor χ_0 can be absorbed into the renormalization of the coupling constant (see below) and should not be counted as an extra variable.

Note that the bare $\chi_0(\mathbf{q}, \omega)$ is real. This is an essential point in our consideration. We argue that the imaginary part of the susceptibility is determined by fermions with energies smaller than Λ and has to be computed within a low-energy theory rather than taken as an input. Indeed, since the spins have no source of damping other than to decay into a particle hole pair, the inverse lifetime of a spin fluctuation coincides with the imaginary part of the fully renormalized particle-hole bubble. Due to the necessity to conserve energy and momentum in a decay process, it involves only low-energy fermions with frequencies *smaller* than the external spin frequency.

In earlier phenomenological studies of the spin-fermion model, the full spin susceptibility, including its imaginary part, was considered as an input [17]. The spin dynamics was assumed to be a simple relaxational one with $\chi^{-1}(\mathbf{Q}, \omega) \propto 1 - i\omega/\omega_{sf}$. The value of ω_{sf} was taken from experiments and assumed to vary with doping independently of other input parameters. The phenomenological assumption about the form of the full susceptibility is roughly consistent with our findings. At the same time, we will see that ω_{sf} is expressed in terms of other input parameters and cannot be varied independently of the spin-fermion coupling.

Note that the damping term in the spin susceptibility only appears if the Fermi surface contains hot spots (points separated by \mathbf{Q}) [70]. For a Fermi surface without hot spots the spin decay is forbidden at low frequencies due to energy constraint. In this situation, the full spin susceptibility is real at small frequencies and differs from (3) only due to effects of quantum criticality. On the other hand, for a Fermi surface with hot spots, the spin damping is permissible down to the lowest energies and overshadows the quadratic in ω term in the bare susceptibility which therefore becomes irrelevant.

The topology of the Fermi surface in cuprates is non-universal and in principle can vary from one material to the other. ARPES data indicate that at least in the best studied Bi-based cuprates, the Fermi surface is centered at (π, π) , i.e., it is an open electron Fermi surface [3,71]. Applying Luttinger theorem which states that the area of electron states, measured in units of the Brillouin zone

area, equals to the density of electrons [72], one can immediately make sure that such Fermi surface necessarily crosses the magnetic Brillouin zone boundary and therefore contains hot spots. As we just said, in this situation, the ω^2 term in the bare spin susceptibility is irrelevant, i.e., $\chi_0(\mathbf{q}, \omega)$ can be approximated by its static part. This in turn implies that the spin-fermion model can be described by the Hamiltonian. This Hamiltonian involves fermions which live near the Fermi surface, spin fluctuations, and the interaction between the two degrees of freedom, and can generally be written as

$$\begin{aligned} \mathcal{H} = & \sum_{\mathbf{k}, \alpha} \mathbf{v}_k(\mathbf{k} - \mathbf{k}_F) c_{\mathbf{k}, \alpha}^\dagger c_{\mathbf{k}, \alpha} + \sum_q \chi_0^{-1}(\mathbf{q}) \mathbf{S}_q \mathbf{S}_{-q} \\ & + g \sum_{\mathbf{q}, \mathbf{k}, \alpha, \beta} c_{\mathbf{k}+\mathbf{q}, \alpha}^\dagger \sigma_{\alpha, \beta} c_{\mathbf{k}, \beta} \cdot \mathbf{S}_{-\mathbf{q}}. \end{aligned} \quad (4)$$

Here, $c_{\mathbf{k}, \alpha}^\dagger$ is the fermionic creation operator for an electron with crystal momentum \mathbf{k} and spin projection α , σ_i are the Pauli matrices, and g is the coupling constant which measures the strength of the interaction between fermionic spins and the collective spin degrees of freedom described by bosonic variables S_q .

Alternatively to the Hamiltonian in Eq. 4, we can also write down the effective action for the model

$$\begin{aligned} S = & - \int_0^\beta d\tau \int_0^\beta d\tau' \sum_{\mathbf{k}, \sigma} c_{\mathbf{k}\sigma}^\dagger(\tau) G_0^{-1}(\mathbf{k}, \tau - \tau') c_{\mathbf{k}\sigma}(\tau') \\ & + \frac{1}{2} \int_0^\beta d\tau \int_0^\beta d\tau' \sum_{\mathbf{q}} \chi_0^{-1}(\mathbf{q}) \mathbf{S}_{\mathbf{q}}(\tau) \cdot \mathbf{S}_{-\mathbf{q}}(\tau') \\ & + g \int_0^\beta d\tau \sum_{\mathbf{q}} \mathbf{s}_{\mathbf{q}}(\tau) \cdot \mathbf{S}_{-\mathbf{q}}(\tau). \end{aligned} \quad (5)$$

where $G_0^{-1}(\mathbf{k}, \tau) = \partial_\tau - \mathbf{v}_k(\mathbf{k} - \mathbf{k}_F)$ is the bare Fermionic propagator. In general, this representation is more advantageous as it allows a time dependence of the bare spin propagator $\chi_0(\mathbf{q}, \tau)$. In our case, as we said, this time dependence is irrelevant, and one can therefore use a conventional Hamiltonian description.

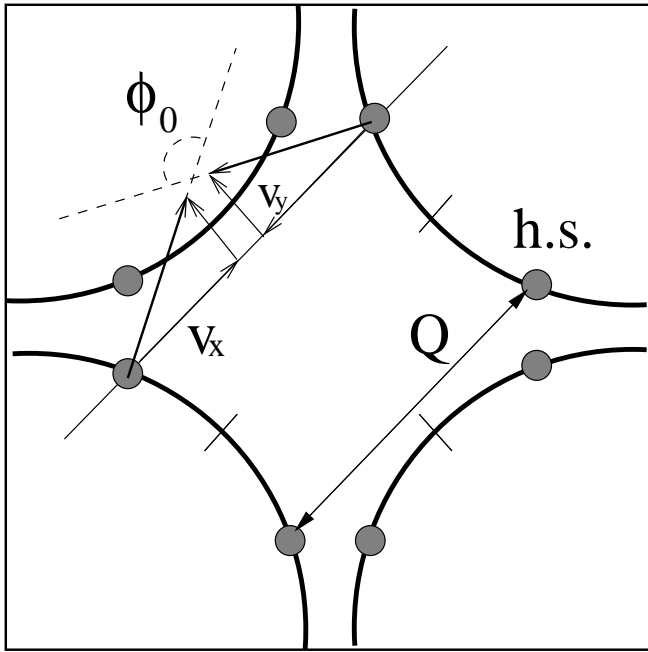


FIG. 5. A schematic picture of the Fermi surface. The notation h.s. stands for “hot spot” – the point on the Fermi surface separated by another point on the Fermi surface by the antiferromagnetic vector \mathbf{Q} . The arrows denote the velocities at hot spots. ϕ_0 is the angle between the velocities at hot spots separated by \mathbf{Q} .

The input parameters in (4) are ξ , the fermionic velocity \mathbf{v}_k and the spin-fermion coupling g . We demonstrate below that the physics associated with the closeness to an antiferromagnetic instability mostly involves fermions near hot spots. For $\mathbf{Q} = (\pi, \pi)$, there are 8 hot spots in the Brillouin zone with the same $v_F \equiv |\mathbf{v}_k|$. The direction of \mathbf{v}_k at two hot spots separated by \mathbf{Q} differs by an angle ϕ_0 . This angle, however, should not be counted as a relevant input parameter as we will see that the physics is insensitive to the actual value of ϕ_0 as long as $\phi_0 \neq \pi$, i.e., there is no nesting at hot spots. The results for the nested Fermi surface are different, and we will not discuss this special case in the paper. Experimentally, in cuprates the hot spots are located not far away from the corners of the Brillouin zone (i.e., from $(0, \pi)$ and symmetry related points). In this situation, ϕ_0 is obviously close to $\pi/2$. For practical purposes, it is more convenient to introduce, instead of v_F and ϕ_0 , the two velocities v_x and v_y via $\epsilon_k = v_x k_x + v_y k_y$ and $\epsilon_{k+Q} = -v_x k_x + v_y k_y$, where k measure a deviation from a hot spot. Obviously, $v_F^2 = v_x^2 + v_y^2$ and $\phi_0 = 2 \tan^{-1} v_x / v_y$. The limit $\phi_0 = \pi$ corresponds to $v_y = 0$. (see Fig. 5)

The spin-fermion coupling constant g is a fully renormalized irreducible vertex for the particle-hole channel. In the Born approximation, g equals to the Hubbard U . Beyond Born approximation g acquires a strong doping dependence and rapidly decreases with increasing dop-

ing. For example, an RPA renormalization of g in the particle-particle channel yields $g = U / (1 + (U/t)F(x))$ where $F(x)$, subject to $F(0) = 0$, is an increasing function of the doping, x . This form shows that $g \sim U$ only at small doping while at larger x it progressively decreases down to $g \sim t$. This form of g is indeed only an approximate one as there is no justification to restrict with one particular renormalization channel at high frequencies. We can only quite generally assume that g is some doping dependent coupling constant which increases as the system approaches half-filling.

To summarize, the relevant input parameters for our model are ξ , v_F , and the effective coupling $\bar{g} = g^2 \chi_0$, which is a combination in which g and χ_0 appear in perturbation series. The first two parameters can be merged into an energy scale $v_F \xi^{-1}$. Out of the two energies, \bar{g} and $v_F \xi^{-1}$, one can construct an overall scale and a single dimensionless ratio

$$\lambda = 3\bar{g} / (4\pi v_F \xi^{-1})$$

which, as we will see in the next section, determines the strength of both fermionic and bosonic self-energy corrections (the numerical factor in λ is introduced for further convenience). Physically, λ measures the ratio of the effective coupling constant and a fermionic energy at a typical fermionic $|k - k_F| \sim \xi^{-1}$, which sets the momentum range for spin-fermion coupling. When λ is small, fermions are nearly decoupled from spin fluctuations and behave as an almost ideal Fermi gas. On the contrary, when λ is large, the bare fermionic dispersion is almost completely overshadowed by the interaction, and this may give rise to a non-Fermi liquid behavior.

The fact that a large number of experimental data for cuprates already near optimal doping differ from the predictions of the Fermi liquid theory indicates that if spin-fermion coupling a relevant mechanism for deviations from the Fermi-liquid theory, λ should be large already for optimally doped samples, and increase with decreasing doping. Our estimates of λ using the photoemission [9,73,74], neutron [75], and NMR [76] data yields $\lambda \sim 2$ near optimal doping (see Sec X). This observation is a challenge to a theory as real systems turns out to be outside the basin of applicability of a conventional, weak coupling perturbation theory and one should instead try unconventional procedures in a search for a strong-coupling solution.

We now proceed with the evaluations of the fermionic and bosonic self-energies.

III. PERTURBATION THEORY FOR THE SPIN-FERMION MODEL AT $T = 0$

In this Section, we analyze the spin-fermion model at $T = 0$. Our strategy is the following: we first present the

results of a formal perturbation theory for both fermionic and bosonic propagators. We show that perturbation expansion for the fermionic self-energy and the spin-fermion vertex holds in powers of λ and obviously breaks down for $\lambda > 1$. We next show that at $\lambda \geq 1$ the self-energy corrections to the spin propagator also become relevant and change the dynamics of spin fluctuations at frequencies which are mostly relevant for fermionic self-energy and vertex renormalization. We then demonstrate that even for large λ , one can construct a variant of perturbation theory in which dominant, $O(\lambda)$ fluctuation contributions are included into new zero-order fermionic and bosonic propagators for which we obtain explicit answers. The remaining fluctuation corrections are logarithmical in λ , and we analyze them in the one-loop RG formalism.

A. A formal perturbation theory

We begin with the direct zero-temperature perturbation expansion in powers of λ . Direct perturbative expansion means that all diagrams are evaluated using the bare values of the spin susceptibility and the fermionic propagator.

1. fermionic self-energy

We start with the fermionic self-energy, $\Sigma(k, \Omega)$ related to the fermionic propagator by $G^{-1}(k, \omega) = \Omega + \Sigma(k, \Omega) - \epsilon_k$. Let's first compute $\Sigma(k, \Omega)$ near a hot spot expanding to first order in frequency and in the quasiparticle energy. We will demonstrate that this supposedly straightforward computation has to be performed with more care than one might expect.

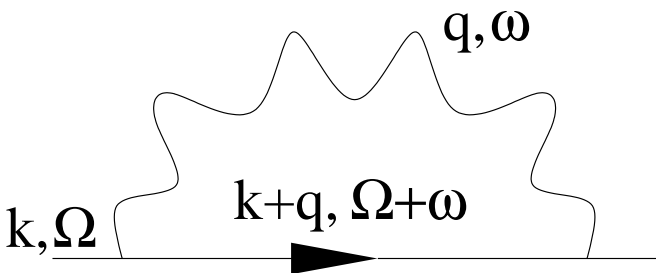


FIG. 6. The lowest-order diagram for the fermionic self-energy.

The lowest-order self-energy correction involves a single spin-fluctuation exchange and is presented in Fig. 6. In the analytical form we have in Matsubara frequencies

$$\begin{aligned} \Sigma(\mathbf{k}, \Omega_m) &= -3g^2 \int \frac{d^2q d\omega_m}{(2\pi)^3} \\ &\times G_0(\mathbf{k} + \mathbf{q}, \omega_m + \Omega_m) \chi_0(\mathbf{q}, \omega_m), \end{aligned} \quad (6)$$

where

$$G_0^{-1}(\mathbf{k}, \omega_m) = i\omega_m - \mathbf{v}_F(\mathbf{k} - \mathbf{k}_{hs}). \quad (7)$$

Subtracting from (6) the self-energy at $\Omega_m = 0$ and $\mathbf{k} = \mathbf{k}_{hs}$ which can be absorbed into the renormalization of the chemical potential, and expanding to first order in $\mathbf{k} - \mathbf{k}_{hs}$ and in frequency, we obtain after simple manipulations

$$\Sigma(\mathbf{k}, \Omega_m) = (i\Omega_m - \epsilon_{k+Q}) I(\mathbf{k}, \Omega_m) \quad (8)$$

where

$$\begin{aligned} I(k, \Omega_m) &= \frac{3\bar{g}}{(2\pi)^3} \int d^2\tilde{q} d\omega_m \frac{1}{\xi^{-2} + \tilde{\mathbf{q}}^2 + (\omega/v_s)^2} \\ &\times \frac{1}{i\Omega_m - \epsilon_{k+Q} + i\omega_m - v_F\tilde{q}_x} \frac{1}{i\omega_m - v_F\tilde{q}_x} \end{aligned} \quad (9)$$

Here $\tilde{\mathbf{q}} = \mathbf{q} - \mathbf{Q}$, and x -axis is chosen along \mathbf{v}_F at $\mathbf{k} + \mathbf{Q}$.

In the spirit on a conventional expansion in Ω_m and ϵ_{k+Q} , it is tempting to evaluate $I(\mathbf{k}, \Omega_m)$ right at $\mathbf{k} = \mathbf{k}_{hs}$ and $\Omega_m = 0$. The corresponding computations are performed in Appendix A, and the result is

$$I(\mathbf{k}_{hs}, 0) = -\lambda \frac{v_s}{v_F + v_s} \quad (10)$$

Substituting this into (8) one would obtain that the self-energy only accounts for the renormalization of the quasiparticle residue, and the magnitude of the renormalization depends on the ratio v_s/v_F . Apparently this is the whole story. However, it turns out that Eq. (10) is not the full result, and

$$\lim_{\Omega_m \rightarrow 0, k \rightarrow k_{hs}} I(\mathbf{k}, \Omega_m) \neq I(\mathbf{k}_{hs}, 0) \quad (11)$$

To show this we evaluate $I(\mathbf{k}, \Omega_m)$ keeping both Ω_m and $\mathbf{v}_F \tilde{\mathbf{k}}$ in the integrand in (8). Analyzing the integrand, we observe that there exists a tiny region of frequencies where the poles in the two fermionic propagators are close to each other, but still are located in different halves of a complex \tilde{q}_x plane. For $\Omega_m > 0$, this region is sandwiched between $\omega_m > -\Omega_m$ and $\omega_m < 0$. The integration over \tilde{q}_x in (8) in this range of frequencies, and a subsequent integration over ω_m yields an extra contribution to $I(k, \Omega_m)$ in the form

$$I_{an}(\mathbf{k}, \Omega_m) = \lambda \frac{i\Omega_m}{i\Omega_m - \epsilon_{k+Q}} \quad (12)$$

We see that $I_{an}(\mathbf{k}, \Omega_m)$ comes from the integration over internal frequencies ω_m which are *smaller* than the external Ω_m . Clearly, this anomalous piece could not be obtained in a conventional perturbation expansion over Ω_m as in the latter one assumes that the internal energies are much larger than the external one. This assumption is generally justified by a simple phase space argument, i.e., the contribution from $|\omega_m| \leq \Omega_m$ is normally small

due to the smallness of the integration range. Here, however, the smallness of the phase space is compensated by the smallness of the denominator in (8) as without Ω_m and ϵ_{k+Q} , the product of two Green's functions contains a double pole. At finite Ω_m and ϵ_{k+Q} , the double pole splits into two single poles, but the energy difference between them is still only $i\Omega_m - \epsilon_{k+Q}$, i.e., is of the same order as the integration range over frequency. The same reasoning is used to extract the effects due to chiral anomaly in quantum chromodynamics [77].

Substituting the total expression for $I(\mathbf{k}, \Omega_m)$ into the self-energy, we obtain

$$\Sigma(\mathbf{k}, \Omega) = \lambda \left[i\Omega_m - (i\Omega_m - \epsilon_{k+Q}) \frac{v_s}{v_s + v_F} \right]. \quad (13)$$

We see that both terms in Σ are of order λ , i.e., there is no strong distinction between ‘‘anomalous’’ and ‘‘normal’’ contributions to the fermionic self-energy. This could be anticipated as, e.g., for $v_s = \infty$, $\chi_0(\mathbf{q}, \omega)$ is purely static, and $\Sigma(\mathbf{k}, \Omega)$ should only depend on ϵ_{k+Q} as the dependence on external Ω_m is eliminated by shifting the internal frequency in the fermionic propagator in (6). We indeed reproduce this result: for $v_s = \infty$ Eq. (13) yields $\Sigma(\mathbf{k}, \Omega_m) = \lambda\epsilon_{k+Q}$.

2. vertex renormalization

We next compute the lowest-order correction to the spin-fermion vertex for fermions at hot spots.

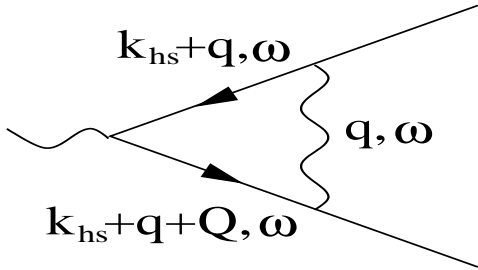


FIG. 7. The lowest-order diagram for the correction to the spin-fermion vertex.

The lowest-order vertex correction diagram is presented in Fig. 7. The vertex correction is obviously the largest for a fermion at a hot spot. For $\mathbf{k} = \mathbf{k}_{hs}$ and $\omega = 0$ we obtain $g^R = g + \Delta g$ where

$$\frac{\Delta g}{g} = i\bar{g} \int \frac{d\omega_m d^2q}{(2\pi)^3} \chi(\mathbf{q}, \omega_m) \times G(\omega_m, \mathbf{k}_{hs} + \mathbf{q}) G(\omega_m, \mathbf{k}_{hs} + \mathbf{q} + \mathbf{Q}) \quad (14)$$

Observe that the overall factor (the result of the summation over spin components) is different from that in

the fermionic self-energy (-1 instead of 3). Expanding, as above, near hot spots as $\epsilon_{k_{hs}+q} = v_x q_x + v_y q_y$, $\epsilon_{k_{hs}+q+Q} = -v_x q_x + v_y q_y$ where $v_x^2 + v_y^2 = v_F^2$, and performing the computations described in Appendix A, we obtain

$$\frac{\Delta g}{g} = \frac{\lambda v_F}{3 v_s} \frac{1}{\beta \sqrt{1 - \alpha^2}} \ln \frac{\alpha (\sqrt{1 - \alpha^2} - \beta)}{\sqrt{(\beta^2 + \alpha^2)(1 - \alpha^2)} - \beta} \quad (15)$$

where $\alpha = v_y/v_s$ and $\beta = v_x/v_s$. For purely static bare susceptibility, i.e., $v_F/v_s \rightarrow 0$, $\Delta g/g$ is a smooth function of v_x and v_y .

$$\frac{\Delta g}{g} = \frac{\lambda v_F}{3 v_x} \sinh^{-1} \frac{v_x}{v_y} \quad (16)$$

In the opposite limit $v_s \ll v_F$, we obtain from (15)

$$\frac{\Delta g}{g} = \frac{\lambda v_s v_F}{3 v_x v_y} \tan^{-1} \frac{v_x}{v_y} \quad (17)$$

Observe that the correction to the spin-fermion vertex vanishes when the velocity of spin excitations tends to zero.

We also verified that the correction to the spin-fermion vertex does not contain a singularity, similar to what we found for a self-energy correction. In other words, the limiting value of Δg at vanishing frequency coincides with Δg evaluated right at zero frequency. The absence of a singular correction to a vertex is associated with the fact that the two internal fermions in the vertex correction diagram have different directions of the velocities, and hence there is no double pole which might give an extra piece after regularization.

3. higher-order diagrams and the structure of the perturbation theory

We see that the perturbative expansion for the fermionic self-energy and the spin-fermion vertex holds in the dimensionless parameter λ . Higher-order diagrams can be easily estimated. They all scale as higher powers of λ . To this end, diagrammatic, perturbative approach clearly fails if λ is large.

There is, however, a hint already at this stage that there are some peculiarities in the perturbation theory at strong coupling. Namely, we expect (and we show below) that at strong coupling, spin fluctuations are completely overdamped, i.e., the frequency dependence of the spin susceptibility is dominated by $i\omega$ term instead of ω^2 term. Crudely, this effect can be modeled by reducing v_s in (13) and (15). We see, that when v_F/v_s becomes very large, the regular part of the fermionic self-energy vanishes leaving only the anomalous piece in (13). Simultaneously, $\Delta g/g$, i.e., vertex correction also vanishes. One can easily make sure that this tendency persists to all orders of the perturbation theory.

Alternatively speaking, at $v_s \rightarrow 0$, the vertex correction and the regular piece of the fermionic self-energy both vanish leaving the anomalous piece in the fermionic self-energy as the only term one has to evaluate.

4. spin polarization operator

To verify that the spin-fermion interaction reduces v_s and makes spin fluctuations softer, we now compute the bosonic self-energy. It comes in our model from a virtual processes in which a spin fluctuation decays into a particle-hole bubble, and hence coincides, up to an overall factor, with the fully renormalized spin polarization operator $\Pi(\mathbf{q}, \omega)$. We define $\Pi(\mathbf{q}, \omega)$ via $\chi^{-1}(\mathbf{q}, \omega) = \chi_0^{-1}(\mathbf{q}, \omega) - \Pi(\mathbf{q}, \omega)/(\chi_0 \xi^2)$, or

$$\chi(\mathbf{q}, \omega) = \frac{\chi_0 \xi^2}{1 + \xi^2(\mathbf{q} - \mathbf{Q})^2 - \Pi(\mathbf{q}, \omega)}. \quad (18)$$

The contributions to the particle-hole bubble from high-energy fermions are already absorbed into the bare susceptibility, and in our consideration we have to consider only fermions with energies smaller than Λ . Also, as static $\chi_0(\mathbf{q})$ is assumed to be peaked at $\mathbf{q} = \mathbf{Q}$, it is sufficient to compute the polarization operator only at $\mathbf{q} = \mathbf{Q}$.

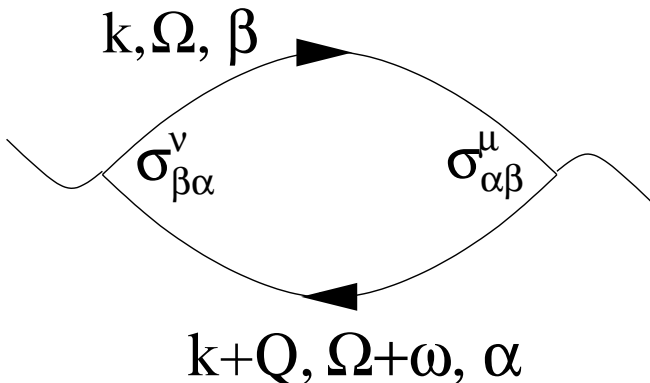


FIG. 8. The lowest-order diagram for the spin polarization operator.

Let's again start with the lowest order perturbation theory in the spin-fermion coupling. The lowest-order diagram for $\Pi(\mathbf{Q}, \omega)$ is presented in Fig. 8. In analytical form, we have in real frequencies

$$\Pi(\mathbf{Q}, \omega) = 2 \bar{g} \xi^2 \int \frac{d^2 \mathbf{k} d\Omega}{(2\pi)^3} G_0(\mathbf{k} + \mathbf{Q}, \Omega + \omega) G_0(\mathbf{k}, \Omega) \quad (19)$$

(a factor of 2 comes from a summation over spin components). Expanding both fermionic energies at \mathbf{k} and $\mathbf{k} + \mathbf{Q}$ to linear order in the deviations from hot spots,

integrating over momentum and frequency in (19) and multiplying the result by the number of hot spots $N = 8$, we obtain,

$$\Pi(\mathbf{Q}, \omega) = i \omega / \omega_{sf} \quad (20)$$

where

$$\omega_{sf} = \frac{4\pi}{N} \frac{v_x v_y \xi^{-2}}{\bar{g}} \equiv \frac{3}{N} \frac{v_x v_y}{v_F^2} \frac{v_F \xi^{-1}}{\lambda} \quad (21)$$

Instead of explicitly inserting $N = 8$, we will keep N as a variable - later we perform a formal expansion in $1/N$.

The independence of $\text{Im}\Pi(\mathbf{Q}, \omega)$ of the fermionic cutoff Λ is indeed the consequence of the energy conservation requirement which confines fermions to hot spots. Observe, however, that Eq. (20) is the full expression for $\Pi(\mathbf{Q}, \omega)$, not only its imaginary part. In other words, as long as one restricts with the linearized fermionic dispersion near the Fermi surface, $\text{Re}\Pi(\mathbf{Q}, \omega) = 0$. This last result implies that there is no universal correction to ξ from low energy fermions. The corrections to ξ only appear when we expand quasiparticle energies further in deviations from the Fermi surface. It is easy to check that these corrections scale as Λ/W and are therefore just minor leftovers from the contributions from high fermionic energies.

We see that the lowest-order spin polarization operator has a simple relaxational, linear in ω form. This implies that at low frequencies, the renormalized spin susceptibility more strongly depends on frequency than the bare susceptibility. This confirms our early conjecture that the effect of the bosonic self-energy can be crudely modeled by increasing v_s .

We next estimate what bosonic momenta and frequencies mostly contribute to the fermionic self-energy in (6) and to the vertex correction in (14). Simple power counting shows that the integrals in (6) and (14) are dominated by $|\mathbf{q} - \mathbf{Q}| \sim \xi^{-1}$ and $\omega \sim v_F \xi^{-1}$. Comparing the full and bare susceptibilities at these momenta and frequencies, we immediately see that for $\lambda \geq 1$ $\Pi(\mathbf{Q}, \omega) \sim \lambda$ dominates over bare $\chi_0(\mathbf{q}, \omega)$. This implies that for large λ , spin fluctuations which mostly contribute to the fermionic self-energy, are completely overdamped due to a strong decay into a particle-hole pair. Clearly, in this situation, one cannot neglect the transmutation of the spin dynamics in evaluating the fermionic self-energy and the correction to the spin-fermion vertex.

B. renormalized perturbation theory

Our next strategy is the following. We assume for a moment that Eq. (20) for $\Pi(\mathbf{Q}, \omega)$ with ω_{sf} given by (21) is valid for all couplings, and re-evaluate the lowest-order fermionic self-energy and vertex correction using the renormalized form of the spin susceptibility. We

then check the self-consistency of this procedure by re-evaluating $\Pi(\mathbf{Q}, \omega)$ with renormalized fermionic propagators and vertices.

1. fermionic self-energy

Consider first the fermionic self-energy. Substituting the renormalized $\chi(\mathbf{q}, \omega)$ instead of $\chi_0(\mathbf{q}, \omega)$ into Eq.6, subtracting, as before, the self-energy at $\omega = \epsilon_{k+Q} = 0$, and expanding to linear order in $\mathbf{k} - \mathbf{k}_{hs}$, we obtain

$$\Sigma(\mathbf{k}, \Omega) = (i\Omega - \epsilon_{k+Q}) I(\mathbf{k}, \omega) \quad (22)$$

but now

$$I(\mathbf{k}, \Omega) = 3\bar{g}\xi^2 \int \frac{d^2\tilde{q}d\omega}{(2\pi)^3} \frac{1}{1 + (\tilde{\mathbf{q}}\xi)^2 + |\omega|/\omega_{sf} + \frac{\omega^2}{v_s^2\xi^2}} \times \frac{1}{i\Omega - \epsilon_{k+Q} + i\omega - v_F\tilde{q}_x} \frac{1}{i\omega - v_F\tilde{q}_x} \quad (23)$$

Consider, as before, the limit $\Omega, \epsilon_{k+Q} \rightarrow 0$ and compute first the regular piece $I(\mathbf{k}_{hs}, 0)$. Without ϵ_{k+Q} and Ω , the last two terms in (23) are equal and produce a double pole at $v_F\tilde{q}_x = i\omega$. Closing the integration contour over \tilde{q}_x by a semi-circle in a half-plane with no double pole, we find that we only have to consider the pole in the spin susceptibility. This pole is located at a much larger $\tilde{q}_x \propto \sqrt{\omega}$ than the double pole. In this situation, one can neglect ω in the Green's functions in comparison with $\tilde{q}_x \propto \sqrt{\omega}$. The remaining computation of $I(\mathbf{k}_{hs}, 0)$ is straightforward. The details are presented in Appendix A, and for $\lambda \gg 1$, the result is, with logarithmic accuracy

$$I_{reg}(\mathbf{k}_{hs}, 0) = -\frac{12v_x v_y}{\pi N v_F^2} \log \lambda \quad (24)$$

We see that the regular piece in $I(\mathbf{k}, \Omega)$ only logarithmically depends on λ , in distinction to a direct perturbation theory where it was of order λ . This result is indeed consistent with our earlier observation that $I_{reg}(\mathbf{k}_{hs}, 0)$ in (10) vanishes in the limit $v_s \rightarrow 0$. The still presence of the $\log \lambda$ factor in (24) is a consequence of $\Pi(\mathbf{Q}, \omega) \propto \omega$, and could not, indeed, be anticipated in a perturbation theory with a bare spin susceptibility.

For completeness, we also present the expression for $I_{reg}(\mathbf{k}_{hs}, 0)$ at arbitrary λ . The calculations are presented in Appendix A. The result is particularly simple for $v_s \rightarrow \infty$, i.e., for purely static bare susceptibility. We obtained

$$I_{reg}(\mathbf{k}_{hs}, 0) = -\lambda \frac{1 + \frac{a}{\pi} \log \frac{a}{2}}{1 + \frac{a^2}{4}} \quad (25)$$

where $a = (v_F\xi^{-1}/\omega_{sf}) = (N\lambda/3) (v_F^2/v_x v_y)$. For $a \ll 1$, we recover the result of a direct perturbation theory, $I_{reg}(\mathbf{k}_{hs}, 0) = -\lambda$. For $a \gg 1$, Eq. (25) reduces to (24).

We next compute an anomalous term in $I(\mathbf{k}, \Omega)$ which, we remind, is a contribution from a regularized double pole in $I(\mathbf{k}, \Omega)$. Integrating, as before, in Eq. (23) over a tiny region $-\Omega < \omega < 0$ where the poles in the two fermionic propagators are located in different half-planes, we obtain

$$I_{an}(\mathbf{k}, \Omega) = \lambda \frac{i\Omega}{i\Omega - \epsilon_{k+Q}} \quad (26)$$

The fact that $I_{an}(\mathbf{k}, \Omega)$ remains the same as in a direct perturbation theory can be easily explained. Indeed, the integration over ω in $I_{an}(\mathbf{k}, \Omega)$ is confined to vanishingly small frequencies for which the dynamical term in the spin susceptibility is small no matter whether the dynamics is ballistic or relaxational.

Substituting the full form for $I(k, \Omega)$ into (22) we obtain $\Sigma(\mathbf{k}, \Omega) = \Sigma_{reg}(\mathbf{k}, \Omega) + \Sigma_{an}(\mathbf{k}, \Omega)$, where for $\lambda \gg 1$

$$\Sigma_{an}(\mathbf{k}, \Omega) = i\lambda\Omega$$

$$\Sigma_{reg}(\mathbf{k}, \Omega) = (i\Omega - \epsilon_{k+Q}) \frac{12v_x v_y}{\pi N v_F^2} \log \lambda \quad (27)$$

We see therefore that the fermionic self-energy consists of two parts – a regular part which accounts for the renormalization of the quasiparticle residue, and a singular part which depends only on ω . The regular part is strongly reduced compared to the direct perturbation theory, and scales as $\log \lambda$ rather than λ . This reduction is due to the fact that at frequencies which determine the fermionic self-energy, the renormalized spin excitations obey relaxational dynamics. On the other hand, the singular part of the self-energy comes from very low internal frequencies, comparable to the external one, and is totally insensitive to the change of the spin dynamics. At strong coupling, the singular, nonperturbative piece in Σ is much larger than the regular piece and obviously should play a central role in all our analysis.

In more general terms, the appearance of $I_{an}(\mathbf{k}, \Omega)$ is the reflection of the singularity in the particle-hole bubble at small momentum and frequency transfer. This follows from the observation that for small $v_F\tilde{q}_x$ and ω' the spin susceptibility, integrated over \tilde{q}_y , can be approximated by a constant, and the anomalous contribution to $I(\mathbf{k}, \omega)$ can be reexpressed as

$$I_{an}(\mathbf{k}, \Omega) = \lambda \tilde{\Pi}(\mathbf{k}, \Omega), \quad (28)$$

where

$$\tilde{\Pi}(\mathbf{k}, \Omega) = -i \int \frac{d\tilde{q}_x d\omega}{(2\pi)^2} G_0(\tilde{q}_x, \omega) G_0(\mathbf{k} + \tilde{q}_x, \omega + \Omega) \quad (29)$$

is the particle-hole polarization bubble with a small momentum/frequency transfer (it differs by an overall constant from $\Pi(\mathbf{k}, \omega)$ introduced in (18)). At vanishing \mathbf{k}

and Ω , this polarization bubble is formally ultraviolet divergent, and its value hence depends on how the regularization is performed [30], i.e., on the order of the integration over frequency and over momentum. Doing frequency integration first, one obtains that $\tilde{\Pi}(\mathbf{k}, \Omega)$ vanishes, while doing momentum integration first, one obtains that

$$\tilde{\Pi}(\mathbf{k}, \Omega) = \frac{\Omega}{\Omega - \mathbf{v}_F \mathbf{k}}. \quad (30)$$

In our case, the regularization of the self-energy is imposed by the fact that $I(\mathbf{k}, \omega)$ is actually a convolution of the polarization bubble and the spin susceptibility. In the above calculations we neglected the dependence of $\chi(\tilde{\mathbf{q}}, \omega)$ on \tilde{q}_x and ω . In reality, however, $\chi(\tilde{\mathbf{q}}, \omega)$ indeed vanishes when either \tilde{q}_x or ω diverge. The general rule of the ultraviolet regularization procedure is that it has to be performed such that to avoid generating extra poles at energies smaller than the energies of the poles in the particle-hole bubble, Eq. (29). The pole in (29) is located at $\omega \propto |\tilde{\mathbf{q}}|$. The pole in the spin susceptibility $\chi(\mathbf{q}, \omega)$ is located at $\omega \propto \tilde{\mathbf{q}}^2$, i.e., at a much *smaller* frequency, and at a much *larger* \tilde{q}_x than those for the pole in (29). Clearly, then, the correct way to regularized (29) is to first integrate over momentum in (29), and only then integrate over frequency. This sequence of integrations yields the anomalous piece in $\tilde{\Pi}(\mathbf{k}, \Omega)$, Eq. (30), which in turn gives rise to the anomalous piece in the fermionic self-energy (28).

Note by passing that in a direct perturbation theory (which operates with the bare susceptibility), a typical frequency scales with a typical momentum. In this situation, the result of regularization strongly depends on the ratio of v_F and v_s (see Eq. (13)). In particular, the absence of the frequency dependence of the self-energy at $v_s = \infty$ is caused the fact that in this situation $\chi_0(\mathbf{q}, \omega)$ is purely static, and the regularization obviously has to be performed by doing frequency integration first.

2. vertex correction

We now re-evaluate the vertex correction with the relaxational form of the spin susceptibility. The analytical expression for $\Delta g/g$ is the same as in (14), but with $\chi(\mathbf{q}, \omega)$ instead of $\chi_0(\mathbf{q})$. Linearizing, as before, the fermionic dispersion near the Fermi surface, and performing momentum and frequency integration as described in Appendix A, we obtain for $\lambda \gg 1$, with logarithmical accuracy,

$$\frac{\Delta g}{g} = \frac{Q(v)}{N} \log \lambda \quad (31)$$

where

$$Q(v) = \frac{4}{\pi} \tan^{-1} \frac{v_x}{v_y} \quad (32)$$

is a smooth function of the ratio of velocities interpolating between $Q = 1$ for $v_x = v_y$, and $Q = 2$ for $v_y \rightarrow 0$. The last limit corresponds to almost nested Fermi surface at hot spots. A similar logarithmical form of the vertex correction has been obtained by Altshuler, Ioffe andMillis [49].

We see that the change of the spin dynamics has a strong effect on the strength of the vertex correction: in a direct perturbation theory, it was of order of λ , now it scales only as $\log \lambda$. This result is fully consistent with our earlier observation from a direct perturbation theory (Eq. (17)) that $\Delta g/g$ vanishes when $v_s \rightarrow 0$. As with the k -dependent piece in the self-energy, the subleading logarithmical dependence of $\Delta g/g$ could not, indeed, be anticipated in a direct perturbation theory with the bare spin susceptibility.

3. higher-order diagrams

We next need to understand what happens when we go to higher-orders in the self-consistent perturbation theory for fermionic self-energy and the spin-fermion vertex. The issue is indeed whether higher order diagrams scale as higher powers of λ or $\log \lambda$. We argue that higher-order terms contribute higher powers of $\log \lambda$ but not higher powers of λ . Our reasoning is based on the fact that in the second-order theory, the vertex correction and the regular part of the fermionic self-energy are $O(\log \lambda)$, and $O(\lambda)$ term in the second-order fermionic self-energy emerges only as a result of a proper regularization of the double pole in the integrand for $\partial \Sigma / \partial \Omega$. Higher-order self-energy and vertex correction diagrams contain more fermionic propagators with different momenta, and one can easily make sure that there is no phase space for a double pole. Accordingly, higher-order vertex correction diagrams just contribute higher powers of $\log \lambda$, while higher-order diagrams for the fermionic self-energy either simply contribute higher powers of $\log \lambda$, or account for $\log \lambda$ corrections to $\Sigma_{an}(\mathbf{k}, \Omega)$. We verified this argument by explicitly computing next order self-energy and vertex corrections.

4. spin polarization operator

A closely related issue is how the fermionic self-energy and vertex renormalization affects the form of the spin polarization operator. We recall that above we evaluated the fermionic self-energy and $\Delta g/g$ assuming that that the spin polarization operator has the same form as in the direct perturbation theory. We now need to verify to which extent this assumption is correct. We show that the renormalization of $\Pi(\mathbf{Q}, \omega)$ from its free-fermion form, Eq. (20) is only due to vertex corrections and to the regular part of $\Sigma(\mathbf{k}, \Omega)$, while a much larger

$\Sigma_{an} = \lambda\Omega$ does not affect the spin polarization operator. To demonstrate this we re-evaluate $\Pi(\mathbf{Q}, \omega)$, Eq. (19), with $G(\mathbf{k}, \Omega) = \Omega + \Sigma_{an}(\Omega) - \epsilon_k$. The computation is rather straightforward as the inclusion of Σ_{an} into fermionic propagator modifies the quasiparticle residue Z and the quasiparticle mass (defined as $v_F = p_F/m$) as $Z = 1/(1 + \lambda)$, $m^* = m(1 + \lambda)$. Substituting the renormalized form of $G(k, \Omega)$ into (19) and performing elementary manipulations, we find that Z and m^*/m appear in $\Pi(\mathbf{Q}, \omega)$ in the combination $Z^2(m^*/m)^2$ which is *independent* of λ . In other words, as long as we restrict with only $\Sigma_{an}(\mathbf{k}, \Omega)$, $\Pi(\mathbf{Q}, \omega)$ remains the same as for free fermions.

The inclusion of $\Sigma_{ref}(\mathbf{k}, \Omega)$ into the fermionic propagator and the corrections to the spin-fermion vertex does affect the form of $\Pi(\mathbf{Q}, \omega)$, but the corrections obviously hold in powers of $\log \lambda$.

C. summary of Sec III

We now summarize what we obtained in this section.

- i We found that the direct perturbation theory for fermionic self-energy and spin-fermion vertex holds in powers of $\lambda \propto \bar{g}/(v_F \xi^{-1})$ and does not converge at strong coupling.
- ii We found that for typical bosonic energies which mostly contribute to fermionic $\Sigma(\mathbf{k}, \Omega)$ and to vertex renormalization, the bosonic self-energy also becomes relevant for $\lambda \geq 1$ and accounts for the change in the bosonic dynamics from a ballistic one to a relaxational one.
- iii We performed the self-consistent perturbative expansion in which we used the relaxational form of the spin susceptibility as an input, and found that it holds in powers of $\log \lambda$, plus there exists the anomalous, nonperturbative piece in the fermionic self-energy which still scales as λ . At strong coupling, this piece much larger than the regular self-energy and obviously should play a central role.
- iv To logarithmical accuracy, the anomalous piece in the fermionic self-energy is given by the second-order diagram, higher-order terms just add extra powers of $\log \lambda$.
- v We found that as long as we restrict with only $O(\lambda)$ piece in the self-energy and neglect vertex corrections and the renormalization of the spin-fermion vertex, the spin-polarization operator remain the same as for free fermions, i.e., the self-consistent perturbation theory is justified.

IV. $N \rightarrow \infty$ LIMIT, $T = 0$

These results of the previous section imply that neglecting logarithms, one can construct a fully self-consistent new “zero-order” theory. In this theory, spin excitations are purely relaxational and vertex corrections are absent. At the same time, the (anomalous) fermionic self-energy is strong and progressively, as λ increases, destroys fermionic coherence.

This new “zero-order” theory indeed makes sense only if one can specify the limit when it becomes “exact” and also construct a controllable perturbative expansion around it. We notice in this regard that all $\log \lambda$ terms contain a factor $1/N$ where, we remind, $N (= 8)$ is the number of hot spots in the Brillouin zone. The presence of $1/N$ is a direct consequence of the fact that the $\log \lambda$ terms appear due to a change from a ballistic to a relaxational spin dynamics. The prefactor for logarithm should then be inversely proportional to the spin damping rate as when this rate is zero, the self-energy and vertex corrections are much larger and scale as $O(\lambda)$. A spin fluctuation with momentum \mathbf{Q} has $N/2$ channels to decay into particle-hole excitation near hot spots, hence the damping rate scales as N , and the prefactor for the logarithm scales as $1/N$. Below we formally treat N as an arbitrary number. Then one can define the $N \rightarrow \infty$ limit, when logarithmical corrections can be totally neglected. In this limit, our new “zero-order” theory becomes exact. At finite but small $1/N$, the perturbation theory around our new vacuum is the expansion in $1/N \log \lambda$.

Instead of introducing an artificially large number of hot spots, one can also extend the spin-fermion model to a large number of electron flavors M ($= 1$ in the physical case) and expand in $1/(8M)$. This later expansion is more appealing from physics perspective as the extension to large N requires a rearrangement of the Fermi surface to a large number of “hot” segments which is difficult to visualize. In both cases, however, the main idea is to enhance the effect of the bosonic damping and therefore reduce the strength of regular self-energy and vertex corrections compared to the anomalous term in the fermionic self-energy. The computations are identical in both cases, and below we will just label the expansion as “large N ” theory. We discuss some formal aspects of the $1/N$ expansion in Appendix XIII.

The limit $N = \infty$ bears some similarity to the Migdal-Eliashberg limit for electron-phonon problem [78–80] although in our case bosonic modes are not independent degrees of freedom. Nevertheless, the smallness in $1/N$ has the same consequence as the smallness of m/M where m is the electronic mass, and M is the ionic mass: one can neglect vertex corrections and also the momentum dependent piece in the fermionic self-energy. Below we will occasionally refer to the $N = \infty$ limit as the Eliashberg-type theory.

We now proceed with the more detailed discussion of the $N = \infty$ limit.

A. derivation of the Eliashberg-type equations

So far our analysis of the fermionic self-energy was restricted to the limit of vanishing fermionic frequency Ω . In this limit, we have at $N \rightarrow \infty$, $\Sigma(\mathbf{k}, \Omega) = \lambda\Omega$. We have also checked that for this $\Sigma(\mathbf{k}, \Omega)$, the spin polarization operator is the same as for free fermions.

We now derive the full form of the fermionic self-energy at $N = \infty$, valid for arbitrary frequencies. The input for the derivation is the knowledge that vertex corrections and the corrections to ϵ_k both scale as $1/N$ and vanish at $N = \infty$. Without them, we have, quite generally,

$$G(\mathbf{k}, \Omega) = \frac{1}{\tilde{\Sigma}(k_{\parallel}\Omega) - \epsilon_k}, \quad (33)$$

where $\tilde{\Sigma}(\Omega) = \Omega + \Sigma(k_{\parallel}\Omega)$, and k_{\parallel} is the momentum component along the Fermi surface. The dependence of the self-energy on k_{\parallel} is a subleading effect which we will be discussing below. This effect is relevant at the lowest frequencies but becomes progressively weaker as Ω increases. We explicitly verified a posteriori that at $N \rightarrow \infty$, typical frequencies are such that the dependence of $G(\mathbf{k}, \Omega)$ of intermediate fermions on k_{\parallel} can be totally neglected. We therefore just ignore it in the derivation below.

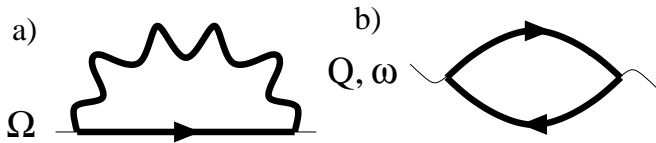


FIG. 9. The diagrams for the fermionic self-energy and spin polarization operator at $N = \infty$.

The full diagram for the self-energy at $N = \infty$ is presented in Fig 9a. Another diagram in Fig 9b is for the full spin polarization operator. We cannot a priori use the free fermion form for $\Pi(\mathbf{Q}, \omega)$ as so far we have only demonstrated that it is preserved if we use the small Ω form of the fermionic self-energy. What we have to do is to derive and solve a set of two coupled equations for $\Sigma(k_{\parallel}\Omega)$ and $\Pi(\mathbf{Q}, \omega)$.

The evaluation of the diagrams is straightforward. Let's first consider fermions near hot spots when $\Sigma(k_{\parallel}\Omega) \approx \Sigma(\Omega)$. Substituting Eqs. (33) and (18) into the diagram for the self-energy and integrating over momenta along the Fermi surface at $\mathbf{k}_{h.s} + \mathbf{Q}$, we obtain

$$\Sigma(\Omega) = \frac{3i\bar{g}}{8\pi^2} \int d\omega d\tilde{q}_x \frac{1}{[\tilde{q}_x^2 + \xi^2(1 - \Pi(\mathbf{Q}, \omega))]^{1/2}} \times \frac{\Sigma(\omega) - \Sigma(\omega + \Omega)}{(v_F\tilde{q}_x - \Sigma(\omega))(v_F\tilde{q}_x - \Sigma(\omega + \Omega))} \quad (34)$$

where as before $\tilde{q} = \mathbf{q} - \mathbf{Q}$.

We already know that the “regular” part of the self-energy vanishes at $N \rightarrow \infty$, so let's focus on the “anomalous” part which should reduce to $\Sigma_{an}(\Omega)$ in the $\Omega \rightarrow 0$ limit. This piece comes from the range of frequencies where the two fermionic poles are in different half-planes of \tilde{q}_x . Since $\text{sign}\Sigma(\omega) = \text{sign}\omega$, this ω range is sandwiched between $-\Omega < \omega < 0$ (for definiteness we set $\Omega > 0$). The next step is to integrate over \tilde{q}_x . At small Ω , we neglected \tilde{q}_x as its inclusion would yield higher powers of Ω . For arbitrary Ω , we cannot use this argument. Still, it turns out that even for high frequencies, keeping \tilde{q}_x in the spin susceptibility give rise to corrections which are at least small by $1/N^2$. We explicitly show this below in a separate subsection. At this moment, we just neglect \tilde{q}_x in the spin propagator and explicitly integrate over \tilde{q}_x in (34). Evaluating the integral, we find that the fermionic self-energy is *canceled out*, and $\Sigma(\Omega)$ takes the form

$$\Sigma(\Omega) = 2\lambda \int_0^\Omega \frac{d\omega}{\sqrt{1 - \Pi(\mathbf{Q}, \omega)}} \quad (35)$$

This cancellation of the self-energy for intermediate fermions implies that self-consistent, FLEX-type calculations in the normal state are not necessary as the dominant piece in $\Sigma(\Omega)$ is captured already by using free-fermion form of the propagator of intermediate fermions.

We next evaluate the spin polarization operator for arbitrary $\Sigma(\Omega)$. Substituting the spin propagator (33) into (19), replacing, as before the momentum integration by the integration over $d\epsilon_k d\epsilon_{k+Q}$, and integrating over energies, we obtain

$$\Pi(\mathbf{Q}, \omega') = \frac{i}{\omega_{sf}} \int_{-\infty}^{\infty} d\omega \left(1 - \frac{\Sigma(\omega)\Sigma(\omega + \omega')}{\sqrt{\Sigma^2(\omega)}\sqrt{\Sigma^2(\omega + \omega')}} \right). \quad (36)$$

Eqs. (35) and (36) form the set of two coupled integral equations for the fermionic self-energy and the spin polarization operator.

B. solution of the Eliashberg-type equations

A more careful look at Eqs. (35) and (36) shows that the solution of the set is straightforward. Indeed, we clearly see that the magnitude and the functional dependence of $\Sigma(\omega)$ is totally irrelevant for $\Pi(\mathbf{Q}, \omega)$, all that matters is the fact that $\text{sign}\Sigma(\omega) = \text{sign}\omega$. The frequency integration in (36) is then straightforward, and performing it we find that

$$\Pi(\mathbf{Q}, \omega) = i \frac{\omega}{\omega_{sf}} \quad (37)$$

i.e., for arbitrary $\Sigma(\Omega)$ it preserves exactly the same form as for free fermions. Substituting this result into (35) we immediately find that

$$\Sigma(\Omega) = \frac{2\lambda\Omega}{1 + \sqrt{1 - i\frac{|\Omega|}{\omega_{sf}}}}. \quad (38)$$

This expression can also be re-written in the scaling form

$$\Sigma(\Omega) = \lambda\omega_{sf}g\left(\frac{\omega}{\omega_{sf}}\right), \quad g(x) = \frac{2x}{1 + \sqrt{1 - i|x|}} \quad (39)$$

At small Ω we indeed recover the previous result $\Sigma(\Omega) = \lambda\Omega$.

The general explanation why the k -independent fermionic self-energy $\Sigma(\Omega)$ does not affect the polarization bubble at a finite momentum was given by Kadanoff [83]. He pointed out that the expansion of the fermionic energy to first order in momentum deviation from k_F is equivalent to imposing an approximate Migdal sum rule on the spectral function $A(\mathbf{k}, \omega) = (1/\pi) \text{Im}\tilde{G}_0(\mathbf{k}, \omega)$

$$\int d\epsilon_{\mathbf{k}} A(\mathbf{k}, \omega) = 1 \quad (40)$$

Expressing $\tilde{G}_0(\mathbf{k}, \omega)$ in terms of $A(\mathbf{k}, \omega)$ via Kramers-Kronig relation and making use of (40), one finds

$$\Pi(\mathbf{Q}, \omega') = -\frac{i}{\omega_{sf}} \int_{-\infty}^{\infty} d\omega \frac{df(\omega)}{d\omega} \omega' + \mathcal{O}(\omega'^2) \quad (41)$$

where $f(\omega)$ is the Fermi function. Eq. (20) then follows from the fact that $f(\omega)$ is 1 at $\omega = -\infty$ and 0 at $\omega = +\infty$.

Eqs. (37) and (38) are the central results of $N = \infty$ analysis. We see that the scale for nonlinear effects in frequency in $\Sigma(\Omega)$ is set by the typical spin relaxation frequency $\omega_{sf} = 4\pi v_x v_y \xi^{-2}/(N\bar{g})$ (the $1/N$ factor in ω_{sf} can be eliminated by rescaling $v \rightarrow vN$ and $\bar{g} \rightarrow \bar{g}N$ as we discuss in Appendix XIII). This ω_{sf} is obviously a measure of the deviation from the QCP. At scales smaller than ω_{sf} , spin susceptibility is nearly static, and $\Sigma(\Omega)$ is expandable in Ω . In this regime, we should generally expect a Fermi liquid behavior with $\Sigma''(\Omega) \propto \omega^2$. However, above ω_{sf} , the system should cross over into a quantum-critical regime, where the system behavior is determined by the fixed point at $\xi = \infty$. In this regime, spin excitations become massless diffusons, and fermionic self-energy should modify such that to eliminate the dependence on ξ .

We indeed find this behavior in our $\Sigma(\Omega)$. We see from (38) that for $|\Omega| < \omega_{sf}$, the self-energy behaves as

$$\Sigma(\Omega) = \lambda\Omega \left(1 + i\frac{|\Omega|}{4\omega_{sf}}\right), \quad (42)$$

For $|\Omega| > \omega_{sf}$, however, it crosses over to a different behavior

$$\Sigma(\Omega) = (i|\Omega|\bar{\omega})^{1/2} \text{sign}\Omega, \quad (43)$$

We see therefore that above ω_{sf} , both $\Sigma'(\Omega)$ and $\Sigma''(\Omega)$ scale as $\sqrt{|\Omega|}$. The normalization energy

$$\bar{\omega} = 4\lambda^2\omega_{sf} = \frac{9\bar{g}}{2\pi N} \frac{2v_x v_y}{v_F^2} \quad (44)$$

does not depend on ξ as it should be in the quantum-critical regime. This $\bar{\omega}$ sets the upper cutoff for the quantum-critical behavior (its dependence on N can again be eliminated by rescaling $g \rightarrow N\bar{g}$).

The $\sqrt{\Omega}$ form of the self-energy at the antiferromagnetic transition was first obtained by Millis [81]. The $\sqrt{\omega}$ form also emerges in the quantum-critical models with disorder [82].

Substituting the quantum-critical form of the self-energy into the fermionic propagator, we obtain that at $\mathbf{k} \approx \mathbf{k}_{hs}$ and $|\Omega| < \bar{\omega}$

$$G(k, \Omega) = \frac{1}{\bar{\omega}} \frac{\sqrt{i|\Omega|\bar{\omega}\text{sign}\Omega + \epsilon_k}}{i|\Omega| - \epsilon_k^2/\bar{\omega}}. \quad (45)$$

We see that in the quantum-critical regime, the system behavior is qualitatively different from that in a Fermi liquid: there is no pole in the fermionic propagator at real frequencies. Instead, $G(k, \Omega)$ has a pole along an imaginary frequency axis, at $|\Omega| = \epsilon_k^{eff} = \epsilon_k^2/\bar{\omega}$. This non-Fermi-liquid pole gives rise to a broad maximum at $\Omega = \epsilon_k^{eff}$. We also verified that in the crossover region $\Omega \sim \omega_{sf}$, the pole in the fermionic propagator gradually moves, with increasing Ω , from real to imaginary frequency axis

At frequencies larger than $\bar{\omega}$, the bare ω term in the fermionic propagator wins over the self-energy, and the spectral function recovers the peak at $\Omega = \epsilon_k$. Still, this behavior is not a Fermi-liquid one as the width of the peak scales as $\sqrt{\Omega}$.

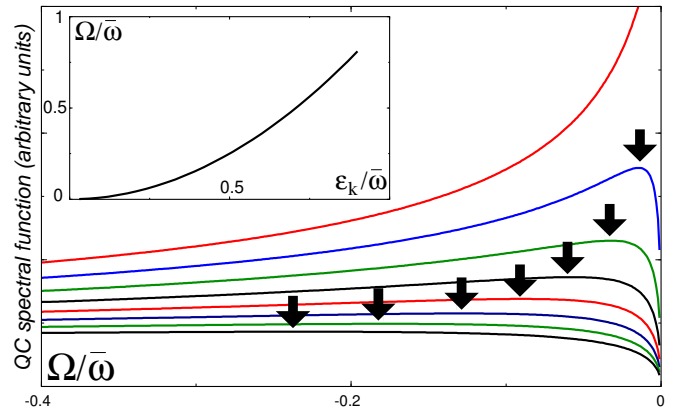


FIG. 10. The behavior of $\text{Im}G(\mathbf{k}, \Omega)$ at $\omega_{sf} = 0$ (45). The inset shows the “quasiparticle” dispersion inferred from the position of the maximum in the spectral function (indicated by arrows).

The behavior of $\text{Im}G(\mathbf{k}, \Omega)$ at $\omega_{sf} = 0$ is shown in Fig. 10 (see Eq. (45)). The inset shows the “quasiparticle” dispersion inferred from the position of the maximum in

the spectral function. We see that the destruction of the Fermi liquid behavior accounts for the effective flattening of the “quasiparticle” dispersion at frequencies below $\bar{\omega}$.

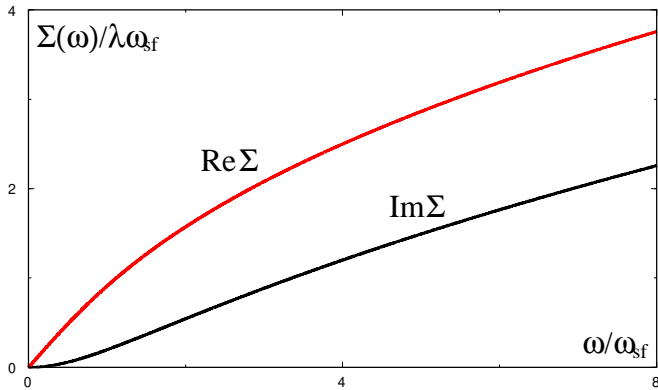


FIG. 11. Real and imaginary parts of the fermionic self-energy, Eq.(39), vs frequency.

In Fig. 11 we present both real and imaginary parts of the fermionic self-energy vs frequency at a finite ω_{sf} . We clearly see a Fermi-liquid behavior at the smallest frequencies, and the $\sqrt{\omega}$ behavior well above ω_{sf} . By numerical reasons, the crossover region in between these two limiting regimes is rather wide - it stretches between $0.5\omega_{sf}$ and $6 - 8\omega_{sf}$. In the crossover regime, $\Sigma''(\mathbf{k}, \omega)$ is, to a surprisingly good accuracy, a linear function of frequency. This linearity, however, does not follow from any theory considerations, and is just a hidden numerical property of the self-energy, Eq. (38). This linearity, however, is relevant for the explanation of the photoemission and optics data in cuprates.

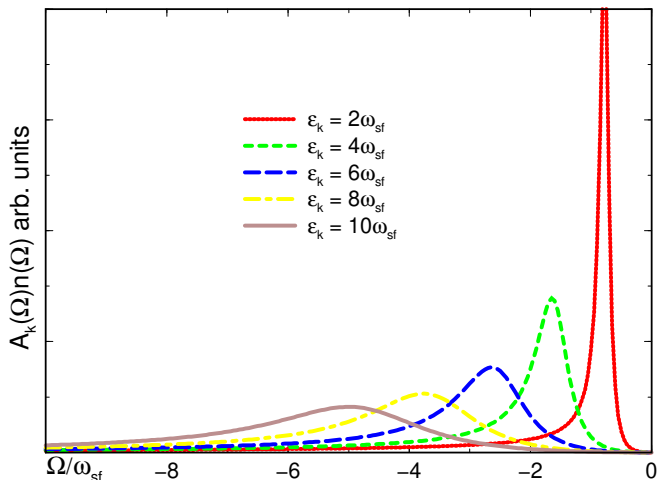


FIG. 12. The behavior of $ImG(\mathbf{k}, \Omega)$ at a finite ω_{sf} . For definiteness we used $\lambda = 1.7$ in which case $\bar{\omega} = 11.56\omega_{sf}$. The high-frequency behavior of $ImG(\mathbf{k}, \Omega)$ is the same as in Fig.(10).

In Fig 12 we present the forms of the spectral function $ImG(\mathbf{k}, \Omega)$ for different values of ϵ_k and finite ω_{sf} . Comparing this result with Fig 10 we see that the quasiparticle peak sharpens up at frequencies comparable to ω_{sf} , as it indeed should as the system crosses over to the Fermi-liquid behavior. Notice, however, that even at $\omega \sim \omega_{sf}$, the width of the peak is comparable to its amplitude.

We next discuss to which extent the full anomalous self-energy depends on the momentum along the Fermi surface. Repeating the same calculations which lead to (38) but for a finite $\tilde{\mathbf{k}} = \mathbf{k} - \mathbf{k}_{hs}$, we find that $\Sigma(\mathbf{k}, \Omega) \equiv \Sigma(k_{\parallel}, \Omega)$ can be rewritten as

$$\Sigma(k, \Omega) = \lambda(k) \frac{2\Omega}{1 + \sqrt{1 - i \frac{|\Omega|}{\omega_{sf}(k)}}} \quad (46)$$

i.e., it still has the same form as at a hot spot, but with k dependent

$$\lambda(k) = \lambda / (1 + (\tilde{k}\xi)^2)^{1/2}, \quad \omega_{sf}(k) = \omega_{sf} (1 + (\tilde{k}\xi)^2) \quad (47)$$

We see that away from the hot spots, the effective coupling gets smaller, and the crossover frequency $\omega_{sf}(k)$ increases. Still, however, at frequencies which exceed $\omega_{sf}(k)$, the system displays the same non-Fermi liquid behavior as at hot spots, i.e., $\Sigma''(k, \Omega)$ first scales linearly with Ω , and crosses over to a $\sqrt{\Omega}$ form at larger frequencies.

In the Fermi liquid regime, the slope of Σ'' depends on k as $(1 + (\tilde{k}\xi)^2)^{-3/2}$. In the non-Fermi liquid regime, this dependence gets weaker and completely vanishes in the $\sqrt{\Omega}$ regime where the overall factor in $\Sigma(k, \Omega)$ becomes $\lambda(k)\sqrt{\omega_{sf}(k)} = \lambda\sqrt{\omega_{sf}}$. This can be seen already from (38). This implies the momentum range where $\Sigma(k, \Omega)$ weakly depends momentum (i.e., the “size” of a hot spot) depends on frequency. For $\Omega < \omega_{sf}$, this range is obviously constrained by $|\tilde{k}\xi| \leq 1$, but for larger frequencies it increases and eventually extends to $|\tilde{k}\xi| < (|\Omega|/\omega_{sf})^{1/2}$. In particular, deep in the quantum-critical regime, i.e., for frequencies comparable $\bar{\omega} = 4\lambda^2\omega_{sf}$, the weak momentum dependence of the fermionic self-energy extends to $|\mathbf{k} - \mathbf{k}_{hs}| \leq \bar{g}/v_F$, i.e, the “size” of a hot spot remains finite even at $\xi \rightarrow \infty$. This result implies that in the quantum-critical regime the momentum variation of the self-energy does not play any significant role and can be safely neglected.

C. the accuracy of the Eliashberg-type theory

We now have to go back and verify the accuracy of the Eliashberg-type Eqs. (35) and (36). We begin with the fermionic self-energy. Recall that in deriving (35) we neglected the dependence on \tilde{q}_x in the spin propagator. Near the singular pole, $\tilde{q}_x^2 \sim (\Sigma(\omega)/v_F)^2$. To

estimate the relative strength of this term, let's evaluate it with $\Sigma(\omega)$ from (38) obtained by neglecting this contribution. At $\omega < \omega_{sf}$, $\Sigma(\omega) \approx \lambda\omega$, hence typical $\tilde{q}_x^2 \sim \lambda^2\omega^2/v_F^2 = (\omega\gamma)(\omega/(4N^2\omega_{sf}))$ are negligible compared to $\omega\gamma$. Clearly, \tilde{q}_x^2 term can be omitted. In the quantum-critical regime, $\omega \gg \omega_{sf}$, we have $\tilde{q}_x^2 \sim \omega\bar{\omega}/v_F^2 = (\omega\gamma)(6v_xv_y/Nv_F^2)^2$. We see that the term which we omitted in (35) and, hence, (38) has the same frequency dependence as the damping term in the spin susceptibility, but has an extra factor $(1/N)^2$ and therefore can be neglected in the $N \rightarrow \infty$ limit.

To understand how $1/N$ expansion works in terms of numbers, we evaluated the overall factor for $\Sigma(\omega)$ in the quantum-critical regime by solving Eq. (34) self-consistently for a physical $N = 8$. Substituting $\Sigma(\Omega) = A(i|\Omega|\bar{\omega})^{1/2}\text{sign}\omega$ as an input into (34), we indeed obtained the same form in the output. Solving for A , we obtained $A = 0.94$ which is very close to $A = 1$ – the result without $1/N$ corrections.

We also compared the $N = \infty$ result with the full second-order expression for $\Sigma(\Omega)$ at arbitrary Ω . The calculations are presented in the Appendix A. The result is particularly simple for $v_s = \infty$ in which case we have from (168)

$$\Sigma(\Omega) = 2\lambda\omega_{sf}a \ln \frac{i\sqrt{K_\Omega - 1} + \sqrt{K_\Omega + 1}}{i\sqrt{K_\Omega - 1} + A_\Omega + \sqrt{K_\Omega + 1} - A_\Omega} \quad (48)$$

where

$$K_\Omega^2 = 1 + \frac{4}{a^2} \left(1 - i\frac{\Omega}{\omega_{sf}}\right); \quad A_\Omega = \frac{2i}{a^2} \frac{\Omega}{\omega_{sf}} \quad (49)$$

and, we remind, $a = (v_F\xi^{-1})/\omega_{sf} = (\lambda N/3)(v_F^2/v_xv_y)$. Our $N = \infty$ result, Eq. (38), is the limiting form of (48) at $a \rightarrow \infty$. The expansion to a linear order in $1/a$ yields a correction to (38) which at low frequencies is logarithmical in λ and coincides with Eqs. (22) and (24).

In Fig. 13 we plot the full second-order result for the self-energy at $N = 8$ and our $N = \infty$ result which is its anomalous part. For definiteness, we set $v_x = v_y$ and $\lambda = 2$ in which case $a = 32/3$. We see that the two curves are very close to each other up at least to $\Omega = \bar{\omega}$, which, we remind, is the upper cutoff frequency for the quantum-critical behavior. We consider this agreement as another evidence that the restriction with only the anomalous contribution to the self-energy works well for the physical $N = 8$.

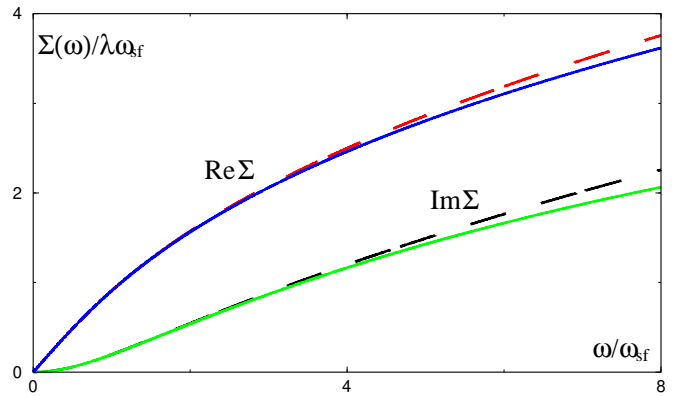


FIG. 13. Real and imaginary parts of the full fermionic self-energy at finite N as a function of frequency. Dashed lines represent the self-energy without the regular part (see Fig. 11).

A minor comment is in order here. In the quantum-critical regime, the second-order expression for $\Sigma(\omega)$ contains a leading $\Omega^{1/2}$ term and a subleading $\Omega \log \Omega$ term. On the other hand, performing computations with the full fermionic propagators, we found a subleading logarithmical term in $\Sigma(\mathbf{k}_{hs}, \Omega)$ but no $\Omega \log \Omega$ term. A careful look into this discrepancy shows that the reason why the subleading (regular) piece in the second-order self-energy has $\Omega \log \Omega$ form is because for free fermions, $\partial G_0^{-1}(\mathbf{k}, \omega)/\partial\omega = -\partial G_0^{-1}(\mathbf{k}, \omega)/\partial\epsilon_k = 1$. In the self-consistent calculations, we still have $\partial G^{-1}(\mathbf{k}, \omega)/\partial\epsilon_k = -1$, but now $\partial G^{-1}(\mathbf{k}, \omega)/\partial\omega = \partial\Sigma(\omega)/\partial\omega$. In the quantum-critical regime, $\partial\Sigma(\omega)/\partial\omega \propto \omega^{-1/2}$. The appearance of the extra $\omega^{1/2}$ in the denominator, transforms $\Omega \log \Omega$ term into $\sqrt{\Omega}/N^2$, exactly as we found.

Finally, we also verify that the renormalization of ϵ_k and of the spin-fermion vertex scale as $\log \lambda/N$ even when we use quantum-critical forms of the self-energy for intermediate fermions. Lets, first analyze $\Sigma(\mathbf{k}, 0)$. Since the fermionic self-energy in (33) does not affect ϵ_k , we can straightforwardly expand $\Sigma(\mathbf{k}, 0)$ in ϵ_{k+Q} . Performing then a simple power counting, we find that in the quantum-critical regime, the inclusion of the self-energy of intermediate fermions only gives rise to $O(1/N^2)$ corrections to the second-order result.

The same result holds for vertex renormalization. Substituting (33) into (14) we obtain

$$\frac{\Delta g}{g} = \frac{i\bar{g}}{(2\pi)^3} \int d^2\tilde{q}d\omega \frac{1}{\xi^{-2} - i|\omega|\gamma + \tilde{\mathbf{q}}^2} \times \frac{1}{\Sigma(\omega) - (v_x\tilde{q}_x + v_y\tilde{q}_y)} \frac{1}{\Sigma(\omega) - (-v_x\tilde{q}_x + v_y\tilde{q}_y)} \quad (50)$$

We immediately see that if we neglect the momentum dependence of the spin susceptibility, then the fermionic self-energy is totally eliminated after the integration over $d^2\tilde{q}$, and the vertex correction remains exactly the same as if we use free fermions (see Eq. (31)). If we keep the

momentum dependence in $\chi(\mathbf{q}, \omega)$, the functional form of $\Delta g/g$ does not change, but the coefficient changes by $1 + O(1/N^2)$.

D. vertices at small momentum transfer

Before we proceed with the $1/N$ expansion, let's consider in more length the issue of vertex renormalization for different bosonic momenta q . Earlier we found that the particle-hole vertex with momentum transfer \mathbf{Q} is only weakly (as $\log \lambda/N$) renormalized by spin-fermion interaction. Mathematically, the smallness of the vertex correction is due to the fact that the two internal fermions in the vertex correction diagram had different directions of Fermi velocities, and hence one can independently integrate over ϵ_k and ϵ_{k+Q} . The vertex correction then can roughly be written as

$$\frac{\delta g}{g} \sim \frac{g^2}{v_F^2} \int d\omega N^2(\omega) \chi(\mathbf{Q}, \omega) \quad (51)$$

where $N(\omega) = \int d\epsilon_k G(\mathbf{k}, \omega) = -i\pi \text{sign}(\omega)$. The frequency dependence then comes only from $\chi(\mathbf{Q}, \omega) \propto v_F^2/(Ng^2\omega)$, and frequency integration yields $\delta g/g \sim (L/N)$ where L is the logarithm of the lower cutoff.

This reasoning is valid for all external q , not necessary $Q = (\pi, \pi)$ (for $\mathbf{q} \neq \mathbf{Q}$, the logarithm is cut also by $|\mathbf{q} - \mathbf{Q}|$). However, it breaks up when one considers a particle-hole vertex with zero momentum transfer. For such vertex, the Ward identity implies [80] that at vanishing bosonic frequency $\delta g/g = 1 + \partial\Sigma(\mathbf{k}, \omega)/\partial\omega$ for a scalar vertex (the one which does not depend on fermionic momentum and conserves spin projection) and $\delta g/g = 1 + \partial\Sigma(\mathbf{k}, \omega)/\partial\epsilon_k$ for a current vertex (which has an extra $\partial\epsilon_k/\partial\mathbf{k}$). In our situation, $\partial\Sigma(\mathbf{k}, \omega)/\partial\epsilon_k$ is small in $1/N$, but $\partial\Sigma(\mathbf{k}, \omega)/\partial\omega$ is not. Moreover, as $\Sigma(\omega) \gg \omega$ at strong coupling and $\omega < \bar{\omega}$, the renormalized scalar vertex well exceeds the bare one.

That the renormalization of the scalar vertex with zero momentum transfer does not contain $1/N$ can indeed be obtained in perturbative calculations. First, we derive the Ward identity for the scalar vertex. It follows from the fact that the integral equation for the full vertex

$$g^{tot}(\mathbf{k}, \omega, \Omega) = g - \frac{3i\bar{g}}{8\pi^2} \int d^2q d\omega' \frac{g^{tot}(\mathbf{k} + \mathbf{q}, \omega', \Omega) \chi(\mathbf{q}, \omega - \omega')}{(\tilde{\Sigma}_{k+q}(\omega' + \Omega) - \epsilon_{k+q})(\tilde{\Sigma}_{k+q}(\omega') - \epsilon_{k+q})} \quad (52)$$

where as before $\tilde{\Sigma}_\omega = \omega + \tilde{\Sigma}_\omega$, is equivalent to the integral equation for $\tilde{\Sigma}_k(\omega + \Omega) - \tilde{\Sigma}_k(\omega)$:

$$\tilde{\Sigma}_k(\omega + \Omega) - \tilde{\Sigma}_k(\omega) = \Omega - \frac{3i\bar{g}}{8\pi^2} \int d^2q d\omega' \frac{(\tilde{\Sigma}_{k+q}(\omega' + \Omega) - \tilde{\Sigma}_{k+q}(\omega')) \chi(\omega - \omega', q)}{(\tilde{\Sigma}_{k+q}(\omega' + \Omega) - \epsilon_{k+q})(\tilde{\Sigma}_{k+q}(\omega') - \epsilon_{k+q})} \quad (53)$$

Comparing (52) and (53) we immediately find that

$$g^{tot}(\mathbf{k}, \omega, \Omega) = g \left(1 + \frac{\tilde{\Sigma}_k(\omega + \Omega) - \tilde{\Sigma}_k(\omega)}{\Omega} \right) \quad (54)$$

In the limit $\Omega \rightarrow 0$ the r.h.s. of (54) yields $1 + \partial\Sigma(\mathbf{k}, \omega)/\partial\omega$.

The very fact that $g^{tot}(\mathbf{k}, \omega, \Omega)$ is related to $\partial\Sigma(\mathbf{k}, \omega)/\partial\omega$ implies that the large renormalization of the scalar vertex with zero momentum transfer is due to the same anomaly which accounts for large $\Sigma(\omega)$. Indeed, consider the lowest-order diagram for the vertex renormalization. When external bosonic frequency is strictly zero, the two fermionic propagators have poles in the same half-plane of frequency, and the integration over ϵ_k does not vanish only due to the fact that the spin susceptibility also has poles at $|\mathbf{q} - \mathbf{Q}| \propto (N\omega)^{1/2}$. Obviously, the resulting vertex correction is small in $1/N$. However, at finite Ω , the poles in the fermionic propagators are split, and there is a nonvanishing contribution from the frequency range where the split poles are in different frequency half-planes. Evaluating this contribution in the same way as for the fermionic self-energy, we indeed find that

$$\frac{\Delta g}{g} = 1 + \lambda \int_0^\Omega \frac{d\omega'}{\tilde{\Sigma}(\Omega - \omega') + \tilde{\Sigma}(\omega')} \frac{1}{(1 + |\omega + \omega'|/\omega_{sf})} \quad (55)$$

It is clear from (55) that the large renormalization of g is due to the same anomaly which gave rise to a large $\Sigma(\omega)$. Collecting the anomalous contributions from the higher-order diagrams and summing them up, one should indeed recover Eq. (54).

Note that this procedure is not as straightforward as one might expect. Indeed, consider the limit when $\Omega, \omega \ll \omega_{sf}$. In this limit, Eq. (55) yields

$$\frac{\Delta g}{g} = 1 + \frac{\lambda}{1 + \lambda}. \quad (56)$$

As for vanishing Ω , the full $g^{tot} = g(1 + \lambda)$, one may suggest that the perturbation series are geometrical, i.e. $1 + \lambda/(1 + \lambda) + \dots > 1/(1 - \lambda/(1 + \lambda)) = 1 + \lambda$. However, the actual situation is not like this: the explicit calculation of the two-loop vertex correction yields

$$\frac{\Delta g}{g}_{|2loop} = \frac{2}{\pi} \left(\frac{\lambda}{1 + \lambda} \right)^2. \quad (57)$$

i.e., the next order diagram contains an extra $\pi/2$ compared to what is would be if the series were geometrical. This peculiarity of the perturbation series emerges because $\Sigma_k(\omega)$ does possess some non-singular k -dependence along the Fermi surface. This momentum dependence is indeed fully accounted for in the Ward

identity but complicates perturbation series in some non-singular way. This is just another example that momentum dependence of the fermionic self-energy complicates calculations but does not affect the physics.

E. summary of Sec IV.

Let' now summarize what we have at the moment.

- i We find that at strong coupling, one can construct a new, fully self-consistent “zero-order” theory which explicitly includes the most divergent $O(\lambda)$ piece in the fermionic self-energy, but neglects vertex corrections and the renormalization of the Fermi velocity which both scale logarithmically with λ . The divergent piece in the self-energy comes from the second-order diagram. Higher order self-energy and vertex correction diagrams only account for totally irrelevant, small numerical corrections to this term.
- ii We demonstrated that this “zero-order” theory becomes exact in the formal limit when $N \rightarrow \infty$. In this theory, fermions are strongly affected by interaction with spin fluctuations and display non-Fermi liquid, quantum-critical behavior at frequencies larger than a typical spin relaxation frequency ω_{sf} . In the quantum-critical regime, the fermionic self-energy interpolates between linear in ω and $\sqrt{\omega}$ forms. At the same time, there is no feedback from fermionic incoherence on spin excitations which remain diffusive with the same diffusion constant as if they were made from free fermions.

Our next step is to develop a perturbation theory in $1/N$. Obviously, our interest is to understand the role of logarithmical vertex and self-energy corrections.

V. THE PERTURBATION THEORY IN $1/N$

A. one loop RG analysis

We recall that the $\log \lambda/N$ terms give rise to the two new features in the theory: vertex corrections which renormalize both fermionic and bosonic self-energies, and static fermionic self-energy $\Sigma(\mathbf{k}, 0)$. To the lowest order in $1/N$, we have from (31) and (135)

$$\frac{\Delta g}{g} = \frac{Q(v)}{N} \log \lambda, \quad (58)$$

$$\Delta \epsilon_k = -\epsilon_{k+Q} \frac{12}{\pi N} \frac{v_x v_y}{v_F^2} \log \lambda \quad (59)$$

where $Q(v) = (4/\pi)\tan^{-1}(v_x/v_y)$ interpolates between $Q = 1$ for $v_x = v_y$, and $Q = 2$ for $v_y \rightarrow 0$.

We see from (58,59) that the $1/N$ corrections to the vertex and to the velocity of the excitations are almost decoupled from each other: the velocity renormalization does not depend on the coupling strength at all, while the renormalization of the vertex depends on the ratio of velocities only through a non-singular $Q(v)$. The absence of the coupling constant in the r.h.s of the Eqs. (58,59) is, we recall, a direct consequence of the fact that the dynamical part of the spin propagator is obtained self-consistently within the model. Due to self-consistency, the overall factors in $\Delta \epsilon_k$ and $\Delta g/g$ are $\bar{g}(\omega_{sf}\xi^2)$. Since the fermionic damping is produced by the same spin-fermion interaction as the fermionic self-energy, ω_{sf} scales as $1/\bar{g}$, and the coupling constant disappears from the Eqs. (58,59).

The fact that the lowest-order corrections diverge at $\lambda = \infty$ obviously implies that the $1/N$ expansion breaks down near the QCP, and one has to sum up the series of the logarithms. We will do this in a standard one-loop approximation by summing up the series in $(1/N) \log \xi$ but neglecting regular $1/N$ corrections to each term in the series (and, indeed, we neglect regular $1/N^2$ corrections from FLEX-type diagrams). We verified that in this approximation, the cancellation of the coupling constant holds even when g is a running, scale dependent coupling. This in turn implies that one can separate the velocity renormalization from the renormalization of the vertex to all orders in $1/N$.

Separating the corrections to v_x and v_y and performing standard RG manipulations, we obtain a set of two RG equations for running v_x^R and v_y^R

$$\begin{aligned} \frac{dv_x^R}{dL} &= \frac{12}{\pi N} \frac{(v_x^R)^2 v_y^R}{(v_x^R)^2 + (v_y^R)^2} \\ \frac{dv_y^R}{dL} &= -\frac{12}{\pi N} \frac{(v_y^R)^2 v_x^R}{(v_x^R)^2 + (v_y^R)^2} \end{aligned} \quad (60)$$

where $L = \log \xi$. The solution of these equations is straightforward and yields

$$v_x^R = v_x Z; v_y^R = v_y Z^{-1}; Z = \left(1 + \frac{24L}{\pi N} \frac{v_y}{v_x}\right)^{1/2} \quad (61)$$

where, we recall, v_x and v_y are the bare values of the velocities (the ones in the Hamiltonian).

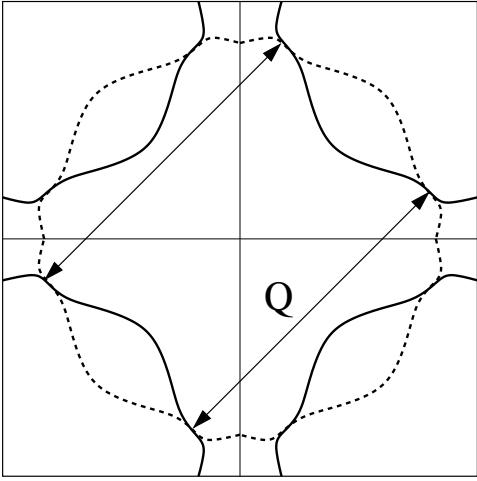


FIG. 14. The nesting of the Fermi surface as the result of the renormalization of the Fermi velocity. Solid line - the Fermi surface. Dashed line - the shadow Fermi surface (shifted by antiferromagnetic \mathbf{Q}). At $\xi = \infty$, the velocities at hot spots become perpendicular to the magnetic Brillouin zone boundary. This creates a “bottle neck effect”: the Fermi surface easily disconnects at hot spots immediately below the magnetic transition.

We see that v_y^R vanishes logarithmically at $\xi \rightarrow \infty$. This implies that right at the QCP, the renormalized velocities at $\mathbf{k}_{h,s}$ and $\mathbf{k}_{h,s} + \mathbf{Q}$ are antiparallel to each other, i.e. the Fermi surface becomes nested at hot spots (Fig. 14). This nesting in turn creates a “bottle neck effect” immediately below the criticality as the original and the shadow Fermi surfaces approach hot spots with equal derivatives (see Fig. 14). Quite generally, the nesting at hot spots is the first step in the evolution of the Fermi surface towards hole pockets [84]. If the nesting occurred at some finite ξ , (as one can judge by formally extending the lowest order result, Eq. (59) outside the range of its applicability), then the system would develop strong SDW precursors already in a paramagnetic phase [85–88]. It turns out, however, that this process is precluded because nesting at finite ξ (i.e., $v_y^R = 0$ at finite v_x^R) would imply that ω_{sf} renormalizes to zero, but renormalized ω_{sf} is the overall factor in the velocity renormalization. The only way to avoid this negative feedback effect is to consider the formal limit of small N , when the spin damping can be neglected [90]. In this limit, the feedback effect on the velocity renormalization is absent, and the Fermi surface evolves towards hole pockets already at a finite ξ .

Another feature of the RG equations (60) is that they leave the product $v_x v_y$ unchanged. This is a combination in which velocities appear in ω_{sf} . The fact that $v_x v_y$ is not renormalized implies that without vertex renormalization, $\omega_{sf} \xi^2$ preserves its form, i.e. spin susceptibility still has a simple diffusion pole.

We next consider vertex renormalization. Using again

the fact that $\bar{g}_{\omega_{sf}}$ does not depend on the running coupling constant, one can straightforwardly extend the second-order result for the vertex renormalization, Eqn (58), to the one-loop RG equation

$$\frac{dg^R}{dL} = \frac{Q(v)}{N} g^R \quad (62)$$

where g^R is a running coupling constant, and $Q(v)$ is the same as in (58) but with renormalized velocities v_x^R and v_y^R instead of v_x and v_y . Observe that the coupling constant *increases* as $\xi \rightarrow \infty$.

At the QCP, the dependence on ξ under the logarithm transforms into the dependence on frequency and external $q - Q$:

$$L \rightarrow (1/2) \log \frac{\bar{\omega}}{\max(|\omega|, (\mathbf{q} - \mathbf{Q})^2/\gamma)}. \quad (63)$$

Using the fact that for $\xi \rightarrow \infty$, $v_y^R/v_x^R \approx N\pi(v_y/v_x)/(24L)$ and expanding $Q(v)$ near $v_y^R = 0$, we find $Q(v) \approx 2(1 - (2/\pi)v_y^R/v_x^R) = 2 - N(v_y/v_x)/(6L)$. Substituting this result into (62) and solving the differential equation we obtain in the limit $L \gg N$

$$g^R = g \exp(2L/N) L^{-v_y/6v_x} \quad (64)$$

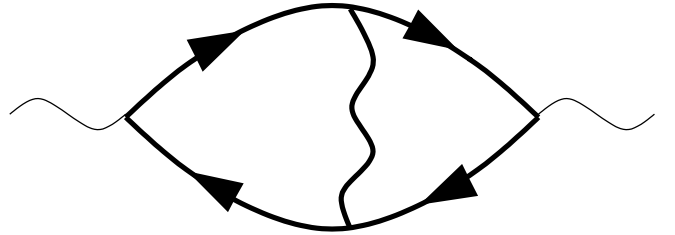


FIG. 15. The polarization bubble with the vertex correction.

We see that the logarithmic factor L appears in the exponent, i.e., series of logarithmical corrections eventually yield power-law dependence of the full vertex on frequency and momentum. This result contradicts the assertion that the quantum critical point is described by a purely bosonic “ ϕ^4 ” theory at the upper critical dimension $d + z = 4$ as in the latter case all logarithmical corrections should sum up into the powers of logarithms. We explain the origin of the power-law behavior below, and in the next subsection compare our results with the bosonic ϕ^4 theory in some detail. Here we just note that the very fact that L appears in the exponent implies that we need to know precisely in which combination $\gamma|\omega|$ and $(\mathbf{q} - \mathbf{Q})^2$ appear in L . To address this issue, we explicitly computed the polarization bubble with a vertex correction at a nonzero momentum and frequency, $\Pi_2(\mathbf{q}, \omega)$. The corresponding diagram is presented in Fig. 15. We normalized $\Pi_2(\mathbf{q}, \omega)$ such that

$\chi(\mathbf{q}, \omega) = \chi_0/(\xi^{-2} + (\mathbf{q} - \mathbf{Q})^2 + \gamma|\omega| + \Pi_2(\mathbf{q}, \omega))$. The computation of the diagram is presented in Appendix C. The result is

$$\Pi_2(\mathbf{q}, \omega) = \frac{Q(v)}{N} ((\mathbf{q} - \mathbf{Q})^2 + \gamma|\omega|) \log \left[\frac{\gamma\bar{\omega}}{(\mathbf{q} - \mathbf{Q})^2 + \gamma|\omega|} \right] \quad (65)$$

We see that $\gamma\omega_{sf}$ and $(\mathbf{q} - \mathbf{Q})^2$ are renormalized in exactly the same way. This result implies that the spin diffusion coefficient *does not* undergo logarithmical renormalization, i.e., the dynamical exponent z remains equal to two despite singularities. Earlier two of us missed the renormalization of the $(\mathbf{q} - \mathbf{Q})^2$ term and erroneously concluded [61] that z becomes larger than 2.

That both ω and $(\mathbf{q} - \mathbf{Q})^2$ terms in the bosonic propagator undergo logarithmical renormalizations requires some extra explanations. We argued earlier that to leading order in $1/N$, the spin polarization bubble has a regular piece, which comes from high fermionic energies and is absorbed into a bare static susceptibility, and an anomalous $\gamma|\omega|$ term which comes from fermionic energies which are smaller than ω . If we linearize fermionic dispersion near k_F and integrate first over momentum, and then over frequency, we only obtain $\gamma|\omega|$, the high-energy piece just does not appear. It is then tempting to conclude that the logarithmical vertex renormalization should yield $\omega \log \omega$ term but no $(\mathbf{q} - \mathbf{Q})^2 \log |\mathbf{q} - \mathbf{Q}|$ term. One should bear in mind, however, that for fermions with a linearized dispersion, the polarization operator is linearly divergent at high energies. Due to divergence, the result of the momentum/frequency integration depends on which integration is performed first. Indeed, evaluating the particle-hole bubble for free fermions by first integrating over frequency and then over momentum, we do obtain, in addition to $\gamma|\omega|$ an extra regular piece, of order of the upper cutoff in the momentum integral.

Consider now what happens when we evaluate the same bubble with the logarithmical vertex correction. Since we are interested in the terms which scale either as ωL or $(\mathbf{q} - \mathbf{Q})^2 L$, we can subtract the result for $\omega = (\mathbf{q} - \mathbf{Q})^2 = 0$. The remaining momentum/frequency integral diverges only logarithmically, and hence the result of the integration no longer depends on which integration is performed first. This implies that while $\gamma\omega$ term in the “zero-order” spin propagator is an anomalous piece which cannot be obtained by expanding in ω , the logarithmical corrections to the spin propagator are *not* anomalous and emerge due to the fact that $d = z = 2$ case is marginal. [Alternatively speaking, these corrections can be found in a standard RG procedure which assumes that typical internal energies are much larger than the external ones.] This reasoning explains why $(\mathbf{q} - \mathbf{Q})^2$ and $\gamma|\omega|$ are renormalized in the same way.

We now discuss why the series of logarithmical vertex corrections yield power-law momentum and frequency

dependence of the renormalized vertex. Mathematically, this is a consequence of the fact that Δg scales as g^3/γ . If γ was independent of g , then δg would be proportional to g^3 , i.e., $dg_R^2/dL \sim (g_R^2)^2$ or $1/(g^R)^2 \propto L$. This would result in a logarithmical behavior of g_R . In our case, however, bosonic dynamics is made by fermions, and $\gamma \propto g^2$. This yields $dg_R/dL \sim g_R$, i.e., $\log g_R \propto L$.

The power-law renormalization of g_R can be understood as follows. Suppose we perform calculations at arbitrary d . The vertex correction contains the product of two fermionic propagators and one bosonic propagator. As we discussed above, typical momenta in the fermionic propagators are much smaller than in the bosonic propagator. Then one can perform a 2D integration over $d\epsilon_k d\epsilon_{k+Q}$ keeping the corresponding momentum dependence only in fermionic propagators. This momentum integration transforms the two fermionic propagators into the constant densities of states. The vertex correction then reduces to the evaluation of the frequency integral of $\chi(q, \omega)$ in dimension $d - 2$. The corresponding integral is logarithmically singular if $d - 2$ is the *lower* critical dimension in the problem. As the lower critical dimension is the upper critical dimension minus two, the vertex correction becomes logarithmically singular if d is the upper critical dimension in the problem. This is precisely what we have in our case. Now, at the lower critical dimension, there is no restriction as to what the series of logarithms should produce, and they can sum either into the inverse power of a logarithm (as in Heisenberg magnets) or into the exponent of a logarithm (as in XY model). It is therefore not surprising that we did find power-law renormalization of g_R at the upper critical dimension.

Note by passing that from general point of view, the spin-fermion model is characterized by two different space-time dimensions. One is obviously $d + z_B = d + 2$, where $z_B = 2$ is the bosonic dynamical exponent. The other space-time dimension is associated with the anomalous piece in $\Sigma(\mathbf{k}, \Omega)$. This piece is produced solely by fermions (bosons can be treated as static). For fermions, the dynamical exponent $z_F = 1$ (typical fermionic momenta and typical fermionic frequencies scale with each other). Accordingly, the space-time dimension associated with the anomaly is $d + z_F = d + 1$. For $d = 2$, it is equal to 3 and is below the upper critical dimension. In particular, one can easily check that for arbitrary d , the anomalous self-energy at $\xi = \infty$ scales as $\Sigma(\Omega) \sim \Omega^{(d-1)/2}$ and accounts for non-Fermi liquid behavior for all $d < 3$.

We now return to Eq. (64). Substituting $L = (1/2) \log(\bar{\omega}\gamma/(\gamma|\omega| + (\mathbf{q} - \mathbf{Q})^2))$, we obtain that at the QCP, the running coupling constant diverges as

$$g^R \propto g (\gamma|\omega| + (\mathbf{q} - \mathbf{Q})^2)^{-1/N} \times |\log(\gamma|\omega| + (\mathbf{q} - \mathbf{Q})^2)|^{-v_y/6v_x} \quad (66)$$

Substituting this result into the spin polarization operator we find that at the QCP,

$$\begin{aligned} \chi^{-1}(\mathbf{q}, \omega) &\propto \left(\frac{g_R}{g}\right)^2 (\gamma|\omega| + (\mathbf{q} - \mathbf{Q})^2) \\ &\propto [\gamma|\omega| + (\mathbf{q} - \mathbf{Q})^2]^{\frac{N-2}{N}} |\log(\gamma|\omega| + (\mathbf{q} - \mathbf{Q})^2)|^{-v_y/3v_x} \end{aligned} \quad (67)$$

This result implies that vertex corrections give rise to anomalous scaling dimension η for the dynamical spin susceptibility,

$$\chi^{-1}(\mathbf{q}, \omega) \propto (\gamma|\omega| + (\mathbf{q} - \mathbf{Q})^2)^{1-\eta}. \quad (68)$$

Up to logarithmic corrections, $\eta = 2/N$. For $N = 8$, $\eta = 0.25$ and $1 - \eta = 0.75$.

We also emphasize that the renormalization of the bosonic propagator has little effect on fermions as the spin susceptibility appears in the fermionic self-energy in the combination with two side vertices, i.e., as $g_R^2 \chi(\mathbf{q}, \omega)$. We see from (67) that this combination retains its bare form $(\gamma|\omega| + (\mathbf{q} - \mathbf{Q})^2)^{-1}$. Accordingly, the only singular correction to fermionic self-energy comes from the logarithmic renormalization of v_F :

$$\Sigma(\Omega) \propto |\Omega|^{1/2} |\log \Omega|^{-1/2} \quad (69)$$

B. a comparison with ϕ^4 theory

The results of the previous subsection imply that the 2D fermionic system at the antiferromagnetic QCP is not described by the effective bosonic theory at the upper critical dimension. This contradicts ϕ^4 theory of the QCP developed mostly by Hertz [55] and Millis [56] (for recent developments, see [91]). Hertz and Millis (HM) departed from the same spin-fermion model as we study, but integrated out fermions in the effective action and obtained the effective Lagrangian for bosonic (spin) degrees of freedom. They conjectured that the expansion of the action in powers of the bosonic variables $S_{q,\omega}$ yields ϕ^4 theory with the dynamical exponent $z = 2$.

$$\begin{aligned} S_{eff} &= T \sum_{\omega, q} (r + \mathbf{q}^2 - i\omega) S_{q,\omega} S_{-q,-\omega} \\ &+ b \sum_{\omega_i, q_i} S_{q_1, \omega_1} S_{q_2, \omega_2} S_{q_3, \omega_3} S_{q_4, \omega_4} \delta(\sum_i q_i) \delta(\sum_i \omega_i) + \dots \end{aligned} \quad (70)$$

where q measures a deviation from (π, π) , r is a distance from the critical point, and b is a constant. At $d = 2$, the ϕ^4 theory is at the upper critical dimension ($d + z = 4$), and the bosonic self-energy is marginally irrelevant. This implies that for $r = 0$ the self-energy only adds fractional power of $\log(\max(\omega, q))$ to the bosonic propagator. One can check this by explicitly computing the self-energy order by order in b .

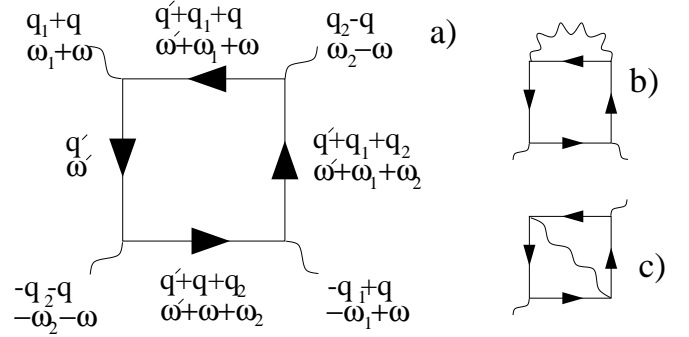


FIG. 16. a) Diagrammatic representation of the four-fold interaction vertex between spin fluctuations. b) and c) Two ways of contracting the external legs of the four-fold vertex.

The bare bosonic propagator in the HM theory is the same as our $N = \infty$ result. We, however, dispute the assertion that b can be approximated by a constant. Indeed, if this approximation is valid, then the first-order correction in b involves one bosonic loop and is infrared finite. We, however, found in the previous subsection that it is logarithmically singular.

The four-boson vertex is diagrammatically given by the graph presented in Fig. 16. At external $\omega_i = q_i = 0$, it becomes (we skip spin indices for a moment)

$$b = N\bar{g}^2 T \sum_{\mathbf{q}', \omega'} G^2(\mathbf{q}', \omega') G^2(\mathbf{q}' + \mathbf{Q}, \omega'). \quad (71)$$

Since

$$\int d\epsilon'_q G^2(\mathbf{q}', \omega') = 0, \quad (72)$$

this vertex vanishes if one linearizes the fermionic dispersion near the Fermi surface. The inclusion of the curvature of the fermionic dispersion (i.e., nonuniversal, lattice effects) makes the momentum integral in (71) and hence b finite [56]. The fact that b is produced by high-energy fermions then implies that it is insensitive to any modifications of the low-energy fermionic dynamics near quantum criticality and can be treated as a constant even at the critical point.

The potential problem with this reasoning is that although the momentum integral in (72) indeed vanishes for a linearized dispersion, the integrand contains a double pole. At finite external ω_i and q_i , the double pole splits into two single poles which in a small frequency range of width ω_i are located in different half-planes. The integration over this range does not produce a smallness in ω_i as the two poles are only separated by a $\max(\omega_i, v_F q_i)$. This implies that even for linearized fermionic dispersion, the value of b is generally finite and depends on the ratio of ω_i and $v_F q_i$.

The evaluation of the four-boson vertex for finite external frequencies and momenta is straightforward. For

simplicity, we restrict with free fermions. One can easily verify that the inclusion of the fermionic self-energy does not affect the results below. Introducing the external momenta and frequencies as in Fig 16a. we obtain (see Appendix C, Eqn. (189))

$$b = \frac{Ng^4}{8\pi v_x v_y} \frac{|\omega_2 + \omega| + |\omega_2 - \omega| - |\omega_1 + \omega| - |\omega_1 - \omega|}{[i(\omega_1 + \omega_2) - \epsilon_{q_1+q_2}][i(\omega_1 - \omega_2) - \epsilon_{Q+q_1-q_2}]}$$
(73)

We see that generally b scales inversely with the incoming frequency, but the coefficient depends on the relative magnitudes of external ω_i and $v_F q_i$. This in particular implies that the bosonic self-energy depends on which external legs of the four-boson vertex are contracted. There are two topologically different self-energy diagrams to first order in b . They are presented in Fig. 16 b and c. If b was independent of momentum and frequency (as is assumed in the HM theory), both diagrams would be equivalent and yield $b \int d^2 q d\omega \chi(\mathbf{q}, \omega)$. This integral is nonsingular in $2D$ and only accounts for a nonessential renormalization of ξ . In our case, the result is different as we already know: the first diagram is equivalent to adding fermionic self-energy to the particle-hole bubble and vanishes if we restrict with linearized fermionic dispersion near the Fermi surface. The second diagram is equivalent to adding a vertex correction to a particle-hole bubble and is logarithmically singular.

For completeness, in Appendix C we explicitly computed both diagrams by choosing the appropriate external frequencies in b , and convoluting b with the spin propagator. This computation indeed yields the same results as we just described, namely the diagram in Fig. 16b vanishes while that in Fig. 16c yields the same logarithmic renormalization as (65).

We see therefore that the explicit computation of the *first-order* bosonic self-energy in the effective ϕ^4 model yields a logarithmically singular piece which comes from a singular momentum/frequency dependence of the ϕ^4 vertex at smallest energies. This singularity is missed if one restricts with a constant four-boson vertex, as it is *assumed* in the ϕ^4 theory.

A very similar computation has been performed by Lercher and Wheatley [53]. They also argued that the four-boson vertex is singular at vanishing external momenta and frequency, and depends on the ratio between momentum and frequency. Our result for the vertex slightly differs from theirs, but the conclusions are identical.

C. summary of Sec. V

Let us now summarize our $1/N$ results.

i We found that the singular corrections to the Fermi velocity cause nesting behavior at hot spots at $\xi = \infty$, but have little effect on the spin dynamics. These corrections are, however, only logarithmically singular at $\xi \rightarrow \infty$. The corrections to the vertex on the other hand do not affect Fermi velocity and fermionic self-energy, but give rise to a nonzero anomalous scaling dimension $\eta = 2/N$ of the bosonic propagator.

ii We demonstrated that the co-existence of the logarithmic renormalization of the Fermi velocity and the anomalous dimension in the spin channel is due to the fact that the corrections to the spin-fermion vertex are structurally equivalent to the renormalization of the order parameter in dimension $d-2$. In the latter case, the logarithmic corrections are not necessary summed up into a series of logarithms.

iii Our results disagree with purely bosonic ϕ^4 theory of the QCP. We argued that the difference is due to the fact that in our model, the four-boson vertex is not a constant but rather has a complex momentum/frequency dependence at the lowest energies. This is another indication of the presence of anomalies in the spin-fermion model. We explicitly demonstrated how our results can be obtained in the effective ϕ^4 theory with full four-boson vertex made by fermions.

iv We also argued that from general perspective, the spin-fermion model has two different space-time dimensions, $d+2=4$ and $d+1=3$. The first is associated with the RG-type physics, and the second is associated with the anomalous piece in the self-energy which comes from low energies and cannot be obtained within RG procedure. For $2 < d < 3$, the bosonic dynamics at criticality is Gaussian, but fermionic self-energy scales as $\Sigma(\Omega) \propto \Omega^{(d-1)/2}$ and accounts for non-Fermi liquid behavior at the critical point.

VI. LARGE N THEORY AT FINITE T

So far, our analysis was restricted to $T = 0$. We now discuss how the fermionic self-energy and the spin polarization operator are modified at finite T .

A conventional wisdom would be that at finite T , the system in the quantum-critical regime possesses ω/T scaling, i.e., fractional powers of frequency are replaced, at small ω , by the same powers of temperature. We will see that this effect, indeed, takes place. We will also find, however, that the fermionic self-energy in the quantum-critical regime contains an extra term which does not fit into ω/T scaling. The strength of this extra term depends on the order of limits $\lambda \rightarrow \infty$ and $N \rightarrow \infty$.

As before, we first present the results of the computations at $N = \infty$ and then extend the theory to finite N

A. $N \rightarrow \infty$ limit

1. spin polarization operator

We begin with the spin polarization operator $\Pi(\mathbf{Q}, \omega)$. Replacing the integration over Matsubara frequencies in Eq. (36) by a summation as

$$\int \frac{d\omega}{2\pi} \rightarrow T \sum_n \quad (74)$$

we obtain

$$\Pi(\omega_m) = \frac{\pi T}{\omega_{sf}} \sum_n \left(1 - \frac{\Omega_n(\Omega_n + \omega_m)}{\sqrt{(\Omega_n)^2 (\Omega_n + \omega_m)^2}} \right), \quad (75)$$

where, as usual, $\omega_m = 2\pi Tm$, $\Omega_n = \pi T(2n + 1)$. The summation over n is elementary and yields

$$\begin{aligned} \Pi_m &= \frac{\pi T}{\omega_{sf}} \sum_n \{1 - \text{sign}([2n + 1][2(n + m) + 1])\} \\ &= \frac{|\omega_m|}{\omega_{sf}} \end{aligned} \quad (76)$$

We see that at finite T , the spin polarization operator preserves exactly the same form as at $T = 0$. In particular, $\Pi(\mathbf{Q}, 0) = 0$, i.e., at finite T , the spin correlation length does not acquire an extra correction from low-energy fermions.

2. fermionic self-energy

As the spin polarization operator does not depend on T , the fermionic self-energy is still given by Eqs. (22) and (23). At $N \rightarrow \infty$ we have

$$\begin{aligned} \Sigma(\mathbf{k}_{hs}, \Omega_m) &= i\pi T \lambda \sum_n \frac{\text{sign}\omega_n}{\sqrt{1 + \frac{|\omega_n - m|}{\omega_{sf}}}} \\ &= i\pi T \lambda \left[1 + \sum_{n=1}^{|m|} \frac{1}{\sqrt{1 + \frac{\omega_n}{\omega_{sf}}}} \right] \text{sign}\Omega_m. \end{aligned} \quad (77)$$

The extension to momenta away from a hot spot proceeds in the same way as at $T = 0$: λ and ω_{sf} are just replaced by $\lambda(k)$ and $\omega_{sf}(k)$ given by (47). The full analysis of self energy as function of frequency and temperature is performed in the Appendix D. For $|\Omega_m|, T \ll \omega_{sf}(k)$, the self-energy obviously has a Fermi-liquid form

$$\Sigma(\mathbf{k}, \Omega_m) = i\lambda(k) \left(\Omega_m + \frac{(\pi T)^2 - \Omega_m^2}{4\omega_{sf}(k)} \text{sign}\Omega_m \right) \quad (78)$$

For $T \ll \omega_{sf}(k)$ and arbitrary Ω_m , the thermal piece in the self-energy preserves T^2 dependence, but the prefactor depends on frequency:

$$\Sigma_T(\mathbf{k}, \Omega_m) = i \frac{\pi^2 T^2}{4\omega_{sf}(k)} F\left(\frac{\Omega_m}{\omega_{sf}(k)}\right) \text{sign}\omega + O(T^4) \quad (79)$$

where $F(0) = 1$, and $F(x \gg 1) \rightarrow 1/3$. The full expression, including T^4 terms is presented in (213).

In the opposite limit $|\Omega_m|, T \gg \omega_{sf}(k)$, the system behavior is quantum-critical. In this limit, the contributions to the sum in Eq. (77) from all $n \neq m$ can be explicitly expressed in terms of Riemann Zeta function (see Eq. (203)). Combining this with the $n = m$ contribution from classical, static spin fluctuations, we obtain

$$\begin{aligned} \Sigma(\mathbf{k}, \Omega_m) &= i\pi T \lambda(k) \\ &+ i \left(\frac{\pi T \bar{\omega}}{2} \right)^{1/2} \left(\zeta\left(\frac{1}{2}\right) - \zeta\left(\frac{1}{2}, 1 + m\right) \right) \end{aligned} \quad (80)$$

where ζ is a Zeta function. For $m \gg 1$, the second term scales as \sqrt{Tm} , i.e., as $\sqrt{\bar{\omega}}$.

In real frequencies, the imaginary part of the self-energy takes the form (see Appendix D)

$$\Sigma''(\Omega) = \frac{\lambda}{2} Im \int_{-\infty}^{\infty} \frac{d\omega}{\sqrt{1 - i\frac{\omega}{\omega_{sf}}}} f(\Omega/2T, \omega/2T) \quad (81)$$

where $f(x, y) = \tanh(x - y) + 1/\tanh(y)$. In the Fermi liquid regime, we obviously have $\Sigma''(\Omega) \propto T^2$, with Ω dependent prefactor, as in (79). In the quantum-critical regime,

$$\Sigma''(\mathbf{k}, \Omega, T) = \pi T \lambda(k) + \left(\frac{T \bar{\omega}}{2} \right)^{1/2} D\left(\frac{\Omega}{T}\right). \quad (82)$$

The scaling function $D(x)$ is given by (214). In the two limits, $D(x \gg 1) = \sqrt{x}$, and $D(x \ll 1) = -1.516 + 0.105x^2$.

The real part of $\Sigma(\mathbf{k}, \Omega)$ is obtained from (82) by Kramers-Kronig transformation. It contains the same \sqrt{T} dependence as (82) with another scaling function of Ω/T , but does not have a λT term. This can be easily understood as static spin fluctuations account for a scattering with a finite transferred momentum and zero transferred frequency, and therefore act as impurities. Not surprisingly, their contribution to the self-energy is purely imaginary.

We see from Eqs. (80), (82) that the piece in the self-energy which comes from nonzero bosonic Matsubara frequencies (i.e., from $n \neq m$ in (77)) yields a conventional scaling form of $\Sigma(\mathbf{k}, \Omega, T)$ in which the $\sqrt{\Omega}$ behavior at $\Omega \gg T$ is collaborated by \sqrt{T} dependence at $T \gg \Omega$, and the prefactor does not depend on the spin correlation length

On the other hand, the $n = m$ term in the sum in (77) yields a linear in T contribution to the self-energy with the prefactor which scales as ξ and diverges at the QCP. This term obviously violates the scaling. This violation is a direct consequence of the fact that in our theory $\xi(T) = \xi(T = 0)$. For the scaling behavior, one would need $\xi^2(T) - \xi^2(0) \propto T$. We discuss this issue in a separate subsection below.

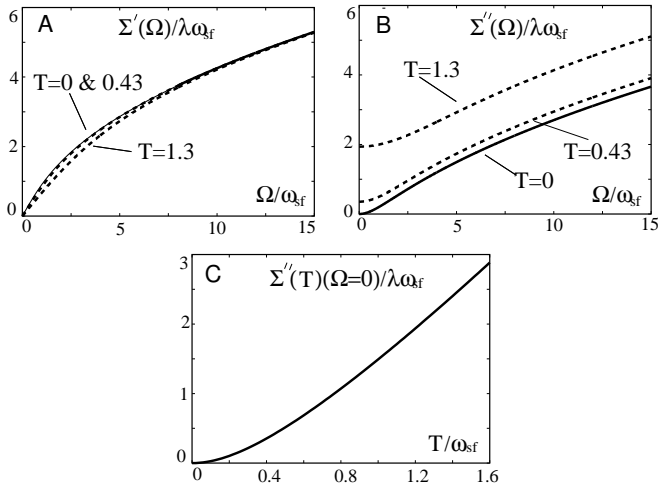


FIG. 17. The results for the fermionic self-energy at $N \rightarrow \infty$.

Finally, at $\Omega = 0$, $\Sigma''(T)$ has a simple form which interpolates between Fermi liquid and quantum-critical regimes. Taking the $\Omega = 0$ limit in (81) we obtain

$$\Sigma''(\Omega = 0) = \pi T \lambda L \left(\frac{T}{\omega_{sf}} \right) \quad (83)$$

where

$$L(x) = \frac{1}{\pi x} \int dy \operatorname{Im} \frac{1}{\sqrt{1-iy}} \frac{1}{\sinh(y/x)} \quad (84)$$

At $x \gg 1$, $L(x) \approx 1$, i.e., $\Sigma''(\Omega = 0) \approx \pi T \lambda$. In the opposite limit of small x , $L(x) = \pi x/4$, and we recover the Fermi liquid behavior.

In Fig. 17 we plot the $N \rightarrow \infty$ result for the self-energy at finite T . We see that at small frequencies, $\operatorname{Im}\Sigma(k, \Omega)$ is linear in T starting already from $T \geq 0.5\omega_{sf}$. At higher frequencies, particularly in the region $\Omega \gg T$, $\operatorname{Im}\Sigma^{ret}(\mathbf{k}, \Omega)$ is linear in ω with almost T -independent slope. A finite temperature only gives rise to an extra constant term in $\operatorname{Im}\Sigma^{ret}(\mathbf{k}, \Omega)$.

B. beyond the $N \rightarrow \infty$ limit

We now consider to which extent we can trust the $N \rightarrow \infty$ results for the fermionic self-energy and the

spin polarization operator, when we apply them to the physical $N = 8$. We will show that there are two problems at finite N which are only partly related: one is how strong are vertex corrections, the effect of keeping the self-energy of intermediate fermions, and the momentum dependent piece in the fermionic self-energy (i.e., the renormalization of the Fermi velocity), and another one is to what accuracy one can factorize the momentum integration in deriving the equation for the fermionic self-energy. [By factorization we mean that in the diagram for fermionic $\Sigma(k, \Omega)$ one integrates over the momentum component along the Fermi surface in the bosonic propagator and over the momentum component transverse to the Fermi surface only in the fermionic propagator. The resulting self-energy is then the convolution of the effective 1D “local” spin susceptibility and the fermionic density of states].

1. accuracy of the factorization of the momentum integration at finite T

Let’s first discuss the second issue. Consider the second-order diagram for the fermionic self-energy. At $T = 0$, the factorization of the momentum integration in this diagram, or, equivalently, the possibility to neglect in the spin susceptibility the momentum component transverse to the Fermi surface, is well justified for all relevant frequencies as the correction to the self-energy from keeping the momentum dependence in the susceptibility has an extra power of Ω in the Fermi liquid regime and is small by $1/N^2$ in the quantum-critical regime. For $T \neq 0$, analogous result holds for the $n \neq m$ contribution to the self-energy, and the proof almost exactly parallels the one for $T = 0$. The situation is, however, different for the $n = m$ contribution to (77). This term comes from static spin fluctuations, and hence typical $(\mathbf{q} - \mathbf{Q})_x \sim |\omega|/v_F$ has to be compared to ξ^{-1} rather than to $(\gamma\omega)^{1/2}$ (x axis is chosen transverse to the Fermi surface at $\mathbf{k}_{hs} + \mathbf{Q}$).

The new frequency scale $v_F \xi^{-1}$ is related to $\bar{\omega}$ and ω_{sf} as

$$v_F \xi^{-1} = \bar{\omega} \frac{v_F^2}{v_x v_y} \frac{N}{12\lambda} = \omega_{sf} \frac{v_F^2}{v_x v_y} \frac{N\lambda}{3} \quad (85)$$

We see that the location of this scale compared to $\bar{\omega}$ depends on the ratio N/λ . In the formal $N \rightarrow \infty$ limit at finite λ , $v_F \xi^{-1} \gg \bar{\omega}$. Then, even at $\omega \sim \bar{\omega}$, $|\omega| \ll v_F \xi^{-1}$, and the factorization of momentum integration is well justified. Alternatively, however, one can keep N finite and study the system behavior at $\lambda \rightarrow \infty$ and finite T . In this limit, $v_F \xi^{-1} \ll \bar{\omega}$, and the corrections to the formal $N = \infty$ result for the static, thermal self-energy are relevant at frequencies $|\omega| \sim \bar{\omega}(N/\lambda) \ll \bar{\omega}$. In reality, for $N = 8$ and $\lambda \geq 1$, $v_F \xi^{-1} \leq \bar{\omega}$, i.e., the modification of the static piece in the fermionic self-energy is a modest effect for $\omega \leq \bar{\omega}$. Note also that this modification is

only relevant in the quantum-critical regime as in the Fermi liquid regime, $|\omega| \leq \omega_{sf}$, and hence $|\omega|/(v_F \xi^{-1}) \leq \omega_{sf}/(v_F \xi^{-1}) = O(1/N)$.

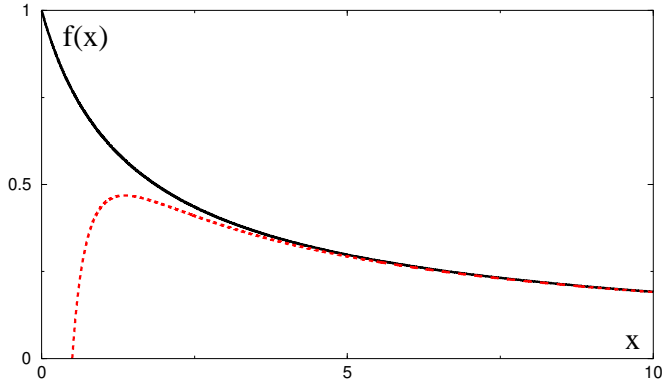


FIG. 18. Function $f(x)$ defined in (89). Dashed line is the asymptotic form $2 \log 2x / (\pi x)$, valid at large x

The exact form of $\Sigma(\Omega_m)$ at a hot spot, can be obtained from the general formula for the self-energy, Eqs. (22) and (23), extended to a finite T . We separate the contributions from dynamical and static spin fluctuations and write $\Sigma(\Omega_m) = \Sigma_{st}(\Omega_m) + \Sigma_{dyn}(\Omega_m)$. As we said, Σ_{dyn} can be safely computed at $N = \infty$ as the corrections scale as regular powers of $1/N$. The result is the second term in Eq. (77):

$$\Sigma_{dyn}(\Omega_m) = i\pi T \lambda \sum_{n=1}^{|m|} \frac{1}{\sqrt{1 + \frac{\omega_n}{\omega_{sf}}}} \text{sign} \Omega_m. \quad (86)$$

In the quantum-critical regime this reduces to the second term in Eq. (80)

$$\Sigma_{dyn}(\Omega_m) = i \left(\frac{\pi T \bar{\omega}}{2} \right)^{1/2} \left(\zeta \left(\frac{1}{2} \right) - \zeta \left(\frac{1}{2}, 1 + m \right) \right) \quad (87)$$

The static contribution has to be evaluated without approximations and reduces to

$$\Sigma_{st}(\Omega_m) = i \lambda T \pi f \left(\tilde{\Omega}_m \right) \quad (88)$$

where $\tilde{\Omega}_m = |\Omega_m| / v_F \xi^{-1}$ and

$$f \left(\tilde{\Omega}_m \right) = \frac{2 \cos^{-1} \tilde{\Omega}_m}{\pi \sqrt{1 - \tilde{\Omega}_m^2}} \quad (89)$$

The limiting values of $f(x)$ are $f(0) = 1$, $f(1) = 2/\pi$, $f(x \gg 1) \approx 2 \log 2x / (\pi x)$. The plot of $f(x)$ is presented in Fig. 18. We see that $\Sigma_{st}(\Omega_m)$ coincides with the $N = \infty$ result $i\pi\lambda$ only at vanishing $\tilde{\Omega}_m$. At finite $\tilde{\Omega}_m$, it is smaller than for $N = \infty$, and for $\tilde{\Omega}_m \gg 1$, $\Sigma_{st}(\Omega_m)$ decreases as $1/\tilde{\Omega}_m$, up to logarithmical corrections. In

this limit, the overall factor in the fermionic self-energy scales as $\lambda v_F \xi^{-1} \sim \bar{g}$, i.e., it no longer depends on ξ . This is indeed what one should expect in the truly quantum-critical regime.

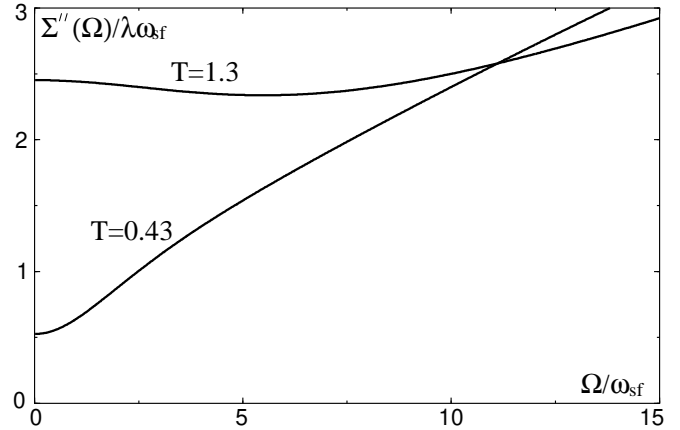


FIG. 19. The modified second-order fermionic self-energy - the sum of Eqs. (90) and (92). It includes the full contribution from thermal, static spin fluctuations, and the $N \rightarrow \infty$ contribution from dynamical spin fluctuations. We used $v_x = v_y = v_F/\sqrt{2}$, and $\lambda = 1$, in which case $v_F \xi^{-1} = 4\bar{\omega}/3 = 16\omega_{sf}/3$.

In real frequencies, $\Sigma''(\mathbf{k}_{hs}, \Omega) = \Sigma''_{st}(\Omega) + \Sigma''_{dyn}(\Omega)$, where $\Sigma''_{dyn}(\Omega)$ is the same as in (81) but with $f_1(x, y) = \tanh(x - y) + 1/\tanh(y) - 1/y$ instead of $f(x, y)$:

$$\Sigma''_{dyn}(\Omega) = \frac{\lambda}{2} \text{Im} \int_{-\infty}^{\infty} \frac{d\omega}{\sqrt{1 - i \frac{\omega}{\omega_{sf}}}} f_1(\Omega/2T, \omega/2T). \quad (90)$$

For $\omega > \omega_{sf}$, this reduces to the second term in (82):

$$\Sigma''_{dyn}(\Omega) = \left(\frac{T\bar{\omega}}{2} \right)^{1/2} D \left(\frac{\Omega}{T} \right). \quad (91)$$

where $D(x)$ is given by (214).

The static contribution is obtained by transferring (88), (89) onto real axis:

$$\Sigma''_{st}(\Omega) = 2T \lambda \text{Im} \frac{\log \left[\tilde{\Omega}^2 + \sqrt{1 + \tilde{\Omega}^2} \right]}{\sqrt{1 + \tilde{\Omega}^2}} \quad (92)$$

For $\tilde{\Omega} \ll 1$, $\Sigma''_{st}(\Omega) \propto (T/\Omega) \log \Omega / v_F \xi^{-1}$. We see that the prefactor depends on ξ only in the logarithmical term. This is indeed the same result as we found earlier by evaluating the thermal self-energy in Matsubara frequencies.

In Fig. 19, we plot $\Sigma''(\mathbf{k}_{hs}, \Omega)$ obtained by combining the the $N = \infty$ form of Σ_{dyn} (Eqn. (90)) and the modified form of Σ''_{st} (Eqn. (92)). Comparing this figure with Fig. 17 where we plotted the formal $N = \infty$ result, we observe that the main difference is in the temperature variation of the self-energy at high frequencies. At

$N = \infty$, the plots at different T differ by a constant. In the modified expression, the thermal piece in $\Sigma''(\mathbf{k}, \Omega)$ decreases with frequency, and the curves at different T progressively come closer to each other.

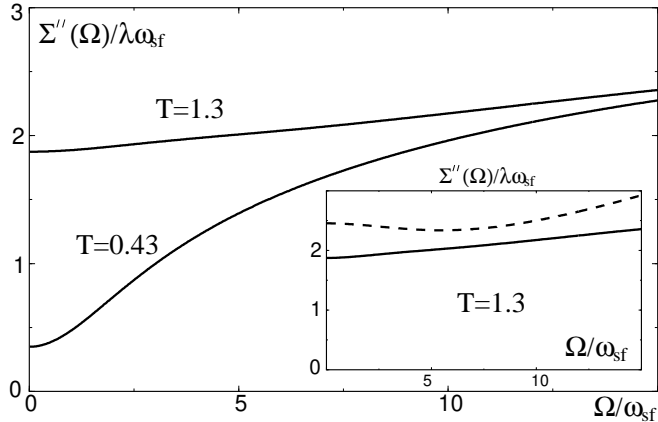


FIG. 20. The full second-order result for the $\Sigma''(k, \Omega)$ obtained without factorizing the momentum integration in both static and dynamics pieces in the self-energy. In the insert the same data for $T = 1.3$ (solid line) is compared with the approximate form of the self-energy from Fig.19 (dashed line). $v_F\xi^{-1}$ is the same as in Fig.19.

To verify how accurate is our “modified $N = \infty$ ” form of the self-energy we present in Fig. 20 the result for the full Σ'' , which we obtained in Appendix D (Eqn (218) with $\tilde{\Sigma}_{R,A}^2 = \Omega - \omega \pm i\delta$) without factorizing the momentum integration in both, static and dynamical parts of Σ'' . Comparing Figs. 19 and 20 we find that the full result is rather close to our approximate one - the only difference is that now the curves at various T progressively come close to each other with increasing frequency, and cross only at very high frequencies.

In Fig. 21 we present the set of the results for the photoemission intensity $I(\Omega) \propto \text{Im}G(\mathbf{k}, \Omega)n_F(\Omega)$ for various ϵ_k . They were obtained using the spectral functions from Fig. 20. For definiteness, we used $\lambda = 1.7$ and $T = 0.43\omega_{sf}$. Comparing these forms with the corresponding results at $T = 0$ (see Fig. 12), we see that a finite temperature gives rise to an additional broadening of the photoemission intensity at small $\Omega \sim \omega_{sf}$, and plays virtually no role for $\Omega \gg \omega_{sf}$.

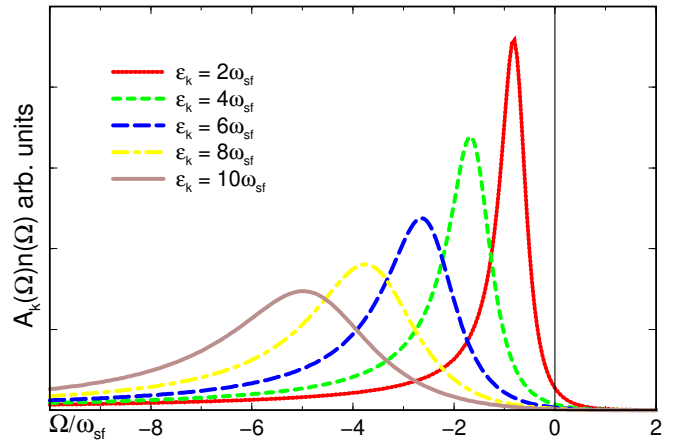


FIG. 21. The photoemission intensity $I(\Omega) \propto \text{Im}G(\mathbf{k}, \Omega)n_F(\Omega)$ for various ϵ_k . For definiteness we used $\lambda = 1.7$ and $T = 0.43\omega_{sf}$.

2. the role of the self-energy of intermediate fermions

In the above analysis we restricted with the second order self-energy diagram. Now we consider what happens if we keep the self-energy of intermediate fermions (i.e., evaluate the self-energy diagram as in Fig. (9)). Recall that at $T = 0$, the self-energy of intermediate fermions is not small in $1/N$ but nevertheless doesn't play any role as the momentum integration can be factorized, and $\Sigma(\omega)$ is expressed in terms of the density of states of intermediate fermions. For the linearized fermionic dispersion, the latter is independent on the self-energy and is the same as for free fermions. This implies that the full expression for the self-energy coincides with the second-order result. At finite T , this is no longer the case as the momentum integration in the static piece in $\Sigma(\Omega)$ cannot be factorized.

In principle, the self-energy of intermediate fermions should include both $T = 0$ and temperature contributions. We will show below that the temperature piece in the self-energy for intermediate fermions becomes relevant for $T \gg N\omega_{sf}$ when also vertex corrections and the renormalization of ϵ_k cannot be neglected. To separate thermal and quantum effects, we focus first on $T \ll N\omega_{sf}$ when the vertex corrections and the corrections to ϵ_k are the same as at $T = 0$, i.e., are small in $1/N$. At these temperatures, the self-energy of intermediate fermions can be approximated by its $T = 0$ value. The latter, in turn, is well approximated by the $N = \infty$ result, $\Sigma_{T=0}(\Omega) = 2\lambda\Omega/(1 + (1 - i\Omega/\omega_{sf})^{1/2})$.

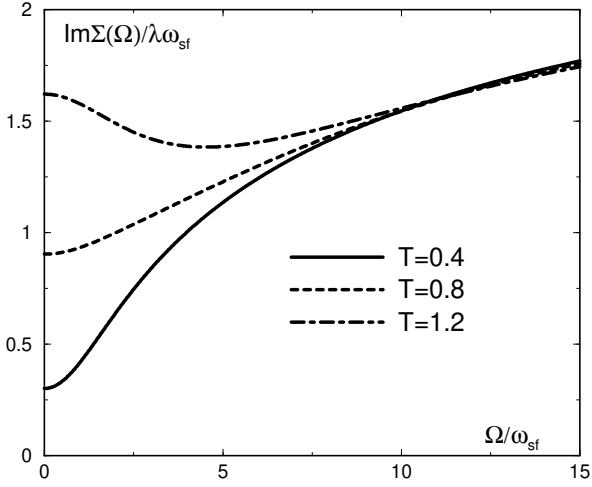


FIG. 22. The full result for the $\Sigma''(k, \Omega)$ (Eqn. 218). The form of $\Sigma''(\Omega)$ at low temperatures is close to the second-order result plotted in Fig.20. The initial decrease of $\Sigma''(\Omega)$ at higher T is probably the artifact associated with the neglect of vertex corrections. $v_F \xi^{-1}$ is the same as in Fig.19.

The full expression for the static part of Σ'' is the same as in Eq. (92), but now $\tilde{\Omega} = (\Omega + \Sigma_{T=0}(\Omega))/v_F \xi^{-1}$. In the quantum-critical regime, $\Omega < \bar{\omega}$, $\Sigma_{T=0}(\Omega)$ exceeds Ω , and $\tilde{\Omega}$ becomes $i\Omega/\bar{\Omega}$ where $\bar{\Omega} = (v_F \xi^{-1})^2/\bar{\omega} = N^2 \omega_{sf} (v_F^2/v_x v_y)/36$. Then, when $\bar{\Omega} < \Omega < \bar{\omega}$, the static piece in the self-energy behaves as $\Sigma''_{st}(\Omega) \propto TN \sqrt{\bar{\omega}/\Omega} \log \Omega/N^2 \omega_{sf}$. We see that up to a logarithmical prefactor, $\Sigma''_{st}(\Omega)$ acquires the same scaling form as the dynamical piece in the fermionic self-energy. In other words, at high enough frequencies, we eventually recover Ω/T scaling.

In Fig. 22 we plot the full expression for Σ'' obtained in the Appendix D, (Eqn. (218)) without factorizing the momentum integration in both static and dynamic parts and keeping the $T = 0$, $N = \infty$ self-energy for intermediate fermions. Comparing this figure with the second-order result, Fig.20, we see that at low T , the two forms of $\Sigma''(\Omega)$ are close to each other, as they indeed should be, as at $T = 0$ keeping the self-energy of intermediate fermions only yields regular $1/N$ corrections. At higher temperatures, Σ''_{prime} in Fig. 22 differs from the second-order result at high frequencies, as we found analytically, but it also initially decreases with frequency due to a stronger downturn renormalization of the static piece then in the second order expression.

This initial decrease poses a dilemma in selecting the theoretical form of Σ'' for experimental comparisons. From theory perspective, the $T = 0$ self-energy of intermediate fermions is not small in $1/N$ and therefore cannot be neglected in evaluating $\Sigma''_{st}(\Omega)$ for which the momentum integration is not factorized. The restoration of the scaling behavior at finite T due to this self-energy is also a good sign. On the other hand, one can include

the self-energy of intermediate fermions but neglect vertex corrections and the momentum dependence of the self-energy only as long as $T < N\omega_{sf}$ (see below). Up to which temperature this can be safely done for a physical $N = 8$ is a priori unclear. It looks to us that the initial drop in $\Sigma''(\Omega)$ in Fig. 22 at $T > \omega_{sf}$ is an artifact of overestimating the reduction of $\Sigma''_{st}(\Omega)$, and should be compensated by vertex corrections. This reasoning implies that for $T > \omega_{sf}$ and $N = 8$, the second-order result for the self-energy, Fig. 20, may be closer to reality than Fig. 22, which explicitly includes the self-energy of intermediate fermions but neglects vertex corrections. In Sec X we will be using the second-order result for the comparisons with the photoemission and optical data. We stress, however, that for $T \leq \omega_{sf}$, the difference between the two results is minor for all experimentally relevant frequencies. In particular, we verified that optical conductivities obtained using the second-order and the full self-energy are almost identical for $T \leq \omega_{sf}$.

We now return to the theoretical discussion and consider what happens at $T \gg N\omega_{sf}$. As we already said, this temperature range is of little use for experimental comparisons with cuprates, at least near optimal doping. However, it is important for the understanding of what is the correct form of the self-energy at a finite T at the QCP, when $\omega_{sf} \rightarrow 0$. Recall in this regard that so far we still have $\Sigma''_{st}(\Omega = 0) = \pi T \lambda \propto \xi$. On the other hand, from general scaling arguments [21] we expect that $\Sigma''_{st}(\Omega)$ in the quantum-critical regime should be independent on ξ .

3. the renormalization of the Fermi velocity

We begin with the velocity renormalization. To estimate it, we need to analyze the strength of the static piece in the self-energy Σ_{k, Ω_m} at $\mathbf{k} \neq \mathbf{k}_{hs}$ and $\epsilon_{k+Q} \gg \Omega_m$. Performing the same computation as in the previous subsection we obtain after simple manipulations,

$$\Sigma(\mathbf{k}, \Omega_m) - \Sigma(\mathbf{k}_{hs}, \Omega_m) = 2T\lambda(k) \log \left[\left(\epsilon_{k+Q} + \sqrt{\epsilon_{k+Q}^2 + v_F^2 \xi^{-2}} \right) / (v_F \xi^{-1}) \right] \quad (93)$$

At small ϵ_{k+Q} , expanding under the logarithm and using the fact that $\epsilon_k = v_x k_x + v_y k_y$ and $\epsilon_{k+Q} = -v_x k_x + v_y k_y$, we obtain

$$\begin{aligned} v_x^R &= v_x(1 + \delta) \\ v_y^R &= v_y(1 - \delta) \\ \delta &= \frac{2v_x v_y}{3v_F^2} \frac{T}{N\omega_{sf}} \end{aligned} \quad (94)$$

We see therefore that velocity renormalization becomes relevant at $T \sim N\omega_{sf}$, as we anticipated.

4. vertex corrections

The result for the vertex renormalization parallels the one for the self-energy. We can split $\Delta g/g$ into the contributions from static and dynamic spin fluctuations. The contribution from dynamical spin fluctuations scales as $(1/N)\log T$ and is small for $T \leq \bar{\omega}$ that we are interested in. The contribution from static spin fluctuations is larger due to the absence of the large $\gamma\omega$ term in the spin susceptibility. Integrating over momenta of two fermionic propagators in the vertex correction diagram in the same way as at $T = 0$, we obtain

$$\left(\frac{\Delta g}{g}\right)_{st} = \frac{2T}{N\omega_{sf}} \tan^{-1} \frac{v_x}{v_y} \quad (95)$$

This expression is valid for small external $\omega < v_F\xi^{-1}$. At larger frequencies, $(\Delta g/g)_{st}$ decreases and eventually scales as $(\bar{g}T/\omega^2)|\log T|$.

We see from (95) that vertex corrections also become relevant at $T > N\omega_{sf}$.

5. the thermal self-energy of intermediate fermions

Finally, we show that at $T > N\omega_{sf}$ we also have to keep the thermal piece in the self-energy for intermediate fermions, The easiest way to estimate this temperature is to consider the limit $\Omega = 0$. At vanishing frequency, the $T = 0$ piece in the fermionic self-energy vanishes, and we are left with only $\Sigma_{st}(T)$. At $N = \infty$, $\Sigma_{st}(T) = \pi T\lambda$. At finite N , this expression is valid if $\Sigma_{st}(T) < v_F\xi^{-1}$, or $T < N\omega_{sf}$. At larger T , the thermal piece in the self-energy for intermediate fermions cannot be neglected, at least at small frequencies.

C. self-consistent theory

We are not familiar with any controlled way to compute the static piece in the self-energy at finite N , finite T , and $\xi \rightarrow \infty$ such that $T \gg N\omega_{sf}$. As an exercise, we performed the FLEX-type computation of $\Sigma_{st}(\Omega, T)$ at vanishing Ω . Specifically, we included the full static fermionic self-energy into the self-energy diagram, but neglected vertex corrections and the renormalization of the Fermi velocity. We solved the self-consistent equation, obtained $\Sigma_{st}(T)$, and then re-calculated the vertex and velocity corrections with the new fermionic propagators. We found that the self-energy no longer diverge at the critical point, and that the vertex and velocity corrections are at most logarithmical even when $T \gg N\omega_{sf}$. While this analysis is by no means a controllable one, it describes the physically appealing effect that the divergence in the self-energy and in the vertex are eliminated

by thermal dressing of intermediate fermionic quasiparticles.

The FLEX-type computation of $\Sigma_{st}(T)$ reduces to the solution of the self-consistent equation in the form

$$\tilde{\Sigma}_{st}(T) = \frac{3T}{N\omega_{sf}} \int_0^\infty \frac{dx}{\sqrt{x^2+1}} \frac{1}{\sqrt{x^2+1} + \tilde{\Sigma}_{st}(T)} \quad (96)$$

where $\tilde{\Sigma}_{st} = \Sigma_{st}/(v_F\xi^{-1})$. The renormalization of the Fermi velocity and the vertex correction depend on $\tilde{\Sigma}_{st}(T)$ as

$$\begin{aligned} \frac{\Delta\epsilon_k}{\epsilon_{k+Q}} &= -\frac{3T}{N\omega_{sf}} \int_0^\infty \frac{dx}{\sqrt{x^2+1}} \frac{1}{(\sqrt{x^2+1} + \tilde{\Sigma}_{st}(T))^2} \\ \frac{\Delta g}{g} &= \frac{T}{N\omega_{sf}} \int_0^\infty \frac{dx}{\sqrt{x^2+1}} \frac{\tilde{\Sigma}_{st}(T)}{(x^2 + \tilde{\Sigma}_{st}^2(T))} \\ &\quad \times \frac{1}{(\sqrt{x^2+1} + \tilde{\Sigma}_{st}(T))} \end{aligned} \quad (97)$$

For simplicity, we set $v_x = v_y = v_F/\sqrt{2}$. The integral in (96) is explicitly evaluated in the Appendix D (see Eqn (216)). The integration in (97) can also be performed exactly, but the results are too lengthy to present here.

At $T \ll N\omega_{sf}$, the self-energy in the denominator can be neglected, and we obtain $\Sigma_{st}(T) = \pi T\lambda$. For these T ,

$$\Delta\epsilon_k = -\frac{3T}{N\omega_{sf}} \epsilon_{k+Q}; \quad \frac{\Delta g}{g} = \frac{\pi T}{2N\omega_{sf}}. \quad (98)$$

In the opposite limit, solving (96) with logarithmical accuracy, we obtain

$$\Sigma_{st}(T) = \bar{\omega} \left(\frac{TN}{6\bar{\omega}}\right)^{1/2} \left(\log \frac{3T}{N\omega_{sf}}\right)^{1/2} \quad (99)$$

At these temperatures

$$\begin{aligned} \frac{\Delta g}{g} &= \frac{T}{N\omega_{sf}} \frac{\log \tilde{\Sigma}_{st}(T)}{\tilde{\Sigma}_{st}^2(T)} = \frac{1}{3} \\ \Delta\epsilon_k &= -\epsilon_{k+Q} \left(1 - \frac{1}{\log \tilde{\Sigma}_{st}(T)}\right) \end{aligned} \quad (100)$$

Analyzing these results, we find that self-consistent solution of the thermal problem yields the results which are qualitatively similar to that at $T = 0$. Namely, the thermal piece in the fermionic self-energy scales as $T^{1/2}$, up to a logarithmical prefactor, the velocities at \mathbf{k}_{hs} and $\mathbf{k}_{hs} + \mathbf{Q}$ logarithmically tend to become antiparallel to each other, and vertex correction remains finite at criticality. The self-consistent solution indeed does not capture full logarithmical physics, nevertheless it clearly demonstrates that higher order diagrams eliminate the unphysical $O(\lambda)$ divergence in the fermionic self-energy and yield \sqrt{T} behavior at the QCP. Alternatively speaking, the self-consistent, finite N solution recovers ω/T scaling in the fermionic variables. From this perspective,

the only real difference between the self-energy at $T = 0$ and $T \neq 0$ in our large N analysis is that at $T \neq 0$, the width of the intermediate regime where $\Sigma'' \propto T$ scales with N ($\omega_{sf} < T < N\omega_{sf}$), while at $T = 0$, the width of the analogous linear regime in $\Sigma''(\omega)$ is, strictly speaking, of order 1 around $T \sim \omega_{sf}$. Curiously enough, for physical $N = 8$, the widths of the linear regimes in ω and in T are comparable as the one in ω occurs in between ω_{sf} and $6 - 8\omega_{sf}$. Whether this is more than just a coincidence is unclear to us. In any event, a more accurate treatment of thermal fluctuations is clearly called for.

Note, however, that while ω/T scaling in the fermionic self-energy is probably recovered in the self-consistent solution, still, there is no ω/T scaling in the dynamical spin susceptibility. Indeed, the thermal correction to the spin-fermion vertex remains finite at criticality, while at $T = 0$, the corrections were logarithmical and eventually yielded an anomalous dimension η . While, as we said, logarithmical physics is not precisely captured by self-consistent solution, there are no reasons to expect $T^{1-\eta}$ behavior as the anomalous power at $T = 0$ emerged due to the presence of anomalies which are purely *quantum* effects.

D. a temperature variation of ξ

Finally, we discuss in some more detail the temperature variation of the correlation length. The issue is whether there exist a universal temperature correction to the correlation length. We recall that in our theory $\xi(T) = \xi(T = 0)$. This independence of T is the consequence of the fact that in the computation of the spin polarization operator, we linearized the fermionic dispersion near the Fermi surface (see Appendix C). Expanding fermionic energies beyond the linear order in $k - k_F$, one indeed obtains thermal correction to ξ^{-2} , but the latter is nonuniversal and is of order $(T/\Lambda)^2$, where Λ (our upper cutoff) is comparable to the fermionic bandwidth. The nonlinearity of the fermionic dispersion also gives rise to a constant term in four-boson vertex $b \propto 1/\Lambda$. For a constant b , the first-order bosonic self-energy in 2D, $\Sigma_b \sim bT \sum_{\omega} \int d^2q \chi(\mathbf{q}, \omega)$ is logarithmically singular at $T \neq 0$ [56]: $\Sigma_b \sim bT \int d^2q / (\mathbf{q}^2 + \xi^{-2}) \sim bT \log \xi$. Cutting the divergence at criticality by 3D effects, we do find that at the QCP, $\xi^{-2}(T) \propto bT$. This correction is larger than T^2 term, but still it is nonuniversal and scales inversely with Λ .

Another widely used approach to the quantum-critical behavior near the antiferromagnetic instability explores the assumption that $\chi(\mathbf{q}, \omega)$ satisfies a temperature independent sum rule constraint $\int d^2q \chi(\mathbf{q}, \omega) = \text{const}$ [19]. One can easily demonstrate that for $z = 2$ dynamics at low-energies, the constraint implies that at the critical point, $\xi^{-2} = aT$ with a model independent, universal a [19,91]. This contradicts the analysis based on

the spin-fermion model. The most likely reason for the discrepancy is that the spin-fermion model is a finite U version of the Hubbard model, while the hard constraint is valid only at infinite U . Indeed, if U is finite, the no-double occupancy constraint is not exact, and there is a finite probability for two electrons to occupy the same site. The spin of this doubly occupied site can be either zero or one, i.e., the “length” of the spin at a given site is not fixed. From this perspective, it is likely that the sigma-model approach captures the physics at very large U , while our theory describes the physics at moderate $U \leq \Lambda$, when lattice effects (such as bT correction to ξ^{-2}) are irrelevant.

E. summary of Sec. VI

We now summarize what we obtained in this section

- i We found that the spin polarization operator at finite T has precisely the same form as at $T = 0$. There is no universal T dependent correction to the spin correlation length.
- ii We found that the $N = \infty$ theory for electronic self-energy at finite T is rather peculiar: the T dependent corrections from scattering on dynamical spin fluctuations (the ones with finite Matsubara frequency) have the same dependence on T as of frequency, i.e., they obey Ω/T scaling. In the quantum-critical regime, this correction scales as $\sqrt{T\bar{\omega}}$. At the same time, the piece in the self-energy from thermal scattering on static spin fluctuations yields impurity-like contribution $\Sigma(T) = i\pi\lambda T$ and still scales with the correlation length ξ . The still presence of ξ in the quantum-critical form of the self-energy is a serious artifact of the $N = \infty$ theory at a finite T .
- iii We demonstrated that this artifact disappears when calculations are performed at a finite N . First, we obtained the full form of the self-energy in the second-order perturbation theory, when intermediate fermions are treated as free particles. We found that at large frequencies, the static piece in the self-energy becomes independent on ξ , up to logarithmical factors. Then we demonstrated that for $T \ll N\omega_{sf}$, one can obtain in a controllable way the full $\Sigma''(\Omega)$, by explicitly including the $T = 0$ self-energy of intermediate fermions. At frequencies which exceed $\bar{\Omega} = N^2\omega_{sf}(v_F^2/v_x v_y)/36$, this self-energy obeys Ω/T scaling. We also found that for $T \geq \omega_{sf}$, this $\Sigma^{prime}(\Omega)$ has a dip at low frequencies which is likely an artifact of overestimation of the reduction of the static part of the self-energy at small but finite Ω . We argued that

the second-order result for the self-energy may be closer to reality at these T .

- iv We found that at small Ω , the controllable calculations of fermionic $\Sigma(\Omega)$ definitely break down when T exceeds $N\omega_{sf}$. For these temperatures, we performed FLEX-type calculations and found that the self-energy recovers $\sqrt{T\bar{\omega}}$ form, up to logarithmic corrections. These calculations are not controlled as the vertex renormalization and the renormalization of the Fermi velocity are $O(1)$. We argued, however, that these renormalizations affect logarithmic factors but not \sqrt{T} dependence.
- v Our finite N analysis indicates that at finite N , the fermionic self-energy likely possesses Ω/T scaling. At $T, \Omega > \omega_{sf}$, $\Sigma(\Omega, T)$ is linear in Ω and T at intermediate energies and crosses over to $\max(\Omega^{1/2}, T^{1/2})$ behavior at high energies. The peculiarity of large N is that the width of the intermediate range along T axis is by a factor of N larger than that along frequency axis.
- vi We found, however, that there is no ω/T scaling in the spin susceptibility, i.e., $\omega^{1-\eta}$ behavior at the QCP at $T = 0$ is not corroborated by the same temperature behavior of the spin correlation length. We argued that this difference is due to the fact that the anomalous dimension η emerges due to the presence of anomalies which are quantum effects.

VII. OPTICAL CONDUCTIVITY

In this section we use the results for the self-energy and study in detail the behavior of the optical conductivity.

The diagonal component of the optical conductivity is given by [80]

$$\sigma_{ii}(\omega) = \sigma_1(\omega) + i\sigma_2(\omega) = \frac{\omega_{pl}^2}{4\pi} \frac{1}{2\pi} \int d\theta \frac{\Pi_\sigma(\theta, \omega)}{i\omega - \delta} \quad (101)$$

where ω_{pl} is the plasma frequency, θ is the angle along the Fermi surface, and $\Pi_\sigma(\theta, \omega)$ is fully renormalized current-current correlator at zero momentum transfer.

Without vertex corrections, $\Pi_\sigma(\theta, \omega)$ is given by

$$\Pi_\sigma(\theta, i\omega_n) = \frac{Q}{\beta} \sum_m \int \frac{d^2k}{(2\pi)^2} G(\mathbf{k}, i\omega_n + i\omega_m) G(\mathbf{k}, i\omega_m) \quad (102)$$

The normalization factor Q has to be chosen such that in an ideal Fermi gas $\Pi(\omega) = 1$. The vertex corrections to Π_σ in our model are due to irreducible corrections to the current vertex. These corrections obviously scale with $d\Sigma/d\epsilon_k$ [80] and can be safely neglected. There are also corrections to Π_σ due to extra interactions which

are neglected in the spin-fermion model. Of particular relevance here is the residual p -wave type four-fermion interaction. This interaction give rise to RPA-type series of particle-hole bubbles [66,92]. How strong these corrections are is a priori unclear and has to be determined by experimental comparisons. We discuss this point in some detail in Sec X).

For a conventional dirty metal with $\Sigma(\mathbf{k}, \omega) = i\text{sign}\omega/2\tau$, Eq. (102) yields the Drude formula $\sigma(\omega) = (\omega_{pl}^2/4\pi)\tau/(1 - i\omega\tau)$. In our case, however, the fermionic self-energy strongly depends on frequency, and the behavior of $\sigma(\omega)$ is more complex.

For experimental comparisons, it is convenient to express the conductivity in terms of the generalized Drude model [10]

$$\sigma(\omega) = \frac{\omega_{pl}^2}{4\pi} \frac{\tau(\omega, T)}{m^*(\omega, T)/m - i\omega\tau(\omega, T)} \quad (103)$$

where the effective relaxation rate $\tau^{-1}(\omega)$ and the effective electron mass $m^*(\omega, T)$ depend on temperature and frequency. Both τ and m^* can be expressed in terms of σ_1 and σ_2 as

$$\tau^{-1}(\omega) = \frac{\omega_{pl}^2}{4\pi} [\text{Re}\sigma^{-1}(\omega)] \quad (104)$$

$$\frac{m^*}{m} = -\frac{1}{\omega} \frac{\omega_{pl}^2}{4\pi} [\text{Im}\sigma^{-1}(\omega)]. \quad (105)$$

Sometimes, the effective relaxation rate is also defined as

$$\frac{1}{\tau^*} = \omega \frac{\sigma_1}{\sigma_2} \quad (106)$$

We now obtain the explicit expression for $\sigma(\omega, T)$. Substituting the fermionic Green's functions into (102), using the spectral representation $G(\mathbf{k}, i\omega_m) = (1/\pi) \int dx \text{Im}G^R(\mathbf{k}, x)/(x - i\omega_m)$ to convert to real frequencies and retarded variables, and integrating over ϵ_k , we obtain after a simple algebra [93,94]

$$\Pi_\sigma^R(\theta, \Omega) = \int d\omega \frac{n_F(\omega + \Omega) - n_F(\omega)}{\Omega + \Sigma_{\omega+\Omega}^A - \Sigma_\omega^R} \quad (107)$$

where $\Sigma_\omega = \Sigma(\theta, \omega)$.

The relaxation rate is related to Π_σ^R by

$$\tau^{-1}(\omega) = \frac{\omega \text{Im} \langle \Pi_\sigma^R(\theta, \omega) \rangle}{(\text{Im} \langle \Pi_\sigma^R(\theta, \omega) \rangle)^2 + (\text{Re} \langle \Pi_\sigma^R(\theta, \omega) \rangle)^2} \quad (108)$$

where $\langle \dots \rangle = \int \frac{d\theta}{2\pi} \dots$ means averaging over the Fermi surface.

The angular dependence of the fermionic self-energy is due to the fact that both the coupling λ and spin relaxation frequency ω_{sf} depend on θ (see Eqn. (47); for small θ , \tilde{k} introduced in (47) is related to θ as $\tilde{k} = k_F\theta$).

One can easily make sure that the integral over θ is determined by $\theta = O(1)$, i.e., the conductivities at low ω and T predominantly come from the momenta away from hot spots. Strictly speaking, this implies that very close to criticality, our forms of the self-energy, obtained by expanding near hot spots, are inapplicable for the computations of the conductivity at small ω and T . Still, however, even at $\xi = \infty$, our formulas for the self-energy can be used to compute conductivity at frequencies above $\omega_{sf}(\theta_{max})$, as at these frequencies, the whole Fermi surface behaves as a hot spot. At small frequencies and $\xi \rightarrow \infty$, the critical behavior is affected by the instability in the pairing channel (see Sec. IX below), and has to be modified anyway.

Below we focus on the forms of conductivities at finite ξ when pairing fluctuations can be neglected. As we already said and will discuss in more detail in Sec X, at these ξ , the self-energy dependence on θ is modest and $\omega_{sf}(\theta_{max})$ is comparable to $\omega_{sf}(\theta = 0)$. In this situation, the θ dependence of the self-energy affects the numbers but not the functional forms of the conductivities. In the calculations below, we just neglect the θ dependence of Σ without further discussions. We now consider the behavior of conductivities at various frequencies and temperatures.

A. $T = 0$

At $T = 0$, there are three different frequency regimes: i) $\omega \ll \omega_{sf}$, ii) $\omega \geq \bar{\omega}$ and iii) $\omega \gg \omega_{sf}$. In the first regime, the fermionic self-energy has a Fermi-liquid form, $\Sigma^R(\omega) = \lambda\omega + i\lambda\omega^2/4\omega_{sf}$, and conductivities indeed also behave as in a Fermi liquid

$$\begin{aligned}
\sigma_1(\omega) &= \frac{\omega_{pl}^2}{24\pi} \left\langle \frac{\lambda}{(1+\lambda)^2\omega_{sf}} \right\rangle \\
\sigma_2(\omega) &= \frac{\omega_{pl}^2}{4\pi} \frac{1}{\omega} \left\langle \frac{1}{1+\lambda} \right\rangle \\
\tau^{-1}(\omega) &= \frac{\omega^2}{6} \frac{\langle \lambda / [(1+\lambda)^2\omega_{sf}] \rangle}{\langle 1/(1+\lambda) \rangle^2} \\
\frac{m^*}{m} &= \frac{1}{\langle 1/(1+\lambda) \rangle}
\end{aligned} \tag{109}$$

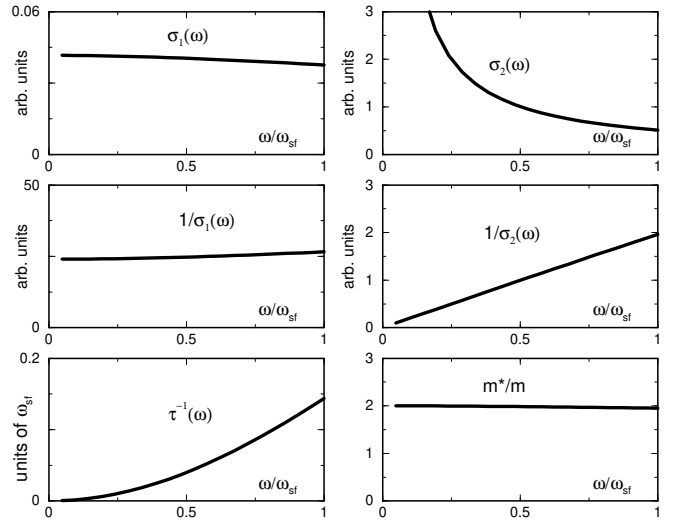


FIG. 23. Real and imaginary parts of conductivity, effective relaxation rate, and effective mass as functions of ω in the Fermi-liquid regime. For definiteness, we used $\lambda = 1$.

In Fig. 23 we plot the two conductivities, the effective relaxation rate and m^*/m at $\omega \leq \omega_{sf}$, obtained by solving (107) with some angular-independent, “average” λ and ω_{sf} . The Fermi-liquid forms are clearly visible at the lowest frequencies. We see, however, that the deviations from the Fermi-liquid behavior become visible already at $\omega \sim \omega_{sf}/2$. This is a consequence of the fact that the fermionic self-energy rapidly deviates from Fermi-liquid form at $\omega > \omega_{sf}/2$.

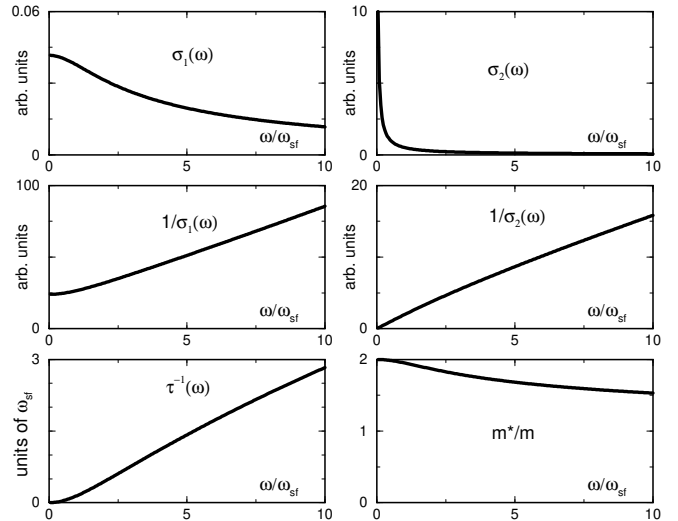


FIG. 24. Frequency dependence of σ_1 , σ_2 , $1/\tau$, and m^*/m at $T = 0$ at intermediate frequencies for $\lambda = 1$.

At intermediate $\bar{\omega} \gg \omega \geq \omega_{sf}$, the fermionic $\Sigma(\omega)$ can be approximated by a linear function of frequency up to $\sim 6 - 8\omega_{sf}$. This results in the linear in ω behavior of

$1/\tau$ and $1/\sigma_1$ In Fig. 24 we show the results for the conductivities, $1/\tau$ and m^*/m in this region. The linearities are clearly visible.

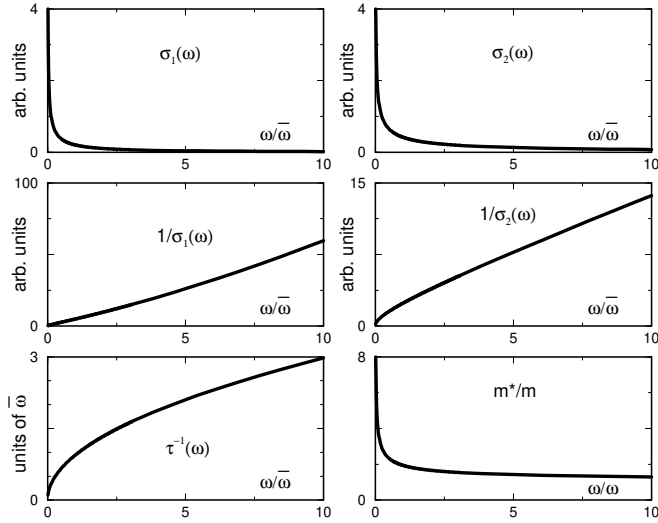


FIG. 25. Frequency dependences of σ_1 , σ_2 , $1/\tau$, and m^*/m at $T = 0$ as functions of $\omega/\bar{\omega}$ at $\omega \gg \omega_{sf}$. For simplicity, we set $\omega_{sf} = 0$.

Finally, at $\omega \gg \omega_{sf}$, $\Sigma^R(\omega) = \sqrt{\bar{\omega}/2|\omega|}(\omega + i|\omega|)$ becomes independent of θ i.e., the whole Fermi surface acts as a hot spot. In this limit, we obtained the exact expression for $\Pi_\sigma(\omega)$.

$$\Pi_\sigma^R(\omega) = 2 - a \frac{\pi}{2} + 4 \frac{a^2 - 1}{\sqrt{a^2 - 2}} \tan^{-1} \frac{(\sqrt{2} - 1)\sqrt{a^2 - 2}}{a + \sqrt{2}} \quad (110)$$

where $a = \sqrt{(i\omega - \delta)/\bar{\omega}}$. This expression can be simplified at $\omega \ll \bar{\omega}$ and $\omega \gg \bar{\omega}$ (i.e., at $a \ll 1$ and $a \gg 1$, respectively). At $\omega \ll \bar{\omega}$ the bare Ω term in the denominator of (107) is small compared to the fermionic self-energy, while at $\omega \gg \bar{\omega}$, the self-energy is smaller than Ω . At $\omega \ll \bar{\omega}$, i.e., $a \ll 1$, we have

$$\begin{aligned} \sigma_1(\omega) &\approx \frac{\omega_{pl}^2}{4\pi} \frac{A}{\sqrt{2\bar{\omega}\omega}} \\ \sigma_2(\omega) &\approx \sigma_1(\omega) \\ \tau^{-1}(\omega) &\approx \frac{1}{A} \sqrt{\frac{\omega\bar{\omega}}{2}} \\ \frac{m^*}{m} &\approx \frac{1}{\omega\tau} \end{aligned} \quad (111)$$

where $A = 2 - \sqrt{2} \log(\sqrt{2} + 1) \approx 0.754$. In the opposite limit, $\bar{\omega} \ll \omega$, i.e., $a \gg 1$, we have

$$\begin{aligned} \sigma_1(\omega) &\approx \frac{\omega_{pl}^2}{4\pi} \frac{2\sqrt{2}}{3} \frac{\bar{\omega}^{1/2}}{\omega^{3/2}} \\ \sigma_2(\omega) &\approx \frac{\omega_{pl}^2}{4\pi} \frac{1}{\omega} \end{aligned}$$

$$\begin{aligned} \tau^{-1}(\omega) &\approx \frac{4}{3} \sqrt{\frac{\omega\bar{\omega}}{2}} \\ m^*/m &\approx 1 \end{aligned} \quad (112)$$

The behavior of the conductivities, the relaxation rate and the effective mass at $\omega \gg \omega_{sf}$ and arbitrary $\omega/\bar{\omega}$ is shown in Fig.25. To emphasize the dependence on $\omega/\bar{\omega}$, we plotted the results right at $\omega_{sf} = 0$. Two features in Fig.25 worth mentioning. First, $1/\tau(\omega)$ scales as $\sqrt{\bar{\omega}}$ and virtually does not change between $\omega < \bar{\omega}$ and $\omega > \bar{\omega}$ (the two limiting results for $1/\tau$ are amazingly close to each other as to a good accuracy $1/A = 4/3!$). Second, $1/\sigma_1(\omega)$ initially (at $\omega \leq \bar{\omega}$) increases as $\sqrt{\bar{\omega}}$, but then remains linear in ω over a substantial frequency range and crosses over to $\omega^{3/2}$ behavior only at very large $\omega/\bar{\omega}$.

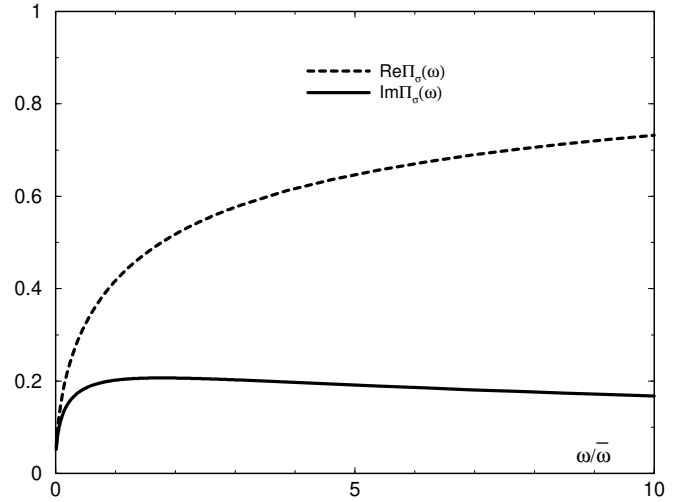


FIG. 26. Frequency dependence of $Im\Pi_\sigma(\omega)$ and $Re\Pi_\sigma(\omega)$ at $T = 0$ and $\omega_{sf} = 0$.

This behavior can also be extracted from the form of the polarization bubble presented in Fig. 26: we see that $Im\Pi_\sigma(\omega)$ first increases as $\sqrt{\bar{\omega}}$, but then nearly saturates at a value near 0.2 and very slowly decreases with increasing ω . It is amazing that $Im\Pi_\sigma(\omega)$ remains flat up to frequencies which by an order of magnitude exceed the lower boundary for $\sqrt{\bar{\omega}}$ behavior in the fermionic self-energy.

We now assemble the $T = 0$ results. For $\lambda \gg 1$, $\bar{\omega} = 4\lambda^2\omega_{sf} \gg \omega_{sf}$, and the scales $\bar{\omega}$ and ω_{sf} are well separated in the sense that the upper boundary of the linear behavior of the fermionic self-energy ($6 - 8\omega_{sf}$) is located below $\bar{\omega}$. In this situation, $\sigma_1^{-1}(\omega)$ is quadratic in ω at the lowest frequencies, becomes linear in ω at $\omega \sim \omega_{sf}/2$, then crosses over to $\sqrt{\bar{\omega}}$ behavior at $\omega \sim 6 - 8\omega_{sf}$, then again becomes linear at $\omega \sim \bar{\omega}$, and eventually behaves as $\omega^{3/2}$ at the highest $\omega \geq \bar{\omega}$. The last crossover is, however, only suggestive as it occurs at very high $\omega \sim 10^2\bar{\omega}$ when our low-energy theory is clearly inapplicable. The inverse σ_2 behaves as ω in the Fermi-liquid regime, changes slope

but remains linear at $\omega > \omega_{sf}$ then crosses over to $\omega^{1/2}$ behavior at $6 - 8\omega_{sf}$, and at higher frequencies behaves as ω . In the “ $\sqrt{\omega}$ ” regime, real and imaginary components of the conductivity are close to each other. The relaxation rate $1/\tau(\omega)$ is quadratic in frequency at the smallest frequencies, becomes linear in ω at $\omega \sim \omega_{sf}/2$, and crosses over to $\sqrt{\omega}$ form at $\omega \sim 6 - 8\omega_{sf}$. This behavior is schematically shown in Fig. 27.

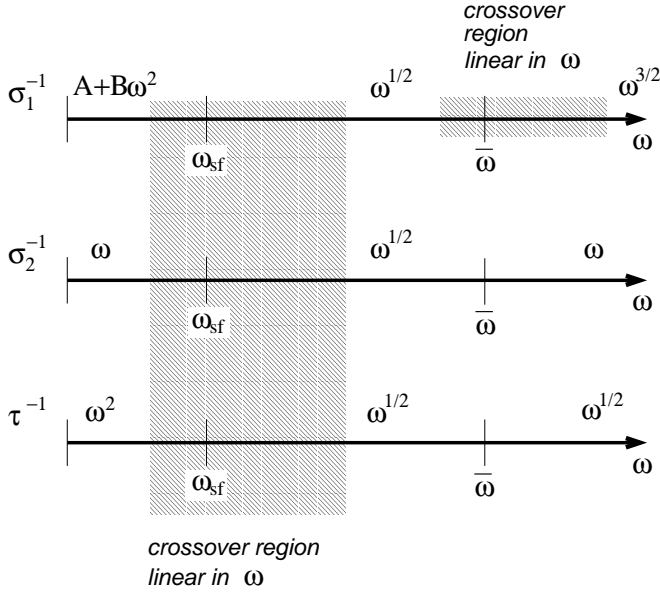


FIG. 27. A sketch of the sequence of crossovers for the two conductivities and the relaxation rate for $\lambda \gg 1$. The shaded regions are the extended crossover regimes. For $\lambda \sim 1$, the crossover region at $\omega \geq \omega_{sf}$ extends over $\bar{\omega}$. In this situation, the two regions of linear behavior of σ_1^{-1} merge. We found numerically that the slope of $\sigma_1^{-1}(\omega)$ does not change much between the two crossover regimes, i.e., $\sigma_1^{-1}(\omega)$ remains nearly linear in ω over a very wide frequency range.

We emphasize that that the behavior of conductivities at $\omega \gg \omega_{sf}$ is fully universal and depends only on the ratio $\omega/\bar{\omega}$ but not on the coupling λ (see Eq. (110)). In particular, at, e.g., $\omega \sim \bar{\omega}/2$,

$$\sigma_1 \approx 0.37 \frac{\omega_{pl}^2}{4\pi\bar{\omega}} \quad \sigma_2 \approx 1.76\sigma_1 \quad \frac{1}{\tau} \approx 0.66\bar{\omega} \quad \frac{m^*}{m} \approx 2.32 \quad (113)$$

For $\lambda \sim 1$, the upper cutoff for the linear behavior of fermionic self-energy exceeds $\bar{\omega}$. In this situation, there should be no intermediate $\sqrt{\omega}$ regime. Numerically, we found that $\Pi(\omega)$ does not change much with frequency between ω_{sf} and $\omega \geq \bar{\omega}$, i.e., the inverse conductivities and the relaxation rate remain linear in ω with little change of the slope over a wide frequency range.

For completeness, in Fig. 28 we present the results for the two conductivities for various λ . We see that while the functional forms of the conductivities do not change

much with λ , the ratio of σ_2/σ_1 indeed depends on λ . This dependence may be used as a guide for selecting λ which best fit the data.

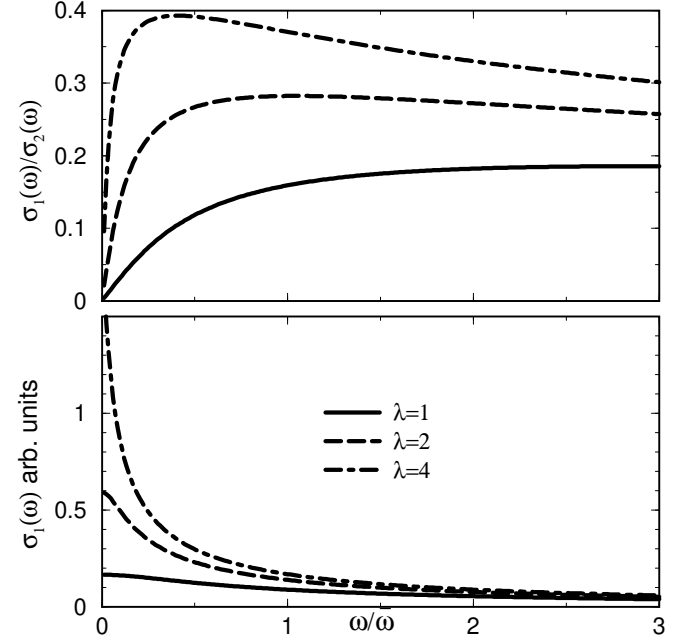


FIG. 28. Real and imaginary parts of the conductivity for various λ .

1. Sum rule for optical conductivity

The optical conductivity satisfies so-called f -sum rule [95] associated with the conservation of the number of carriers

$$\int_0^{\infty} \sigma_1(\omega) d\omega = \frac{\omega_{pl}^2}{4\pi} \quad (114)$$

This sum rule has a practical application as it is used to extract the plasma frequency ω_{pl} from the experimental data. The issue we consider is up to which frequency one has to integrate to satisfy the sum rule. We will demonstrate that the integral in (114) is poorly convergent, and one has to integrate up to an unexpectedly high frequency to get the right value of ω_{pl} .

The results of the numerical integration of the conductivity $\sigma_1(\omega)$ up to some frequency ω are presented in Fig. 29. We see that the convergence is very slow. This is related to the fact that over a very substantial frequency range, the imaginary part of the polarization bubble remains almost a constant (see Fig. 26), and hence $\sigma_1(\omega)$ scales as $1/\omega$ in which case the integral logarithmically depends on the upper cutoff in frequency integration. Only at very high $\omega \gg \bar{\omega}$, the conductivity crosses over to $\omega^{-3/2}$ behavior, and the integral over σ_1 converges.

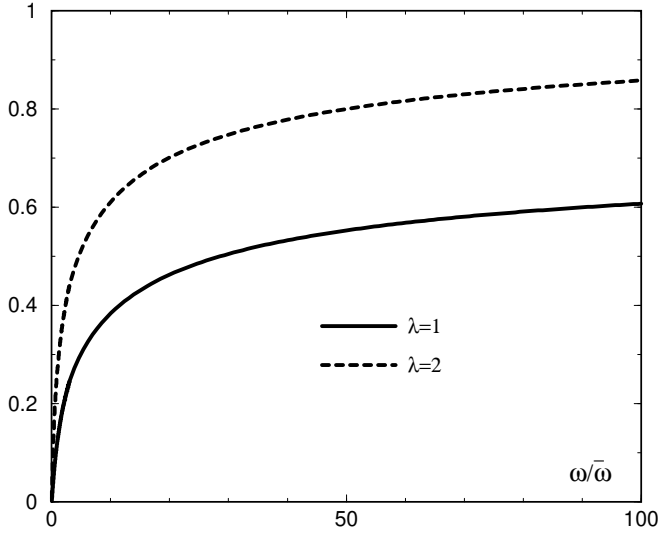


FIG. 29. The sum rule (114) as a function of the upper limit of integration. We used $T = 0$, $\lambda = 1$.

In cuprates, the value of the plasma frequency is normally obtained by integrating the measured $\sigma_1(\omega)$ up to about $2 - 2.5eV$ [10,96–99]. We will argue below that this scale roughly corresponds to about $10\bar{\omega}$ Fig 29 then indicates that the value of the plasma frequency extracted from these measurements is somewhat smaller than the actual value of ω_{pl} , the difference decreases with increasing λ .

B. finite T

We next consider the behavior of the optical conductivity at finite T . We begin with the limit $\omega \rightarrow 0$.

1. finite T , $\omega \rightarrow 0$

At finite T , $Im\Sigma(\omega)$ becomes finite at $\omega = 0$, and $\Pi_\sigma(\omega)$ at the lowest frequencies can be obtained by just expanding in ω in (107). Performing the expansion, we obtain

$$\begin{aligned}\sigma_1(T) &= \frac{\omega_{pl}^2}{4\pi} \frac{1}{8T} \int_{-\infty}^{\infty} \frac{1}{Im\Sigma_\omega^R} \frac{d\omega}{\cosh^2(\omega/2T)} \\ \tau^{-1}(T) &= \frac{\omega_{pl}^2}{4\pi} \sigma_1^{-1} \\ m^*/m &= \frac{\sigma_1^{-2}}{16T} \int_{-\infty}^{\infty} \frac{1 + \partial Re\Sigma_\omega^R/\partial\omega}{[Im\Sigma_\omega^R]^2} \frac{d\omega}{\cosh^2(\omega/2T)}\end{aligned}\quad (115)$$

Obviously, the typical frequency in these integrals is of order of temperature. At small $T \ll \omega_{sf}$, the self energy has the Fermi-liquid form (see Eq. (78)). The straightforward calculations then yield

$$\begin{aligned}\sigma_1(T) &= \frac{\omega_{pl}^2 \langle \omega_{sf} \rangle}{4\pi \cdot 6T^2} \\ \tau^{-1}(T) &= \frac{6T^2}{\langle \omega_{sf} \rangle} \\ m^*/m &= \frac{6}{\pi^2} \frac{\langle (1 + \lambda)\omega_{sf}^2 \rangle}{\langle \omega_{sf} \rangle^2} \left(1 + \frac{6}{\pi^2} \zeta(3) \right)\end{aligned}\quad (116)$$

where $\zeta(z)$ is Riemann zeta function.

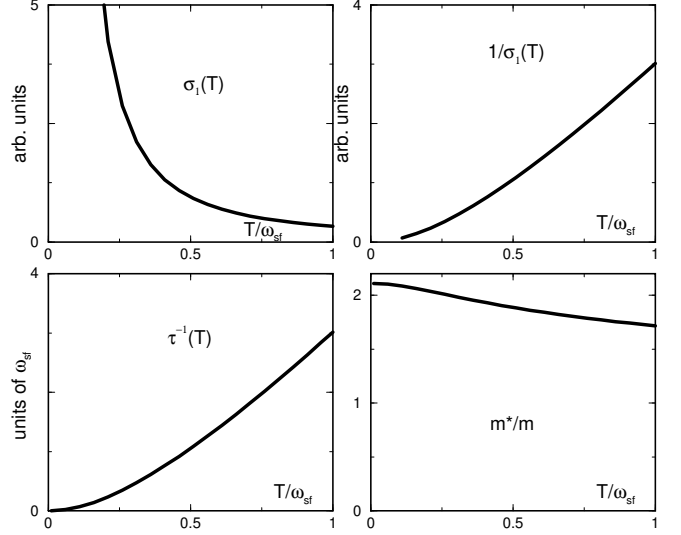


FIG. 30. Temperature dependences for σ_1 , σ_2 , $1/\tau$, and m^*/m at finite $T < \omega_{sf}$ and $\omega = 0$. We used $\lambda = 1$.

To obtain the conductivity at $T \gg \omega_{sf}$ we need as an input the self energy at $\omega \gg \omega_{sf}$. The dominant contribution to its imaginary part comes from static spin fluctuations. At $T \ll N\omega_{sf}$ which we assume to hold, this static piece is independent of frequency and just reduces to $\lambda\pi T$. Substituting this result into (115), we immediately obtain

$$\begin{aligned}\sigma_1(T) &\approx \frac{\omega_{pl}^2}{8\lambda\pi^2 T} \\ \tau^{-1}(T) &\approx 2\lambda\pi T\end{aligned}\quad (117)$$

We see that both σ_1^{-1} and τ^{-1} are linear in T , and the slopes scale with the coupling constant. The computation of the mass ratio requires more care as it involves $Re\Sigma_\omega^R$. For intermediate $\omega_{sf} \ll \omega \ll \bar{\omega}$, $\partial Re\Sigma_\omega^R/\partial\omega \gg 1$. Substituting $Re\Sigma_\omega^R$ into (115) and evaluating the frequency integral we obtain

$$m^*/m \approx 0.48\sqrt{\bar{\omega}/T}\quad (118)$$

In the opposite limit $\omega \gg \bar{\omega}$, $\partial Re\Sigma_\omega^R/\partial\omega \ll 1$. The integral in (115) is then trivially evaluated and yields

$$m^*/m \approx 1\quad (119)$$

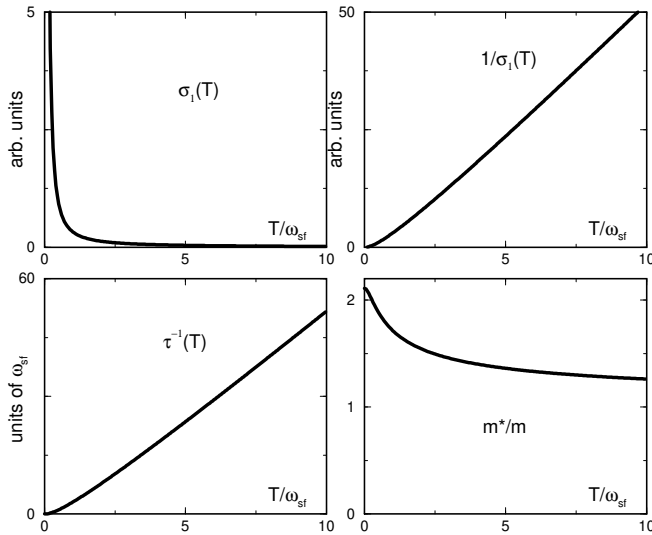


FIG. 31. Temperature dependences for $\sigma_1(T)$, $\rho(T) = 1/\sigma_1(T)$, $1/\tau$, and m^*/m at $\omega = 0$ and $T \geq \omega_{sf}$. We used $\lambda = 1$.

In Fig.31 we present the results for the dc conductivity, resistivity, relaxation rate and the mass ratio at $T \geq \omega_{sf}$. We see that although the asymptotic “high temperature” behavior of the conductivity and the relaxation rate, Eq. (117) is reached only at rather high temperatures, the linear in T behavior of σ_1^{-1} and τ^{-1} (and, accordingly, the linear in T behavior of the resistivity) begins already at a low $T \sim \omega_{sf}$ and over a wide temperature range can be well approximated by $AT - B$ where A is somewhat smaller than in (117), and B is a small positive number.

2. finite T , finite ω

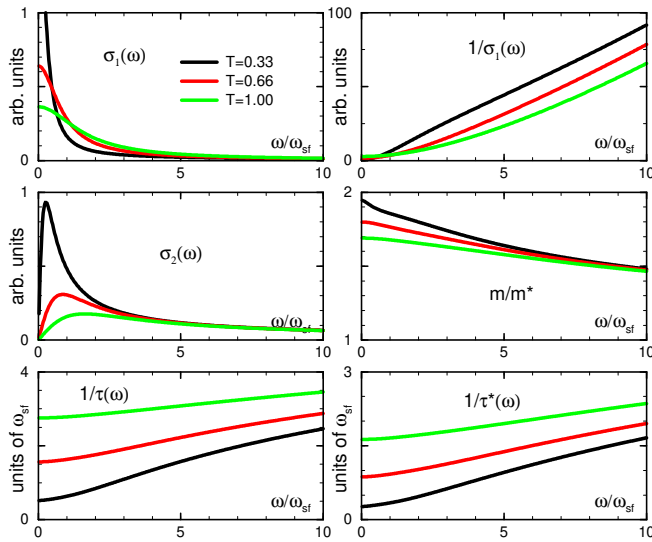


FIG. 32. Frequency dependence of the conductivities, inverse σ_1 , mass ratio and the relaxation rates $1/\tau$ and $1/\tau^*$ at different temperatures. We used $\lambda = 1.7$. The results were obtained with the second-order self-energy (see Fig20).

Finally, in Fig. 32 we present the results for the conductivities, the mass ratio, and the relaxation rates $1/\tau$ and $1/\tau^*$ when both frequency and temperature are finite. We see that for any T , the inverse conductivity σ_1 is still linear in ω over a substantial frequency range, and the slope is almost independent of T . Observe also that the conductivity curves for various T cross each other such that at small ω , conductivity decreases with T , while at large ω it increases with the temperature. The conductivities in Fig. 32 are obtained with the second-order fermionic self-energy (its imaginary part is plotted in Fig. 20). We verified that if we use the “full” self-energy (218), we obtain almost identical results for the conductivities, mass ratio and relaxation rates.

C. summary of Sec. VII

We now summarize the main results of this section

1. At $T = 0$, real and imaginary parts of the optical conductivity, $\sigma_1(\omega)$ and $\sigma_2(\omega)$, and the effective scattering rate $1/\tau(\omega)$ undergo a series of crossovers schematically shown in Fig 27. In particular, for moderate couplings, σ_1^{-1} and σ_2^{-1} are linear in ω over a substantial frequency range. The relaxation rate $1/\tau$ is also linear in ω but over a smaller range of frequencies, and then crosses over to $\sqrt{\omega}$ behavior.
2. We found that the f -sum rule for σ_1 is recovered only if the integration in $I(\omega) = \int_0^\omega \sigma_1(x)dx$ is extended up to extremely high frequencies. If the integration is performed up to frequencies about 10 times larger than $\bar{\omega}$, $I(\omega)$ saturates (see Fig. 29) at some intermediate value which depends on λ . The implication of this result for experiments is that ω_{pl} extracted from integrating up to a particular cutoff is somewhat smaller than the actual plasma frequency.
3. At finite T , the most important features are the development of the peak in $\sigma_2(\omega)$ at ω comparable to T , and the crossing between $\sigma_1(\omega)$ curves at different T : the conductivity at the lowest T is the largest at the smallest ω , but become the smallest at larger ω (see Fig. 32). The relaxation rate on the other hand do not display this kind of behavior.
4. The effective mass m^* is by a factor $1 + \lambda$ larger than the bare electron mass, but the ratio m^*/m decreases with increasing frequency and temperature.

VIII. OTHER OBSERVABLES

In this section, we briefly discuss the behavior of other observables - the fermionic density of states, the NMR relaxation rate and the Raman intensity.

A. fermionic density of states

The fermionic density of states (DOS) is given by

$$N(\omega) = \frac{1}{\pi} \sum_k |\text{Im}G(\mathbf{k}, \omega)| \quad (120)$$

Assume for simplicity that the Fermi surface is circular. Then we can split momentum integration into the integration over $d\theta$ along the Fermi surface, and over $d\epsilon_k = v_F dk_\perp$, where k_\parallel is a momentum component along the Fermi surface. Substituting $G^{-1}(\mathbf{k}, \omega) = \omega + \Sigma(k_\parallel, \omega) - \epsilon_k$ and integrating over $d\epsilon_k$ first we obtain that

$$N(\omega) = \text{const} \quad (121)$$

independently of the strength of the fermionic self-energy. It is only essential that the self-energy does not depend on ϵ_k .

For more complex Fermi surface, $N(\omega)$ does acquire some frequency dependence which, however, is completely unessential from physics perspective. Also, Eq. (121) is indeed only valid at frequencies much smaller than the fermionic bandwidth, when one can linearize the fermionic dispersion near the Fermi surface. At frequencies comparable to bandwidth, $N(\omega)$ curves down and eventually vanishes.

B. neutron scattering and NMR relaxation rate

The neutron scattering measures the dynamical structure factor $S(\mathbf{q}, \omega) = (1 + 2n_B(\omega))\chi''(\mathbf{q}, \omega)$. Substituting the expression for the susceptibility, Eqs (18), (20), we obtain

$$S(\mathbf{q}, \omega) = \frac{\chi_0 \xi^2}{\omega_{sf}} \frac{\omega(1 + 2n_B(\omega))}{(1 + \xi^2(\mathbf{q} - \mathbf{Q})^2) + (\omega/\omega_{sf})^2} \quad (122)$$

At $\omega \gg T$, the Bose factor is irrelevant, $S(\mathbf{q}, \omega)$ at a given q has a simple $x/(1 + x^2)$ form where $x = \omega/(\omega_{sf}(1 + \xi^2(\mathbf{q} - \mathbf{Q})^2))$ is a rescaled frequency.

The NMR relaxation rate $1/T_1$ is proportional to the momentum integral of $S(\mathbf{q}, \omega)$ weighted with the momentum dependent formfactor $F(\mathbf{q})$ [27]:

$$T_1^{-1}(\omega) \propto \sum_q F(\mathbf{q})S(\mathbf{q}, \omega) \quad (123)$$

The typical frequencies in the NMR experiments are in the range of few MHz ($\sim 10^{-4}K$), hence $T \gg \omega$ for all reasonable T . Then $1 + 2n_B(\omega) \approx 2T/\omega$, and

$$T_1^{-1} \propto 2T \lim_{\omega \rightarrow 0} \sum_q F(\mathbf{q}) \frac{\chi''(\mathbf{q}, \omega)}{\omega} \quad (124)$$

The form factor $F(\mathbf{q})$ depends on the local environment of the isotope atom. For *Cu* NMR, $F(\mathbf{q})$ does not vanish at $\mathbf{Q} = (\pi, \pi)$. Substituting $\chi''(\mathbf{q}, \omega)$ into (124), one can easily check that the momentum integration in (124) is then confined to small $|\mathbf{q} - \mathbf{Q}| \sim \xi^{-1}$, and hence

$$\frac{1}{T_1 T} \approx \frac{F(\mathbf{Q})\chi_0}{4\pi\omega_{sf}} \quad (125)$$

As the product $F(\mathbf{Q})\chi_0$ can be extracted independently from Knight shift data [27], the measurements of $1/T_1$ allow one to determine ω_{sf} which, we remind, is one of the two input parameters in our theory.

C. Raman intensity

Another observable sensitive to the form of the fermionic self-energy is the intensity of the Raman absorption. In a Fermi gas, a transferred photon energy ω can be absorbed by a metal only if ω is smaller than $v_F|q|$ when q is a transferred momentum (this is the Fermi golden rule) [100]. As photon momentum is vanishingly small, the absorption is possible only for extremely small $\omega \sim \omega_{in}v_F/c$ where ω_{in} is the incident photon frequency, and c is the velocity of light. However, if fermions have a nonzero $\text{Im}\Sigma$, the absorption is possible for all frequencies: the energy extracted from photons is dissipated due to a finite lifetime of fermionic excitations.

The intensity of the (non-resonance) Raman absorption $R(\omega)$ is generally proportional to the imaginary part of the particle-hole bubble at zero external momentum and finite frequency, weighted with the form-factors which depend on the scattering geometry [101,102]. For the most studied B_{1g} scattering, the form-factor $F_R(\mathbf{k}) \propto \cos k_x - \cos k_y$ is at maximum near hot spots, and can be approximated by a constant. The Raman intensity is then simply given by

$$R(\omega) \propto \text{Im}\Pi_R(\omega) \quad (126)$$

The Raman bubble $\Pi_R(\omega)$ differs from $\Pi_\sigma(\omega)$ as side vertices are now scalars. As we discussed in Sec. IV, a scalar vertex with zero total momentum is subject to strong vertex corrections. For a density-density correlator with momentum independent vertices, vertex corrections fully cancel fermionic self-energy, and as a result there is no dissipation [103]. [This cancellation is the consequence of the fact that the number of particles is conserved]. However, for B_{1g} Raman scattering, the side vertex has d -wave symmetry, and the renormalization of the vertex requires a d -wave component of the interaction. In this situation, there is no exact relation between

fermionic self-energy and vertex corrections. We explicitly verified that for magnetically-mediated scattering, the correction to the B_{1g} Raman vertex is nonsingular even when $\xi \rightarrow \infty$. Neglecting this nonsingular vertex renormalization, we obtain a simple relation between the normal state Raman intensity and the normal state conductivity:

$$R(\omega) \sim \omega \sigma_1(\omega). \quad (127)$$

In particular, at $T = 0$, $R(\omega) \propto \omega$ at small frequencies, then saturates, then crosses over to $R(\omega) \propto \sqrt{\omega}$, and then (if lattice effects do not interfere) first saturates and then begins decreasing as $\omega^{-1/2}$. This last regime, however, is likely already masked by the development of a “two-magnon” peak from short-range spin fluctuations [104].

IX. PAIRING VERTEX

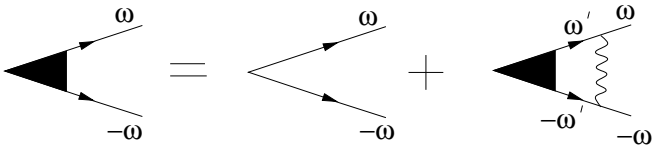


FIG. 33. The diagram for the full vertex in the particle-particle channel. The bare (unshaded) vertex is infinitesimally small. The wavy line is the spin propagator. Since the spin-mediated interaction is retarded, the full vertex depends on frequency ω .

Finally, we briefly discuss the development of the pairing instability in the spin-fermion model. It is customary for the analysis of the pairing problem to introduce an infinitesimally small particle-particle vertex $g_{pp}^0(k, -k) \equiv g_{pp}^0(k)$ and study its renormalization by magnetically mediated interaction. The corresponding diagram is presented in Fig 33. The temperature where the renormalized vertex diverges is obviously the onset of pairing. The magnetically-mediated pairing interaction is repulsive for s -wave pairing, but is attractive in the $d_{x^2-y^2}$ channel [17,25]. Accordingly, we will be searching for a d -wave solution for the full pairing vertex $g_{pp}(k)$. For momenta near hot spots, the d -wave constraint implies that $g_{pp}(k + Q) = -g_{pp}(k)$.

We demonstrate in this section that the renormalization of the pairing vertex is not a $1/N$ effect, and hence the pairing instability is possible even in the limit when $N \rightarrow \infty$, when our Eliashberg-type theory becomes exact.

For a particle-hole vertex with a nonzero momentum transfer, the $1/N$ smallness of the vertex renormalization comes from the fact that for large N , the momentum dependence of the spin susceptibility can be neglected, and the vertex correction is a convolution of the two fermionic

densities of states and the dynamical spin susceptibility at momentum \mathbf{Q} . The latter contains N in the denominator, and this gives rise to the overall $1/N$ factor in the correction to a particle-hole vertex. For zero momentum transfer, the $1/N$ does not appear, but as we discussed in Sec IV D, this is the consequence of the fact that the momentum integral is singular and has to be properly regularized.

For a particle-particle vertex, the situation is different as now vertex renormalization involves fermions with opposite momenta and frequencies, and hence at a given frequency, the poles in the two fermionic propagators are located in different half-planes of ϵ_k . As a result, there is no double pole in the momentum integral. The latter in turn implies that at $N \rightarrow \infty$, one can again factorizing the momentum integration i.e., neglect in the spin susceptibility the momentum component transverse to the Fermi surface. Still, however, one *has to* integrate the susceptibility over the momentum component along the Fermi surface. This last procedure changes the power of $1/N$ in the denominator such that eventually $1/N$ is eliminated from the equation for $g_{pp}(k)$ (see below).

Two of us and Finkel'stein have demonstrated explicitly [40] that for relevant k near each of hot spots, the momentum variation of $g_{pp}(k)$ is irrelevant and can be neglected. The momentum integration then can be performed explicitly, and at $T = 0$ we obtain

$$\frac{\delta g_{pp}}{g_{pp}^0} \propto \frac{3g^2}{8\pi^2 v_F} \int \frac{d\omega_m}{|\omega_m - i\Sigma(\omega_m)|} \chi_L(\omega_m - \Omega_m) \quad (128)$$

where Ω is the external frequency ($g_{pp} = g_{pp}(\Omega, -\Omega)$), and $\chi_L(\omega) = \pi\chi_0\xi/(1 + |\omega|/\omega_{sf})^{1/2}$ is the “local” 1D susceptibility obtained by integrating over momentum component along the Fermi surface and neglecting $\mathbf{q} - \mathbf{Q}$ transverse to the Fermi surface. Substituting this susceptibility into (128), we obtain

$$\frac{\delta g_{pp}}{g_{pp}^0} = \frac{1}{4} \int \frac{d\omega_m}{\omega_m} \frac{\sqrt{\omega_{sf}} + \sqrt{\omega_{sf} + |\omega_m|}}{\sqrt{\omega_{sf} + |\omega_m - \Omega_m|}} \frac{2\lambda}{1 + (2\lambda) + \sqrt{1 + |\omega_m|/\omega_{sf}}} \quad (129)$$

We see that the vertex correction is positive, i.e., the addition of a spin-fluctuation exchange enhances the particle-particle vertex. Rescaling frequency as $x = \omega/\omega_{sf}$ we immediately find that $\delta g_{pp}/g_{pp}^0$ depends only on N -independent effective coupling λ . The origin of this result is rather transparent in the quantum-critical regime $\omega_m \gg \omega_{sf}$. Here $\chi_L \propto \sqrt{\omega_{sf}/\omega_m}$ scales as $(1/N)^{1/2}$. Simultaneously,

$$\omega_m - i\Sigma(\omega_m) \approx \sqrt{\omega_m \bar{\omega}} \sim \lambda \omega_m \sqrt{\frac{\omega_{sf}}{\omega_m}} \quad (130)$$

also scales as $(1/N)^{1/2}$. Taking the ratio of the two expressions we obtain N -independent result

$$\frac{g^2}{v_F} \frac{\chi_l(|\omega_m - \Omega_m|)}{\omega_m - i\Sigma(\omega_m)} \sim \frac{1}{\omega_m} \left(\frac{\omega_m}{|\omega_m - \Omega_m|} \right)^{1/2}. \quad (131)$$

Another issue is how large is the pairing instability temperature. For $\lambda \leq 1$, the answer is rather obvious as the pairing problem is very similar to the BCS phonon problem with ω_{sf} playing the same role as the Debye frequency for phonons. Indeed, when $\lambda \leq 1$, ω_{sf} in (129) provides a natural upper cutoff for the frequency integral. Extending Eq. (129) to finite T in a standard way and evaluating the frequency sum with logarithmical accuracy, we obtain

$$\frac{\delta g_{pp}}{g_{pp}^0} = \frac{\lambda}{1 + \lambda} \log \frac{\omega_{sf}}{T} \quad (132)$$

Obviously then, $T_{ins} \propto \omega_{sf} \exp^{-(1+\lambda)/\lambda}$. This is similar to the McMillan formula for phonons [105]. The $1 + \lambda$ factor in the numerator accounts for the mass renormalization at frequencies below ω_{sf} .

Eq. (132) is formally valid for all couplings λ provided that the pairing problem is *confined* to a region $\omega \leq \omega_{sf}$ where the system has a Fermi-liquid behavior. However, we see from (129) that the pairing kernel preserves $1/\omega$ form also at frequencies larger than ω_{sf} and crosses over to $1/\omega^{3/2}$ form only at $\omega > \bar{\omega}$. For $\bar{\omega} \gg \omega_m \gg \omega_{sf}$, we have from (129)

$$\frac{\delta g_{pp}}{g_{pp}^0} = \frac{1}{4} \int \frac{d\omega_m}{\sqrt{|\omega_m(\omega_m - \Omega_m)|}} \quad (133)$$

Alternatively speaking, the kernel for the pairing problem remains $O(1/\omega)$ not only in the Fermi-liquid regime, but also in the quantum-critical regime where the system does not behave as a Fermi-liquid. This implies that T_{ins} in principle can be of order $\bar{\omega}$, i.e., substantially higher than in the McMillan formula. This is not guaranteed, however, as the pairing kernel in (129) depends on both internal and external frequency, and the logarithm in the r.h.s. of (133) is cut by Ω_m . In the latter case, the ladder series are not geometrical, and there is no a priori guarantee that they yield an instability at $T \sim \bar{\omega}$.

The full analysis of the pairing problem requires extra care and is beyond the scope of the present paper. We just cite the result [40]: the instability temperature T_{ins} does scale with $\bar{\omega}$ at strong coupling, and saturates at $T_{ins} \approx 0.17\bar{\omega}$ at $\xi = \infty$. Numerically, the saturation of T_{ins} was detected in Ref. [106]. The behavior below T_{ins} is rather involved, as we discussed in the Introduction (see Fig. 4).

Note in passing that the studies of the pairing instability at the verge of the magnetic transition yield rather nontrivial results also when the pairing is mediated by ferromagnetic spin fluctuations [107].

The fact that the pairing instability temperature scales with $\bar{\omega}$ which, we remind, is the upper cutoff frequency

for the quantum-critical behavior, implies that our normal state analysis which neglects pairing channel is valid only in a restricted frequency and temperature range. Still, however, numerically $T_{ins} \ll \bar{\omega}$, and hence there exists a wide region of frequencies/temperatures where normal state quantum-critical analysis is valid. A related issue is how strong are the pairing fluctuations above T_{ins} . We show below that the pairing susceptibility has an overall factor $1/N$ and hence pairing fluctuations only affect fermionic self-energy in a narrow range near T_{ins} . Outside this region, they contribute only $1/N$ corrections to the fermionic self-energy and hence do not affect our $N = \infty$ analysis.

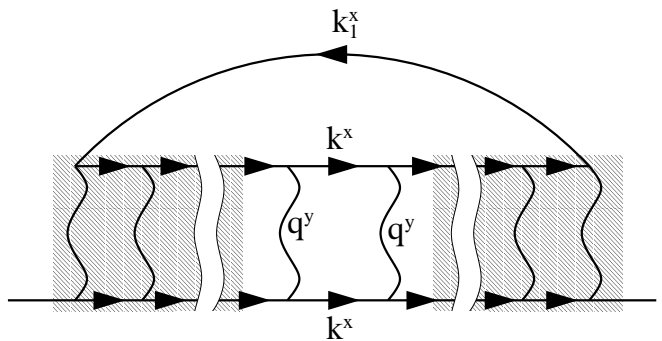


FIG. 34. The diagram for the correction to the electronic self-energy due to fluctuations in the pairing channel.

The corrections to the electronic self-energy due to pairing fluctuations are shown diagrammatically in Fig 34. Consider first the shaded regions in Fig. 34. Each time we add an extra bosonic line to the ladder, we also add two fermionic lines. As we demonstrated above, this addition does not contribute extra powers of $1/N$. The $1/N$ factor comes from the unshaded part of this diagram. It contains a pair of fermionic propagators, and a *pair* of bosonic propagators, i.e., it contains an extra bosonic propagator compared to the building block in the shaded part of the diagram. The bosonic propagator scales as $1/N$ as there are N channels for spin decay. We explicitly verified that this $1/N$ appears as the overall factor in the diagram, i.e.,

$$\Sigma_{pp}(\Omega) \propto \sqrt{\omega\bar{\omega}} \frac{\Gamma}{N} \quad (134)$$

where Γ is the enhancement factor from the shaded part of the diagram. The divergence in Γ implies pairing instability and obviously affects fermionic self-energy. However as long as $\Gamma \leq N$, $\Sigma_{pp}(\Omega)$ has a prefactor of $1/N$, and can be neglected in the limit $N \rightarrow \infty$.

A final comment. The pairing instability at a finite T_{ins} at $\xi = \infty$ obviously implies that there exists a dome on top of the magnetic quantum critical point. Inside this dome, the quantum-critical theory has to be reconsidered as the fermions near hot spots become gaped. In other

words, the quantum-critical behavior which causes the pairing instability at a finite T_{ins} by itself gets affected as a feedback from the pairing. In particular, we explicitly verified that the correction to the spin-fermion vertex is saturated at finite value below T_{ins} , i.e., it is no longer logarithmically singular. This, in particular, implies that the anomalous magnetic response in the quantum-critical regime, which we found in Sec. V exists only at intermediate energies and cannot be extended to the lowest ω (which fall inside the dome). The quantum-critical behavior inside the dome is a subject of a separate study and we will not discuss it here.

X. SUMMARY AND EXPERIMENTAL COMPARISONS

In this paper, we presented the full scale calculations for the normal state properties of the spin-fermion model. The model involves low-energy fermions interacting with their own spin collective excitations which are assumed to be peaked at the antiferromagnetic momentum $\mathbf{Q} = (\pi, \pi)$. We argued that this model is the low-energy version of the lattice, Hubbard-type models for strongly interacting fermions, provided that the spin fluctuations are the only low-energy collective bosonic excitations. The model indeed makes sense only if the spin-fermion coupling does not exceed fermionic bandwidth which we assume to hold. If this condition is not satisfied, the separation between low-energy and high-energy excitations becomes problematic.

We demonstrated that near magnetic instability, the model falls into the strong coupling limit, where the conventional perturbation theory does not work. The corrections to the Fermi-gas behavior are the strongest for fermions near hot spots - the points at the Fermi surface separated by antiferromagnetic \mathbf{Q} . The presence of hot spots is essential for our study - without them the critical theory at $T = 0$ would have had a different dynamical exponent $z = 1$.

We developed a controlled way to perform calculations in the strong coupling limit by expanding in $1/N$ where $N (= 8$ for the physical case) is the number of hot spots in the Brillouin zone. Equivalently, one can extend the model to a large number of electron flavors M and expand in $1/M$.

Our major results are summarized in Figs. 11 and 20 for the fermionic spectral function, and Fig. 32 for optical conductivity. For the dynamical structure factor, our major result is Eqn (67). We demonstrated that near the QCP, the dimensionless spin-fermion coupling $\lambda \propto \xi$ is large, i.e., the system falls into the strong coupling regime. This strong coupling behavior can also be reached at intermediate ξ when the spin-fermion interaction \bar{g} increases.

At strong coupling, the region near the QCP is divided into the Fermi liquid regime and the quantum-critical regime where the system behavior is the same as at criticality. The quantum-critical behavior extends roughly up to frequencies comparable to the spin-fermion coupling constant \bar{g} . The crossover from the Fermi liquid to the quantum-critical behavior on the other hand occurs at energies of order $\omega_{sf} \sim \lambda^{-2}\bar{g} \ll \bar{g}$. We found that there is a single crossover energy for both electronic and magnetic properties of the system.

We now list the catalog of our key results. We first list the results at $T = 0$ and then show how they are modified at finite T .

A. $T = 0$

1. Fermi-liquid regime

In the Fermi-liquid regime, we found for the fermionic self-energy

$$\Sigma(k, \Omega) = \Omega\lambda(k) + i\lambda(k)\frac{\Omega|\Omega|}{4\omega_{sf}(k)} \quad (135)$$

The momentum-dependent coupling constant $\lambda(k)$ and $\omega_{sf}(k)$ are given by

$$\lambda(k) = \lambda/(1 + (\tilde{k}\xi)^2)^{1/2}, \quad \omega_{sf}(k) = \omega_{sf}(1 + (\tilde{k}\xi)^2) \quad (136)$$

where \tilde{k} is the deviation from a hot spot along the Fermi surface ($\tilde{k} = \epsilon_{k+Q}/v_F$). These Fermi liquid forms are valid when $\Omega < \omega_{sf}(k)$. Obviously, the self-energy corrections are the largest for fermions near hot spots. For the same frequencies, we found that the spin susceptibility near the antiferromagnetic momentum \mathbf{Q} can be well approximated by its static form

$$\chi(\mathbf{q}, \omega) \approx \frac{\chi_0\xi^2}{1 + (\mathbf{q} - \mathbf{Q})^2\xi^2} \quad (137)$$

In this limit, $\sigma_1(\omega)$ weakly depends on ω , and $\sigma_2(\omega)$ scales as ω^{-1} .

2. quantum-critical regime, intermediate frequencies

At intermediate frequencies $\omega_{sf}(k) \leq \Omega \leq 6 - 8\omega_{sf}$, we found that to a surprisingly good accuracy, the imaginary part of the fermionic self-energy is linear in frequency:

$$\Sigma''(k, \Omega) \approx 0.3\lambda(k)(\Omega - 0.7\omega_{sf}) \quad (138)$$

Note, however, that this behavior is *not* an intermediate asymptotic which width could be controlled by some parameter of a system, but rather a peculiar behavior

in a wide crossover region between truly Fermi-liquid and truly quantum-critical (high frequency) regimes. The real part of the self-energy $\Sigma'(k, \Omega)$ roughly follows $\omega \log |\omega|$ behavior which is the Kramers-Kronig transform of (138), but this form is only approximate as the linearity in Σ'' exists only in a limited frequency range.

At frequencies larger than ω_{sf} , one also has to use the full expression for the dynamical spin susceptibility as neither the gap in the static susceptibility nor the dynamical piece can be neglected

$$\chi(\mathbf{q}, \omega) = \frac{\chi_0 \xi^2}{1 + (\mathbf{q} - \mathbf{Q})^2 \xi^2 - i|\omega|/\omega_{sf}} \quad (139)$$

Finally, at these frequencies, both $\sigma_1(\omega)$ and $\sigma_2(\omega)$ scale as $1/\omega$.

3. quantum-critical regime, high frequencies

At high frequencies, $\Omega \sim \bar{\omega} \gg \omega_{sf}(k)$, the whole Fermi surface behaves as a hot spot. We found that in this regime, the fermionic self-energy scales as $\sqrt{\omega}$:

$$\Sigma(\Omega) = e^{i\frac{\pi}{4}} \sqrt{\bar{\omega} |\Omega|} \text{sign} \Omega \quad (140)$$

This form of the self-energy implies that fermionic Green's function $G^{-1}(k, \Omega) \propto (i\Omega - \epsilon_k^2/\bar{\omega})$. Comparing this with the Fermi liquid result $G^{-1}(k, \Omega) \propto \Omega - \epsilon_k/(1 + \lambda(k))$, we see that as the system crosses over to the quantum-critical regime, the pole in the fermionic propagator gradually moves from the real frequency axis onto the imaginary axis. The pole along imaginary axis implies that fermions are completely overdamped and can only propagate diffusively.

Simultaneously, the dynamic spin susceptibility acquires a strong frequency dependence which also gives rise to the diffusive behavior near $q = Q$:

$$\chi(\mathbf{q}, \omega) \approx \frac{\chi_0}{(\mathbf{q} - \mathbf{Q})^2 - i|\omega|\gamma} \quad (141)$$

where $\gamma = (\omega_{sf} \xi^2)^{-1}$ is independent of ξ . Alternatively speaking, both fermionic and spin excitations are diffusive at $\omega \sim \bar{\omega} \gg \omega_{sf}$.

Finally, in the true quantum-critical regime $\sigma_1(\omega)$ interpolates between $\omega^{-1/2}$ at $\omega < \bar{\omega}$, and $\omega^{-3/2}$ at the highest frequencies. The imaginary part of conductivity interpolates between $\omega^{-1/2}$ for $\omega < \bar{\omega}$ and ω^{-1} for $\omega > \bar{\omega}$. We found that the crossover region for $\sigma_2(\omega)$ is rather narrow, but that for $\sigma_1(\omega)$ is very wide, and in a wide range of frequencies $\omega > \bar{\omega}$, $4\pi/\omega_{pl}^2 \sigma_1(\omega)$ is close to $0.2\omega^{-1}$.

4. quantum-critical point

Finally, we analyzed the forms of the self-energy and the spin susceptibility when $\omega_{sf} \rightarrow 0$, and for fermions

near hot spots the quantum-critical behavior extends down to the lowest frequencies. In this limit, there exists a wide frequency range where on one hand $\omega \gg \omega_{sf}$, and on the other hand $\omega \ll \bar{\omega}$, i.e., a truly *low-energy* quantum-critical regime. We found that in this regime, Eqs (140) and (141) are modified by subleading, $\log(\omega/\bar{\omega})$ terms in the perturbation series. We studied the effects of extra logarithms in the one-loop RG theory assuming that the number of hot spots N is large and neglecting nonlogarithmic corrections in $1/N$ ($N = 8$ in real situation). We found that the spin dynamics is still described by the dynamical exponent $z = 2$, but the dynamical susceptibility acquires an anomalous dimension:

$$\chi(\mathbf{q}, \omega_m) \propto (\gamma|\omega_m| + (\mathbf{q} - \mathbf{Q})^2)^{-1+\eta} [\log(\gamma|\omega_m| + (\mathbf{q} - \mathbf{Q})^2)]^{-v_y/3v_x} \quad (142)$$

where $\eta = 2/N = 0.25$, and v_y and v_x are the components of the bare Fermi velocity near hot spots: $\epsilon_k = v_x k_x + v_y k_y$; $\epsilon_{k+Q} = -v_x k_x + v_y k_y$. The appearance of a finite η is the consequence of the fact that the spin-fermion model contains anomalies which give rise to a complex structure of the four-boson vertex at the QCP. In this respect, our theory differs from the effective bosonic ϕ^4 theory, which is marginal in $d = 2$ since $z + d = 4$.

The fermionic self-energy is not affected by the anomalous dimension η and differs from (140) only by a logarithmic factor:

$$\Sigma(\Omega_m) \propto |\Omega_m|^{1/2} |\log \Omega_m|^{-1/2} \quad (143)$$

Finally, the Fermi velocity is also logarithmically renormalized in the quantum-critical region:

$$v_x^R = v_x \left(1 + \frac{24L v_y}{\pi N v_x}\right)^{1/2}; v_y^R = v_y \left(1 + \frac{24L v_y}{\pi N v_x}\right)^{-1/2} \quad (144)$$

where $L = |\log[\min(\xi^{-1}, \gamma\omega)]|$. This renormalization implies that as ξ diverges, $v_x^R \rightarrow 0$, and the velocities at \mathbf{k}_{hs} and $\mathbf{k}_{hs} + \mathbf{Q}$ become antiparallel to each other, i.e., the Fermi surface becomes “nested” at hot spots. This “nesting” is the first step in the transformation from a large Fermi surface to a small one, consisting of hole pockets. If this effect occurred at a finite ξ , then one might expect a subsequent topological transition in which a large Fermi surface disconnects into hole pockets and the rest. We found, however, that the “nesting” occurs only right at $\xi = \infty$, and is only a weak logarithmic effect. This is a consequence of the fact that the low frequency spin excitations are diffusive rather than propagating. If the Fermi surface did not contain hot spots or the damping was just weaker, one could expect more stronger nesting effects and, accordingly, some spin-density-wave precursors in the normal state.

The logarithmical modification of the fermionic self-energy gives rise to logarithmical modifications of the conductivities: both real and imaginary parts of the conductivity behave as $\sigma(\omega) \propto |\log \omega|^{1/2}/\sqrt{\bar{\omega}}$.

We next list the results at finite T .

B. finite T

1. Fermi liquid regime

The Fermi liquid regime for T dependent terms in the fermionic self-energy is confined to $\pi T \leq 0.5\omega_{sf}(k)$. For these temperatures we obtained $\Sigma(k, \Omega) = \Sigma(k, \Omega, T = 0) + \Sigma_T(k, \Omega)$ where $\Sigma(k, \Omega, T = 0)$ is given by (135), and $\Sigma_T(k, \Omega)$ predominantly affects the imaginary part of the self-energy:

$$\Sigma_T(k, \Omega) = i \frac{\pi^2 T^2}{4\omega_{sf}(k)} \text{sign}\Omega F\left(\frac{\Omega}{\omega_{sf}(k)}\right) + O(T^4) \quad (145)$$

where $F(x)$ is a smooth function of x with the limits $F(0) = 1$, $F(x \gg 1) \rightarrow 1/3$. The full expression, including T^4 terms, is presented in (213).

We found that the spin susceptibility is not affected by a finite temperature except for a regular, $O((T/\Lambda)^2)$ correction to the correlation length. The conductivities are affected and change to $\sigma_1(\omega) \propto T^{-2}$ and $\sigma_2(\omega) \propto \omega/T^4$ at $\omega < T^2/\omega_{sf}$. The resistivity indeed obeys a Fermi liquid form $\rho(T) \propto T^2$.

2. quantum-critical regime, intermediate temperatures

At intermediate temperatures, $0.5\omega_{sf} < T < N\omega_{sf}$, we found that the thermal contribution to the self-energy is predominantly linear in T . In the formal limit $N \gg 1$, there are two different types of linear behavior. One occurs at relatively high T , when on one hand, $T < N\omega_{sf}$, and on the other hand, T is larger than $6 - 8\omega_{sf}$. In this regime, the dominant piece in $\Sigma_T(\mathbf{k}, 0)$ is the impurity-like contribution from the scattering by static spin fluctuations. It yields $\Sigma_T(\mathbf{k}, 0) = i\pi T\lambda_k$. The contribution to $\Sigma_T(\mathbf{k}, 0)$ from dynamical spin fluctuations is smaller and scales as \sqrt{T} . In explicit form (see Eqn (213))

$$\Sigma_T''(k, 0) = \pi T\lambda(k) - 1.516 \left(\frac{T\bar{\omega}}{2}\right)^{1/2} \quad (146)$$

At $T < 6 - 8\omega_{sf}$, the scattering from dynamical spin fluctuations also yields a linear in T piece in the fermionic self-energy. In this temperature range, we found, to a good accuracy

$$\Sigma_T''(k, 0) = 0.4 \pi T\lambda(k) \quad (147)$$

At finite Ω the self-energy is more involved and is generally given by Eq. (218). The dynamical piece in the self-energy is well approximated by the $N = \infty$ result, Eqns. (90) and (91). In the static piece, the corrections to the $N = \infty$ result $i\pi T\lambda$ become relevant above typical frequency evolves is $\bar{\Omega} = N^2\omega_{sf}(v_F^2/v_x v_y)/36$. At $N = \infty$ and finite λ , this $\bar{\Omega}$ exceeds $\bar{\omega} = 4\lambda^2\omega_{sf}$. However, at finite N and large λ , $\bar{\Omega} \ll \bar{\omega}$. We found a controllable way to compute the full fermionic $\Sigma(\Omega)$ at $T \ll N\omega_{sf}$ and arbitrary $\Omega/\bar{\Omega}$. We found that at $\bar{\omega} > \Omega > \bar{\Omega}$, the static piece in the fermionic self-energy decreases as $\Sigma_{st}''(\Omega) \propto TN\sqrt{\bar{\omega}/\Omega} \log(\Omega/(N^2\omega_{sf}))$. At these frequencies, the full self-energy (sum of dynamical and static pieces) obeys the scaling form $\Sigma(\Omega, T) \propto \sqrt{T}f(\Omega/T)$, up to logarithmic corrections. For completeness, we presented both the full result for the self-energy, Fig. 22, and the second-order result, Fig 20. We argued that although the derivation of the full self-energy is justified for $T < N\omega_{sf}$, by numerical reasons, vertex corrections may become relevant by numerical reasons already at $T \geq \omega_{sf}$. We conjectured that at these temperatures, the second-order result may be closer to reality than the “full” expression which includes self-energy of intermediate fermions but neglects vertex corrections.

The dynamical spin susceptibility is the same as in (139), and the conductivities scale, at vanishing ω , as $\sigma_1 \propto 1/T$, $\sigma_2 \propto \omega/T^2$. The behavior of conductivities at finite frequencies is rather involved and we refrain from discussing the limits. The full result is presented in Fig. 32.

3. quantum-critical regime, high temperatures

At high temperatures, $\pi T > N\omega_{sf}$, vertex corrections and the corrections to the Fermi velocity cannot be neglected, and our controlled computational scheme breaks down. In this regime we obtained the results by neglecting vertex corrections without justification and performing self-consistent FLEX-type calculations. We then verified that the vertex correction, evaluated using the full fermionic propagators remain $O(1)$, i.e., at least they do not diverge. We found that the contribution to $\Sigma_T(\mathbf{k}, 0)$ from scattering on static spin fluctuations scales down from $\pi T\lambda$ and at the highest T behaves, up to logarithms, as \sqrt{T} with ξ -independent coefficient, i.e., in the same way as the contribution from the scattering on dynamical spin fluctuations. Combining the two contributions, we obtained

$$\Sigma_T''(k) = \bar{\omega} \left(\frac{TN}{6\bar{\omega}}\right)^{1/2} \left(\log \frac{3T}{N\omega_{sf}} - 1.516 \left(\frac{3}{N}\right)\right)^{1/2} \quad (148)$$

This evolution of the thermal piece in the self-energy affects the conductivities which scale at $\omega \rightarrow 0$ as

$$\sigma_1(T) \propto T^{-1/2}, \sigma_2(T) \propto \omega/T.$$

4. quantum-critical point

At $\omega_{sf} \rightarrow 0$, the temperature range $\pi T > N\omega_{sf}$ extends down to the lowest frequencies. We found at vanishing ω_{sf} and a finite T that the fermionic self-energy scales as

$$\Sigma_T'' \propto T^{1/2} |\log T| \quad (149)$$

The angle between the Fermi velocities at \mathbf{k}_{hs} and $\mathbf{k}_{hs} + \mathbf{Q}$ scales as $1/|\log T|$ (see (100)). Both of these results are identical to what we obtained at $T = 0$, if we substitute T by Ω (see Eqs. (143) and (144)). Equal powers of logarithms at $T = 0, \Omega \neq 0$ and $T \neq 0, \Omega = 0$ mean that the system at the QCP possesses ω/T scaling for fermionic variables. This is quite expected, in view of the fact that the fermionic self-energy is not affected by the anomalous exponent in the spin susceptibility. However, as we said, the self-consistent FLEX solution is uncontrolled, and therefore the equivalence between Ω and T in our solution is not the proof that the ω/T scaling actually exists.

On the other hand, our theory definitely yields no ω/T scaling for the dynamical spin susceptibility. At $T = 0$, we found the anomalous exponent η (see (142)). At finite T and $\omega = (\mathbf{q} - \mathbf{Q})^2 = 0$, we found that the susceptibility behaves regularly, as $\chi \propto 1/T^2$. This behavior is certainly modified due to ϕ^4 interaction between bosonic modes. This effect is, however, beyond the scope of our theory as the ϕ^4 interaction is produced by high-energy fermions and scales as $1/\Lambda$. The anomalous behavior at $T = 0$ on the other hand is universal and survives in the limit $\Lambda \rightarrow \infty$.

C. comparison with experiments

We now compare our key results for the spectral function and conductivity with the experimental data on optimally doped high T_c cuprate *Bi2212* for which both photoemission and conductivity data are available. We remind that the two inputs in our theory are the coupling constant λ and the overall scale $\bar{\omega} = 4\lambda^2\omega_{sf}$. Alternatively, we can reexpress λ as $\lambda = 3v_F\xi^{-1}/(16\omega_{sf})$ and use $v_F\xi^{-1}$ and ω_{sf} as input parameters.

The value of the Fermi velocity can be obtained from the photoemission data at high frequencies, when the self-energy corrections to the fermionic dispersion become relatively minor. The three groups which reported the MDC data on *Bi2212* for momenta along zone diagonal [9,73,74] all agree that that the bare value of the Fermi velocity along the diagonal is rather high: $2.5-3eV\text{\AA}$, or $0.7-0.8eV\text{\AA}$ where $a \sim 3.8\text{\AA}$ is the *Cu-Cu*

distance. We used the $t-t'$ model to relate this velocity with that at hot spots. Using the value of the velocity and the experimental facts that the Fermi surface is located at $\mathbf{k} \approx (0.4\pi/a, 0.4\pi/a)$ for momenta along zone diagonal and at $\mathbf{k} \approx (\pi/a, 0.2\pi/a)$ for k_x along the zone boundary, we found $t \sim 0.2 - 0.25eV$, $t' \approx -0.36t$ and $\mu \approx -1.1t$. These numbers roughly agree with other studies [33]. The hot spots are located at $\mathbf{k}_{hs} = (0.16\pi, 0.84\pi)$ and symmetry related points, and the velocity at a hot spot is approximately a half of that at zone diagonal. This yields $v_F \approx 0.35 - 0.4eV\text{\AA}$.

The values of ω_{sf} and ξ can in principle be extracted from neutron scattering data on $S(\mathbf{q}, \omega) \propto \omega/((1 + (\mathbf{q} - \mathbf{Q})^2\xi^2)^2 + (\omega/\omega_{sf})^2)$, and from NMR data. We are not familiar with the detailed analysis of the normal state neutron and NMR data for *Bi2212* and will rely on the data for near optimally doped *YBCO*. The NMR analysis [76] yields $\omega_{sf} \sim 20meV$ and $\xi \sim 2a$. The neutron data in the normal state are more difficult to analyze because of the background which increases the width of the neutron peak and masks some frequency dependence. The data show [75] that the dynamical structure factor in the normal state is indeed peaked at $\mathbf{q} = \mathbf{Q} = (\pi/a, \pi/a)$, and the width of the peak increases with frequency and at $\omega = 50meV$ reaches 1.5 of its value at $\omega = 0$. A straightforward fit to the theoretical formula, Eqn(139), yields $\omega_{sf} \sim 35-40meV$ and $\xi \sim a$ which are predictably larger than ω_{sf} and ξ extracted from NMR. We will use NMR values $\omega_{sf} \sim 20meV$ and $\xi = 2a$ for further estimates.

Combining the results for v_F , ξ and ω_{sf} , we obtain $\lambda \sim 2$. This in turn yields $\bar{\omega} \sim 0.3eV$. As an independent check of the internal consistency of the estimates, note that our recent analysis of the superconducting state [39] yields the resonance neutron frequency at $\omega_{res} \sim 0.25\bar{\omega}/\lambda$, i.e., at $\omega_{res} \sim 40meV$. This is quite consistent with the data.

Away from hot spots, the effective coupling decreases as $\lambda(k) = \lambda(1 + (\epsilon_{k+Q}/v_F\xi^{-1})^2)^{1/2}$. This formula is indeed valid only in some vicinity near hot spots as we didn't include in the theory the variation of the Fermi velocity along the Fermi surface. Nevertheless, experimentally, even for $k = k_F$ along zone diagonal (the furthest k point away from a hot spot), $\epsilon_{k_F+Q}/v_F(k_F)\xi^{-1} \approx 1.4$ [8]. This shows that the coupling does vary along the Fermi surface, but this variation is modest: λ is reduced by at most 1.7 when we move from hot spots towards zone diagonal. Actual reduction can be even smaller as v_F by itself increases as one approaches zone diagonal. For $\omega_{sf}(k)$, our theory predicts that it increases with the deviation from hot spots. Note, however, that $\omega_{sf} \propto \sin \phi_0$, where ϕ_0 is the angle between velocities at \mathbf{k} and $\mathbf{k} + \mathbf{Q}$. In our theory, we assumed that this angle does not change. In reality, ϕ_0 angle tends to π as \mathbf{k} approaches the zone diagonal, and this *reduces* ω_{sf} .

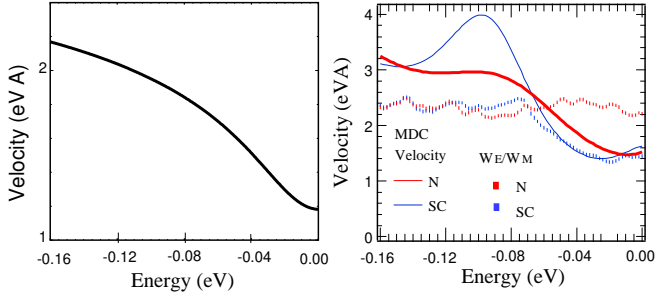


FIG. 35. a. The theoretical result for the effective velocity of the quasiparticles $v_F^* = v_F / (1 + \partial\Sigma'(\omega)/\partial\omega)$. For definiteness we used $\omega_{sf} = 20\text{meV}$, $\lambda = 1.7$ and $v_F = 3\text{eV}\text{\AA}$. b. Experimental result for the effective velocity, extracted from the MDC dispersion [9] along zone diagonal. Observe the bump in the frequency dependence of the velocity at $70 - 80\text{meV}$ in the data and at about $3 - 4\omega_{sf}$ in the theory.

Since for both $\lambda(k)$ and $\omega_{sf}(k)$ there are competing effects which we cannot fully control, we believe that effective $\omega_{sf}(k)$ and $\lambda(k)$ should just be obtained from the fit to the photoemission data. In particular, ω_{sf} can be extracted from the MDC (momentum distribution curve) measurements of the electronic dispersion $\omega + \Sigma'(\omega) = \epsilon_k$. In Fig 35 we compare our $(1 + \partial\Sigma'(\omega)/\partial\omega)$ with the measured variation of the effective velocity $v_F(\omega)$ of the electronic dispersion along zone diagonal [9]. We see that the theoretical dispersion has a bump at $\omega \sim 3\omega_{sf}(k_{diag})$. Experimental curves look quite similar and show the bump at $\sim 70 - 80\text{meV}$ [9,73,74]. This yields $\omega_{sf}(k_{diag}) \sim 25\text{meV}$, i.e., almost the same as near hot spots.

Note in passing that although $\epsilon_{k+Q}/v_F\xi^{-1}$ does not vary much when k moves along the Fermi surface, the fact that the Fermi velocity is very high implies that ϵ_{k_F+Q} is roughly $v_F\sqrt{2} * 0.22\pi/a \approx 0.8\text{eV}$, i.e., it is comparable to a bandwidth. This implies that one certainly cannot neglect the curvature of the Fermi surface in the theoretical analysis. In other words, the Fermi-surface is very different from a near square which one would obtain for only nearest neighbor hopping. Furthermore, the fact that the Fermi velocity is large implies the physics at energies up to few hundred meV is confined to a near vicinity of the Fermi surface, when one can safely expand ϵ_k to a linear order in $k - k_F$. Finally, van-Hove singularities (which we neglected) do play some role [108,109] but as $\epsilon_{0,\pi} \approx 0.34t \sim 85\text{meV}$, we expect that the van-Hove singularity softens due to fermionic incoherence and should not substantially affect the physics.

We now briefly compare the experimental and theoretical forms of the fermionic spectral function and optical conductivity.

1. spectral function

We first use our form of the fermionic self-energy to fit the MDC data which measure the width of the photoemission peak as a function of k at a given frequency. In Fig. 36 we compare our results for $\Delta k = \Sigma''(k, \Omega)/v_F$ with the measured [9] Δk vs frequency at $T \sim 100\text{K}$ and temperature at $\Omega \rightarrow 0$ [73]. For definiteness we used $\lambda = 1.7$ and $\omega_{sf} = 20\text{meV}$. The slope of Δk is chiefly controlled by λ . We see that $\lambda \leq 2$ yields rather good agreement with the data on both, frequency and temperature dependence of the self-energy. On the other hand, the magnitude of our Σ'' is smaller than in the data. To account for the values of Δk , we had to *add* a constant of about 50meV to Σ'' . The origin of this constant term is unclear. It may be the effect of impurities [110], and it also may be the effect of other scattering channels which we ignored [92]. It is essential, however, that the functional dependence of $\Sigma''(\Omega T)$ is captured by spin-fluctuation scattering.

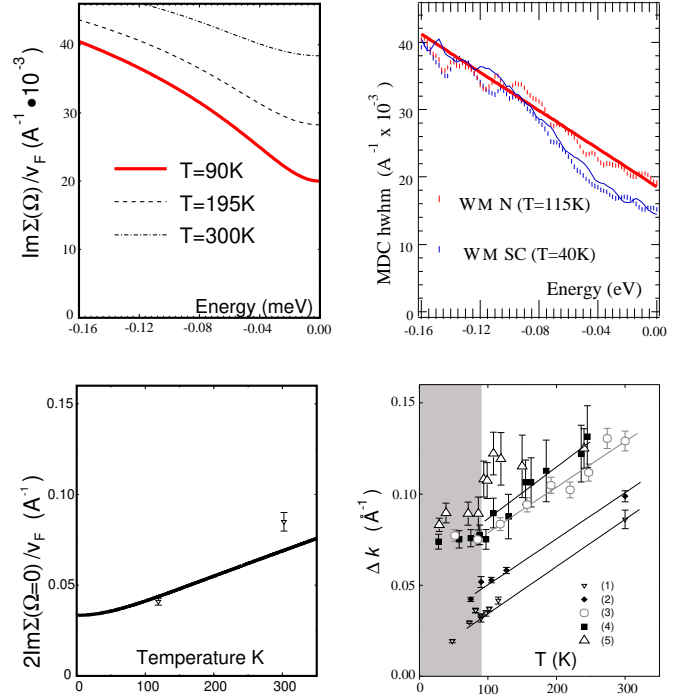


FIG. 36. A comparison between theoretical results and the photoemission MDC data. For the Lorentzian lineshape of the MDC signal, observed in experiments, the MDC hwhm equals to Σ''/v_F . Upper panel - the results for the MDC hwhm vs frequency at a given T . The experimental results are taken from [9]. Lower panel - the MDC fwhm vs temperature at $\Omega = 0$. The experimental results (right figure and the points on the left figure) are taken from [73].

In Fig 37 we present our results for the hwhm of the EDC (energy distribution curve) which measures fermionic $I_k(\Omega) = A_k(\Omega)n_F(\Omega)$ as a function of

frequency at a given k ($A_k(\Omega) = (1/\pi)ImG(k, \Omega)$). For Lorentzian lineshape, the EDC hwhm is given by $\Sigma''(\Omega)/(1 + \Sigma'(\Omega)/\Omega)$ [9]. The data are taken at $T = 115K$ [9]. Again, the theoretical slope reasonably agrees with the experimental one. Some discrepancy is associated with the fact that the experimental lineshape is not a Lorentzian and hence the measured hwhm is not exactly $\Sigma''(\Omega)/(1 + \Sigma'(\Omega)/\Omega)$.

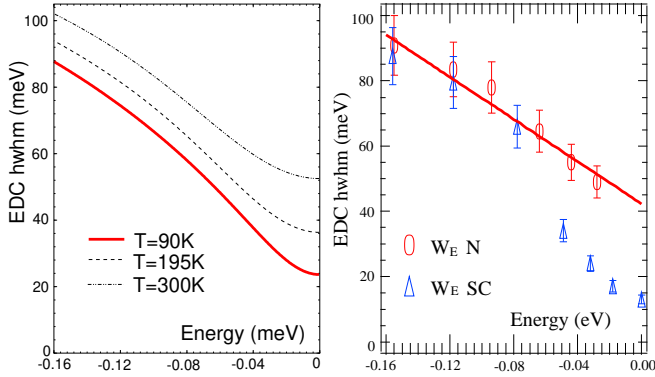


FIG. 37. The theoretical result for $\Sigma''(\Omega)/(1 + \Sigma'(\Omega)/\Omega)$. The points are the experimental hwhm of the EDC dispersion from [9].

2. conductivity

In Fig. In Fig. 38 we compare our theoretical results for the conductivity with the experimental data for σ_1 and σ_2 at different temperatures [98]. For definiteness we used the same $\lambda = 1.7$ and $\omega_{sf} = 20meV$ as in the fit to the photoemission data along zone diagonals. We checked that the change in λ affects the ratio σ_2/σ_1 at high frequencies, but does not change the functional forms of the conductivities. We adjusted the plasma frequency to obtain the agreement between dc conductivity and Σ'' extracted from the MDC photoemission data using $v_F \sim 3eV/\text{\AA}$. This adjustment yields $\omega_{pl} \sim 20000cm^{-1}$. This value is somewhat larger than $\omega_{pl} \sim 16000cm^{-1}$ obtained experimentally by integrating σ_1 up to about $2 - 2.5eV$ [97–99]. This discrepancy is consistent with our theoretical result that the sum rule is satisfied only at extremely high frequencies (see Fig. 29).

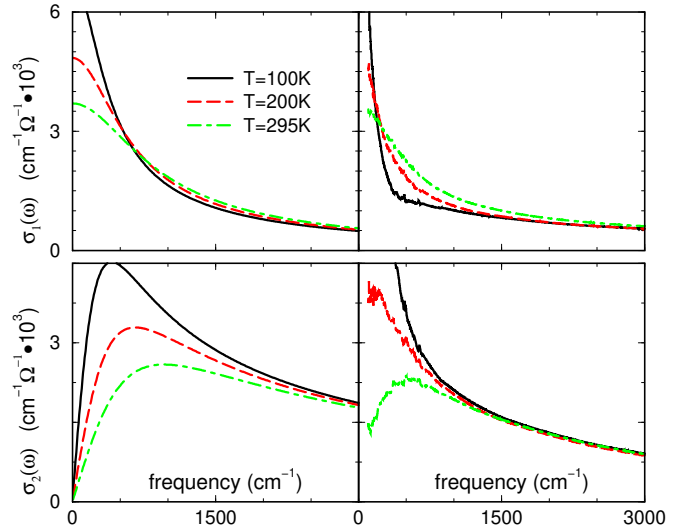


FIG. 38. The theoretical and experimental results for the real and imaginary parts of optical conductivity. The data are from [98].

We see that theoretical $\sigma_1(\omega)$ and $\sigma_2(\omega)$ capture the essential features of the measured forms of the conductivities. In particular, the curves of σ_1 at different temperatures cross such that at the lowest frequencies, the conductivity decreases with T which at larger frequencies it increases with T (the same behavior has also been detected in [10,99]). The imaginary part of conductivity decreases with T at any frequency, and the peak in $\sigma_2(\omega)$ increases in magnitude and shifts to lower T with decreasing T [98,99,111]. At frequencies above $1500cm^{-1}$ both σ_1 and σ_2 weakly depend on T and are comparable in the amplitude.

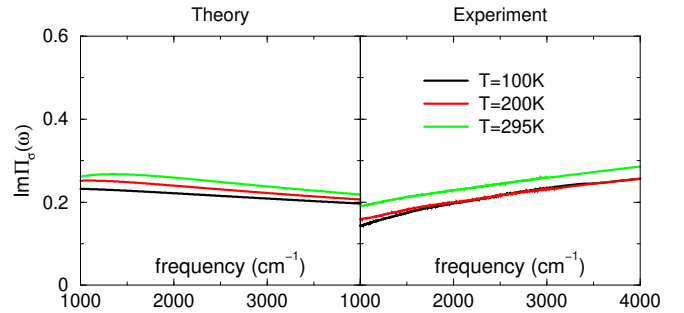


FIG. 39. The theoretical and experimental results for $\Pi''_{\sigma}(\omega) = 4\pi\sigma_1\omega/\omega_{pl}^2$. The data are from [98].

In Fig 39 we compare experimental and theoretical results for the imaginary part of the full particle-hole polarization bubble $\Pi''_{\sigma}(\omega) = 4\pi\sigma_1\omega/\omega_{pl}^2$. Theoretically, at $T = 0$, $\Pi''_{\sigma}(\omega)$ saturates at a value of about 0.2 *independently* on λ and remains almost independent on frequency over a very wide frequency range (see Fig. 26). We see that the theoretical value of Π_{σ} does not change much

with T . Experimental data also clearly show a near saturation of Π''_{σ} at a value close to 0.2. We consider this agreement as a strong argument in favor of our theory.

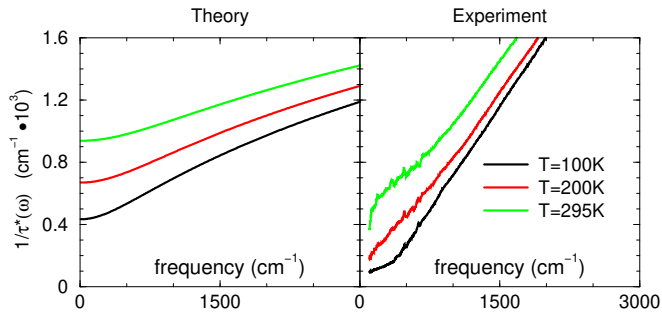


FIG. 40. The theoretical and experimental results for $1/\tau^* = \omega\sigma_1/\sigma_2$. The data are from [98].

The agreement between our theory and the experiment is, however, not a perfect one. In Fig. 40 we show theoretical and experimental results for $1/\tau^* = \omega\sigma_1/\sigma_2$. The advantage of comparing $1/\tau^*$ is that this quantity does not require one to know what the plasma frequency is. We see that while both experimental and theoretical curves are linear in frequency, the slopes are off roughly by a factor of 3. This discrepancy is related to the fact that in our theory, at high enough frequencies, $Pi'_{\sigma}(\omega)$ is roughly 3 times larger than $\Pi''_{\sigma}(\omega)$ (see Fig. 26) and hence $\sigma_2/\sigma_1 \sim 3$, while experimentally σ_1 and σ_2 nearly coincide at high frequencies. Also, at zero frequency, the theoretical value of $1/\tau^*(\omega = 0)$ at, say, $T = 300K$ is larger than in the data [98,99]. From Fig 40 the ratio of theoretical and experimental $1/\tau^*(\Omega = 0)$ is roughly 1.5.

The discrepancy in $1/\tau^*$ is important for the theory as it indicates that either the averaging over the Fermi surface and vertex correction within a bubble, or the RPA-type corrections to conductivity [66,92] do play some role. Still, however, Figs. 38 and 39 indicate that the general trends of the behavior of the conductivities, at least near optimal doping, are reasonably well captured by the spin-fluctuation theory.

In this paper we collected all what we know at the moment about the normal state properties of the spin-fermion model. The next step is to consider what happens below the pairing instability. We plan to present the detailed account of these results in the near future.

XI. ACKNOWLEDGEMENTS

It is our pleasure to thank A. M. Finkel'stein for stimulating discussions on numerous aspects of strong coupling effects in cuprates. We are also thankful to E. Abrahams, A.A. Abrikosov, B.L. Altshuler, D. Basov, G. Blumberg, J.C. Campuzano, P. Coleman, L.P. Gor'kov, M. Grilli, L. Ioffe, P. Johnson, R. Joynt, B. Keimer, R. Laughlin, M.

Lavagna, D. Khveschenko, G. Kotliar, H. von Löhneysen, A. Millis, M. Norman, C. Pépin, D. Pines, A. Rosh, S. Sachdev, Q. Si, O. Tchernyshyov, A. Tsvelik, J. Tu and J. Zasadzinski for useful conversations. We are also thankful to D. Basov and J. Tu for sharing their unpublished results with us and to M. Norman for bringing ref. [53] to our attention. The research was supported by NSF DMR-9979749 (Ar. A and A. Ch.), and by the Ames Laboratory, operated for the U.S. Department of Energy by Iowa State University under contract No. W-7405-Eng-82 (J.S). This work was partly done while A.C. was on a sabbatical leave at the Rutgers University and the NEC Research Institute. The hospitality of both places is acknowledged with thanks.

XII. APPENDIX A

In this Appendix, we evaluate several integrals presented in Sec. III.

A. direct perturbation theory

We first compute the second order fermionic self-energy and the vertex correction in a direct perturbation theory for the spin-fermion model. ‘‘Direct’’ means that the calculations are performed with the bare value of the spin susceptibility.

We begin with the perturbative fermionic self-energy $\Sigma(\mathbf{k}, \Omega_m) = (\Omega_m - \epsilon_{\mathbf{k}+Q}) I(\mathbf{k}_{hs}, 0)$, where $I(\mathbf{k}_{hs}, 0)$ is given by (9)

$$I(\mathbf{k}_{hs}, 0) = \frac{3\bar{g}}{(2\pi)^3} \int d^2\tilde{\mathbf{q}} d\omega_m \frac{1}{\xi^{-2} + \tilde{\mathbf{q}}^2 + (\omega/v_s)^2} \times \frac{1}{(i\omega_m - v_F\tilde{q}_x)^2} \quad (150)$$

Here $\tilde{\mathbf{q}} = \mathbf{q} - \mathbf{Q}$, and x -axis is chosen along \mathbf{v}_F at $\mathbf{k} + \mathbf{Q}$. Rescaling the momentum and frequency $\tilde{q}_x = \xi^{-1}x$, $\tilde{q}_y = \xi^{-1}y$, and $\omega = \xi^{-1}v_s z$, transforming to the spherical coordinates and integrating over $r = \sqrt{x^2 + y^2 + z^2}$, we obtain ($\eta = v_F/v_s$)

$$I(k_{hs}, 0) = -\frac{\lambda}{2\pi\eta} \int_0^{\pi/2} \frac{d\theta}{\sin\theta} \int_0^{2\pi} \frac{d\phi}{(i\eta^{-1}\cot\theta - \cos\phi)^2} = -\lambda\eta \int_0^{\pi/2} \frac{\sin\theta \cos\theta d\theta}{[1 + (\eta^2 - 1)\sin^2\theta]^{3/2}} = -\frac{\lambda}{1 + \eta}, \quad (151)$$

Similar analysis works also for the vertex correction. We have from (14)

$$\frac{\Delta g}{g} = -\frac{\bar{g}}{8\pi^3} \int d^2\tilde{q} d\omega \frac{1}{\xi^{-2} + \tilde{\mathbf{q}}^2 + (\omega/v_s)^2} \times \frac{1}{i\omega - (v_x\tilde{q}_x + v_y\tilde{q}_y)} \frac{1}{i\omega + v_x\tilde{q}_x - v_y\tilde{q}_y} \quad (152)$$

Rescaling the momentum and frequency in the same way as before, we obtain from (152)

$$\frac{\Delta g}{g} = -\frac{\lambda}{6\pi^2} \frac{v_F}{v_s} \int \frac{dxdydz}{1+x^2+y^2+z^2} \frac{1}{(iz-\alpha y)^2 - \beta^2 x^2} \quad (153)$$

where $\alpha = v_y/v_s$ and $\beta = v_x/v_s$ ($\alpha^2 + \beta^2 = \eta^2$). Introducing spherical coordinated and integrating over r we obtain

$$\begin{aligned} \frac{\Delta g}{g} &= -\frac{\lambda v_F}{6\pi v_s} \int_0^{\pi/2} \frac{d\theta}{\cos\theta} \int_0^{2\pi} \frac{d\phi}{(i \tan\theta - \alpha \sin\phi)^2 - \beta^2 \cos^2\phi} \\ &= \frac{\lambda v_F}{3v_s} \int_0^{\pi/2} \frac{d\theta \cos\theta \sin\theta}{[\sin^2\theta + \alpha^2 \cos^2\theta] \sqrt{\sin^2\theta + (\alpha^2 + \beta^2) \cos^2\theta}} \\ &= \frac{\lambda v_F}{3} \frac{1}{v_s \beta \sqrt{1-\alpha^2}} \ln \frac{\alpha(\sqrt{1-\alpha^2} - \beta)}{\sqrt{(\beta^2 + \alpha^2)(1-\alpha^2)} - \beta} \end{aligned} \quad (154)$$

At $v_s \rightarrow \infty$, i.e., for a purely static bare spin susceptibility, $\Delta g/g$ becomes

$$\frac{\Delta g}{g} = \frac{\lambda}{3} \frac{v_F}{v_x} \sinh^{-1} \frac{v_x}{v_y} \quad (155)$$

For $v_x = v_y$, we have $\frac{\Delta g}{g} = \frac{\lambda\sqrt{2}}{3} \ln(1+\sqrt{2}) \approx 0.415\lambda$.

In the opposite limit $v_s \ll v_F$, we obtain from (154)

$$\frac{\Delta g}{g} = \frac{\lambda}{3} \frac{v_s v_F}{v_x v_y} \tan^{-1} \frac{v_x}{v_y} \quad (156)$$

B. renormalized perturbation theory

We next repeat these computations using the relaxational form of the spin susceptibility. We first re-evaluate $I(\mathbf{k}_{hs}, 0)$. From Eq. (23) we have

$$\begin{aligned} I(\mathbf{k}_{hs}, 0) &= 3\bar{g}\xi^2 \int \frac{d^2\tilde{q}d\omega_m}{(2\pi)^3} \frac{1}{1 + (\tilde{\mathbf{q}}\xi)^2 + \frac{|\omega_m|}{\omega_{sf}} + \frac{\omega_m^2}{v_s^2\xi^{-2}}} \\ &\quad \times \frac{1}{(i\omega_m - v_F\tilde{q}_x)^2} \end{aligned} \quad (157)$$

The key difference with the direct perturbation theory is that now the ω^2 term in the susceptibility becomes subleading at low frequencies. Let's first neglect this term. Introducing, as before, $\tilde{q}_x\xi = x$, $\tilde{q}_y\xi = y$, and also $\omega_m = \omega_{sf}t$, we then rewrite Eq. (157) as

$$\begin{aligned} I(\mathbf{k}_{hs}, 0) &= \frac{3v_x v_y}{2\pi^2 N v_F^2} \int dx dy dt \frac{1}{1+x^2+y^2+|t|} \\ &\quad \times \frac{1}{(x-it/a)^2} \end{aligned} \quad (158)$$

where $a = (v_F\xi^{-1}/\omega_{sf}) = (N\lambda/3)(v_F^2/v_x v_y)$. One can easily make sure that the neglect of the ω^2 term in the

susceptibility is justified when $a \gg 1$ (see also below). The integration over y is straightforward and yields

$$\begin{aligned} I(\mathbf{k}_{hs}, 0) &= \frac{3v_x v_y}{2\pi N v_F^2} \int \frac{dxdt}{(1+x^2+|t|)^{1/2}} \\ &\quad \times \frac{1}{(x-it/a)^2} \end{aligned} \quad (159)$$

The last term in (159) is a double pole. The integral over x then does not vanish only because the first term contains a branch cut. Deforming the contour of integration over x to include the branch cut along imaginary x , and integrating over the branches of the branch cut, we obtain

$$I(\mathbf{k}_{hs}, 0) = -\frac{12v_x v_y}{\pi N v_F^2} \int_0^{\sim 1/a} dt \frac{1}{1+t}. \quad (160)$$

Evaluating the integral with logarithmical accuracy, we obtain

$$I_{reg}(\mathbf{k}_{hs}, 0) = -\frac{12v_x v_y}{\pi N v_F^2} \log \lambda \quad (161)$$

This is the result we cited in the Eq. (24).

With little more efforts, one can evaluate $I(\mathbf{k}_{hs}, 0)$ for arbitrary a and v_s/v_F which are two parameters for $I(\mathbf{k}_{hs}, 0)$. To avoid presenting very long formulas, we only consider the two limits $v_s \rightarrow \infty$ (i.e., a purely static bare spin susceptibility), and $v_F = v_s$. In the first case, performing the same computations as above but keeping a arbitrary, we obtain after some algebra

$$I(\mathbf{k}_{hs}, 0) = -\frac{\lambda}{\pi} \int_0^\infty \int_0^\infty \frac{ydydx}{(1+x+ay)(x+y^2)^{3/2}} \quad (162)$$

The straightforward integration yields

$$I_{reg}(\mathbf{k}_{hs}, 0) = -\lambda \frac{1 + \frac{a}{\pi} \log \frac{a}{2}}{1 + \frac{a^2}{4}} \quad (163)$$

This is the result we cited in the Eq. (25).

Similar considerations for $v_s = v_F$ yield

$$I(\mathbf{k}_{hs}, 0) = -\frac{4\lambda}{\pi a^2} \left(\pi - a - \sqrt{4-a^2} \cot^{-1} \frac{a}{\sqrt{4-a^2}} \right) \quad (164)$$

At $a \rightarrow 0$, $I(\mathbf{k}_{hs}, 0) \rightarrow -\lambda/2$ in agreement with (151).

We next show how to compute the full (regular plus anomalous) second-order $\Sigma(\mathbf{k}_{hs}, \Omega)$ at arbitrary Ω . We have

$$\begin{aligned} \Sigma(\mathbf{k}_{hs}, \Omega_m) &= 3\bar{g}\xi^2 \int \frac{d^2\tilde{q}d\omega_m}{(2\pi)^3} \\ &\quad \frac{1}{1 + (\tilde{\mathbf{q}}\xi)^2 + |\omega_m|/\omega_{sf} + \frac{\omega_m^2}{v_s^2\xi^{-2}}} \frac{1}{i\Omega_m + i\omega_m - v_F\tilde{q}_x} \end{aligned} \quad (165)$$

Introducing the same variables x, y, t as before, and also $\Omega = s\omega_{sf}$ and using the spectral representation of the Green's functions we obtain

$$Im\Sigma(\Omega) = \frac{\lambda\omega_{sf}}{\pi} Im \int_0^s dt \int \frac{dy}{y^2+1-it + ((s+t)^2 - \eta^2 t^2)/a^2}$$

The integration is straightforward, and the result is

$$Im\Sigma(\Omega) = Im \frac{\lambda\omega_{sf}a}{\sqrt{1-\eta^2}} \ln \frac{\sqrt{s+t_1} + \sqrt{s+t_2}}{\sqrt{t_1} + \sqrt{t_2}} \quad (166)$$

where t_1 and t_2 are the roots of the quadratic equation

$$(1+it)a^2 = (s+t)^2 - \eta^2 t^2 = 0 \quad (167)$$

For purely static bare susceptibility ($v_s = \infty$, or $\eta = 0$), Eqn (166) is simplified to

$$\Sigma(k_{hs}, \Omega) = 2\lambda\omega_{sf}a \ln \frac{i\sqrt{K_\Omega - 1} + \sqrt{K_\Omega + 1}}{i\sqrt{K_\Omega - 1} + A_\Omega + \sqrt{K(\Omega) + 1 - A_\Omega}} \quad (168)$$

where

$$K_\Omega^2 = 1 + \frac{4}{a^2} \left(1 - i \frac{\Omega}{\omega_{sf}}\right); \quad A_\Omega = \frac{2i}{a^2} \frac{\Omega}{\omega_{sf}} \quad (169)$$

(we used Kramers-Kronig relation to obtain $Re\Sigma$)

We next evaluate the lowest order correction to the spin-fermion vertex at the bosonic momentum \mathbf{Q} . The expression for Δg in terms of fermionic Green's functions is given by Eq. (14). Neglecting the subleading ω_m^2 in the spin propagator, introducing $x = \tilde{q}_x \xi$, $y = \tilde{q}_y \xi$, and $t = \omega/\omega_{sf}$, and expanding the quasiparticle energies to linear order in deviations from hot spots we obtain from (14)

$$\frac{\Delta g}{g} = \frac{v_x v_y}{2\pi^2 N} \int dx dy dt \frac{1}{1+x^2+y^2+|t|} \times \frac{1}{(v_x x)^2 - (v_y y - iv_F t/a)^2} \quad (170)$$

we remind that $a = (N\lambda/3) (v_F^2/v_x v_y) \gg 1$. Let's perform the integration over y first. As both poles in the last term in (170) are in the same half-plane, it is convenient to close the integration contour over a different half-plane where only the spin susceptibility has a pole. Evaluating the integral we obtain,

$$\frac{\Delta g}{g} = \frac{v_x v_y}{\pi N} \int_0^\infty dt \int_{-\infty}^\infty \frac{dx}{\sqrt{1+x^2+|t|}} \times \left[(v_F x)^2 + v_y^2(1+t) + v_F^2 (t/a)^2 + 2v_y v_F \frac{t}{a} \sqrt{1+x^2+|t|} \right]^{-1}. \quad (171)$$

To a logarithmical accuracy, we can neglect $1/a$ terms in the integrand of (171) and set the upper limit of frequency integration to be $t_{max} \sim a^2$. Introducing next

$x = (1+t)^{1/2}p$, and performing the integration over p first, we obtain from (171)

$$\frac{\Delta g}{g} = \frac{1}{2N} Q \left(\frac{v_x}{v_y} \right) \int_0^{a^2} \frac{dt}{1+t} \quad (172)$$

where

$$Q \left(\frac{v_x}{v_y} \right) = \frac{4}{\pi} \frac{v_x v_y}{v_F^2} \int_0^\infty \frac{dp}{\sqrt{1+p^2}} \frac{1}{p^2 + (v_y/v_F)^2} = \frac{4}{\pi} \tan^{-1} \frac{v_x}{v_y} = \frac{4\phi_0}{\pi} \quad (173)$$

and ϕ_0 is the angle between the directions of velocities at hot spots separated by \mathbf{Q} . The integration over t in (172) is elementary, and we obtain

$$\frac{\Delta g}{g} = \frac{1}{N} Q \left(\frac{v_x}{v_y} \right) \log \lambda \quad (174)$$

This is the result we quoted in the text. For $\lambda \rightarrow \infty$, the logarithmic dependence on λ transforms into the logarithmic dependence on the external frequency: $\log \lambda \rightarrow (1/2) \log \omega_{max}/|\omega|$ where $\omega_{max} \sim v_F^2/\bar{g}$.

It is instructive to observe that the same result can also be obtained by noticing that the ω terms in the fermionic propagators are much smaller than the $\sqrt{\omega}$ term from the spin susceptibility, Eq. (170). These ω terms can then be neglected, and the vertex correction can be straightforwardly simplified to

$$\frac{\Delta g}{g} = \frac{2v_x v_y}{\pi^2 N} I \log \xi, \quad (175)$$

where

$$I = \int \frac{d\tilde{x} d\tilde{y}}{1+\tilde{x}^2+\tilde{y}^2} \frac{1}{(\tilde{x}v_x + \tilde{y}v_y - i0)(\tilde{x}v_x - \tilde{y}v_y + i0)} \quad (176)$$

and compared to our previous notations, we introduced $\tilde{x} = x/t^{1/2}$, $\tilde{y} = y/t^{1/2}$. Naively, one might expect that the 2D integral in (176) is determined by the two poles at vanishing \tilde{x} and \tilde{y} . However, the contribution to the integral from small \tilde{x}, \tilde{y} diverges as \log^2 , and has to be regularized. The extra $1+x^2+y^2$ in the denominator of (176) provides such a regularization. We checked that for $v_x = v_y$, the regularization is irrelevant, and the result for $\Delta g/g$ comes from the two poles at vanishing \tilde{x}, \tilde{y} . For other ratios of velocities, the regularization yields an extra contribution to the integral from the range where $\tilde{x}, \tilde{y} = O(1)$. A straightforward calculation then yields $I = (2\pi/(v_x v_y)) \tan^{-1} v_x/v_y$, and hence the same $\Delta g/g$ as in (174). Physically, this result implies that except for the case when $v_x = v_y$, a part of the vertex correction comes from small momenta (in reality, of order ω/v_F), and a part comes from much larger momenta, of order $(\omega/(\omega_{sf}\xi^2))^{1/2} \gg \omega/v_F$.

Above we computed $\Delta g/g$ with the logarithmical accuracy. One can easily check, however, that the 3D

integration over momentum and frequency in (14) is convergent, i.e., the subleading, non-logarithmical term can also be determined within the low-energy model. This calculation is more convenient to perform in polar coordinates, by expressing $\epsilon_k = v_F \tilde{q} \cos(\phi + \phi_0/2)$, $\epsilon_{k+Q} = v_F \tilde{q} \cos(\phi - \phi_0/2)$. The integration over \tilde{q} is straightforward, and performing it we obtain

$$\frac{\Delta g}{g} = -\frac{2|\sin \phi_0|}{\pi^2 N} \text{Re} \int_0^\pi d\phi \frac{\log[\sin(\phi/2)]}{\cos \phi + \cos \phi_0} \times (2 \log a + \log \sin \phi/2) \quad (177)$$

where, we remind, $a = v_F \xi^{-1} / \omega_{sf} = (N\lambda/3)v_F^2/(v_x v_y)$. The $\log a$ term in (177) is indeed the same as in (174). The second piece is the regular contribution to $\Delta g/g$. Evaluating this piece numerically we find that for $\phi_0 = \pi/2$ i.e., $v_x = v_y$, which is close to the actual situation in cuprates, $\Delta g/g = (1/N)(\log a - 0.93)$. This result implies that for moderate λ , vertex correction is rather small numerically: $\Delta g/g \approx 0.09$ for e.g., $\lambda = 1$, and $\Delta g/g \approx 0.18$ for $\lambda = 2$.

XIII. APPENDIX B

In this Appendix we discuss the general structure of the $1/N$ expansion. Suppose for definiteness that we keep the number of hot spots finite and extend the theory to a large number of fermionic flavors. As usual, the extension of the theory to large N implies an appropriate rescaling of the coupling constant \bar{g} . In our case, however, we also have to rescale the Fermi velocity in the same way as \bar{g} . Indeed, consider the lowest order fermionic loop (the particle-hole bubble). We found above that it is proportional to $\bar{g}N/v_F^2$. The power of the Fermi velocity in the denominator accounts for the number of fermion propagators in the diagram. Evidently we would like this diagram to be of order one. Then we will have a “zero-order” theory with no factor of N . Usually this is achieved by assuming that the coupling constant is inversely proportional to N . However if we do this extension, we find that the anomalous fermionic self energy, which is also a part of the “zero-order” theory scales as $1/N$ as it is proportional to \bar{g}/v_F . (recall that the fermionic self-energy contains only one fermionic line and no summation over the flavor index). A proper extension which makes both particle-hole bubble and anomalous fermionic self-energy of order 1 is

$$\bar{g} \rightarrow \bar{g}N \quad (178)$$

and

$$v_F \rightarrow v_F N. \quad (179)$$

We now consider the general structure of the Feynman diagrams not included into the “zero-order” theory. Since

v_F scales with N , each running fermionic line acquires a factor $1/N$. Similarly, since \bar{g} scales with N , a diagram with n vertices acquires a prefactor $N^{n/2}$ (recall that $\bar{g} \propto g^2$). Finally, if a given diagram to the thermodynamic potential has m closed fermion loops, a summation over fermionic flavors yields an additional prefactor N^m results. As a result, a diagram with n -vertices and m closed fermionic loops behaves as

$$D(n, m) \propto N^{m-n/2}, \quad (180)$$

We used the fact that the number of internal fermionic lines in the diagram is n .

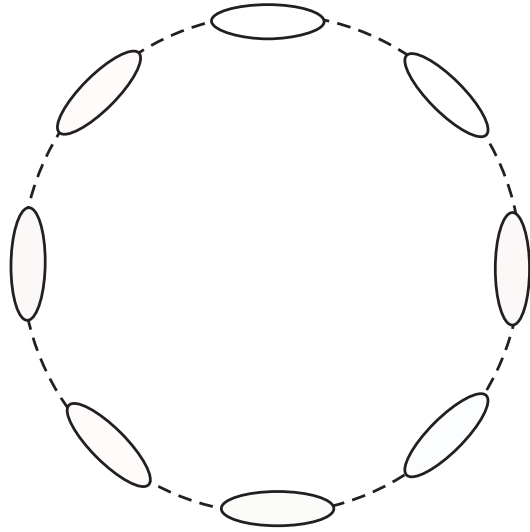


FIG. 41. A diagram for the thermodynamic potential to zero order in $1/N$.

The thermodynamic potential for the “zero-order” theory is given by the diagram shown in Fig.41. In this diagram, $m = n/2$ and hence $D = O(1)$. The fermionic and bosonic self energies are obtained by cutting one fermionic (or bosonic) line, and are also of order 1 as they indeed should be in the “zero-order” theory. Note, however, that this independence of N is the result of the interplay between \bar{g} and v_F as if one cuts a fermionic line one loses one factor N since one closed fermionic loop disappears. This is compensated by the fact that there is one running fermionic line less in the diagram.

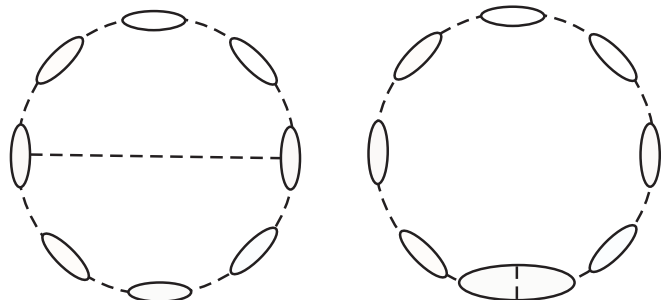


FIG. 42. The diagrams for the thermodynamic potential to order $1/N$.

The diagrams which constitute the expansion in $\frac{1}{N}$ are then obtained by reducing the number of internal fermionic loops at a given number of \bar{g} . The leading corrections are shown in Fig. 42. These diagrams have $m = n/2 - 1$ and hence are of order $1/N$. Cutting fermionic or bosonic lines yields self energy and vertex corrections to order $1/N$. Higher order diagrams are obtained by further reducing the number of closed fermionic loops.

XIV. APPENDIX C

In this Appendix we evaluate the polarization bubble with the vertex correction. We first compute this bubble explicitly. Then we redo computations in a different way: we first evaluate the effective four-fermion vertex and then contract two of its opposite external legs (see Fig. 16) and convolute the vertex with the spin propagator. This last computation allows us to directly compute our theory with the ϕ^4 theory of critical behavior for the dynamical exponent $z = 2$.

A. direct computation

The diagram which we need to compute is presented in Fig. 16c In the analytical form we have for $\xi = \infty$

$$\begin{aligned} \Pi_2(\mathbf{q}, \Omega) = & -\frac{2\bar{g}^2 N}{(2\pi)^4} T^2 \sum_{\omega, \omega'} \int d^2 k d^2 k' \frac{1}{\gamma|\omega - \omega'| + (\mathbf{k} - \mathbf{k}')^2} \\ & \frac{1}{\epsilon_k - i\omega} \frac{1}{\epsilon_{k+q} - i(\omega + \Omega)} \\ & \frac{1}{\epsilon_{k'+q} - i(\omega' + \Omega)} \frac{1}{\epsilon_{k'+Q} - i\omega'} \end{aligned} \quad (181)$$

where, as before $\epsilon_k = v_x k_x + v_y k_y$, $\epsilon_{k+Q} = -v_x k_x + v_y k_y$, and k measures a deviation from a hot spot. The combinatoric factor $2N$ comes from spin summation and summation over hot spots, and $\gamma = N\bar{g}/(4\pi v_x v_y)$.

Consider for simplicity the case $v_x = v_y$. Introducing first $k_x + k_y = k_+$, $k_y - k_x = k_-$, $k'_x + k'_y = k'_+$, $k'_y - k'_x = k'_-$, $q_+ = q_x + q_y$, $q_- = q_y - q_x$, and then $(k_+ + k'_+) = 2b_+$, $k_+ - k'_+ = b_-$, $(k_- + k'_-) = 2c_+$, $k_- - k'_- = c_-$, and substituting into (181) we obtain

$$\begin{aligned} \Pi_2(\mathbf{q}, \Omega) = & -\frac{2\bar{g}^2 N}{(2\pi)^4} \frac{1}{4v_x^4} T^2 \sum_{\omega, \omega'} \int db_- dc_- \\ & \frac{1}{\gamma|\omega - \omega'| + (b_-^2 + c_-^2)/2} \end{aligned}$$

$$\begin{aligned} & \times \int db_+ \left[\frac{1}{b_+ + \frac{b_-}{2} - i\frac{\omega}{v_x}} \frac{1}{b_+ - \frac{b_-}{2} + q_- - i\frac{\omega' + \Omega}{v_x}} \right] \\ & \times \int dc_+ \left[\frac{1}{c_+ - \frac{c_-}{2} - i\frac{\omega'}{v_x}} \frac{1}{c_+ + \frac{c_-}{2} + q_+ - i\frac{\omega + \Omega}{v_x}} \right] \end{aligned} \quad (182)$$

The integration over db_+ and dc_+ is straightforward and yields

$$\begin{aligned} \Pi_2(\mathbf{q}, \Omega) = & \frac{2\bar{g}^2 N}{(2\pi)^4} \frac{1}{4v_x^4} T^2 \sum_{\omega, \omega'} \int db_- dc_- \\ & \frac{1}{\gamma|\omega - \omega'| + (b_-^2 + c_-^2)/2} \\ & \frac{[\text{sign}(\omega' + \Omega) - \text{sign}\omega][\text{sign}\omega' - \text{sign}(\omega + \Omega)]}{[b_- - q_- + i\frac{\omega' - \omega + \Omega}{v_x}][c_- + q_+ - i\frac{\omega - \omega' + \Omega}{v_x}]} \end{aligned} \quad (183)$$

Shifting the momenta $b_- - q_- = \tilde{b}_-$, $c_- + q_+ = \tilde{c}_-$ we rewrite (183) as

$$\begin{aligned} \Pi_2(\mathbf{q}, \Omega) = & \frac{2\bar{g}^2 N}{(2\pi)^4} \frac{\pi^2}{4v_x^4} T^2 \sum_{\omega, \omega'} \int d\tilde{b}_- d\tilde{c}_- \\ & \frac{1}{\gamma|\omega - \omega'| + ((\tilde{b}_- + q_-)^2 + (\tilde{c}_- + q_+)^2)/2} \\ & \frac{[\text{sign}(\omega' + \Omega) - \text{sign}\omega][\text{sign}\omega' - \text{sign}(\omega + \Omega)]}{[\tilde{b}_- + i\frac{\omega' - \omega + \Omega}{v_x}][\tilde{c}_- - i\frac{\omega - \omega' + \Omega}{v_x}]} \end{aligned} \quad (184)$$

Next step is to observe that typical \tilde{b}_- and \tilde{c}_- are of order of a typical frequency, and hence can be safely neglected in the bosonic propagator, in which typical momenta scale as a square root of a typical frequency. The remaining momentum integration then proceeds straightforwardly, and we obtain

$$\begin{aligned} \Pi_2(\mathbf{q}, \Omega) = & \frac{2\bar{g}^2 N}{(2\pi)^4} \frac{\pi^4}{4v_x^4} T \sum_{\omega} \frac{\text{sign}(\tilde{\omega} + \Omega)\text{sign}(\Omega - \tilde{\omega})}{\gamma|\tilde{\omega}| + q^2} \\ & \times T \sum_{\omega'} (\text{sign}(\omega' + \Omega) - \text{sign}(\omega' + \tilde{\omega})) \\ & \times (\text{sign}\omega' - \text{sign}(\omega' + \tilde{\omega} + \Omega)) \end{aligned} \quad (185)$$

where $\tilde{\omega} = \omega - \omega'$. At $T \rightarrow 0$, the summation over ω' is elementary and yields $4(|\tilde{\omega}| - \Omega)$. Substituting this result and the expression for γ into (185), evaluating the integral over $\tilde{\omega}$ up to an upper cutoff A , and re-analyzing the computational steps for $v_x \neq v_y$ (this adds a factor $Q(v) = (4/\pi) \tan^{-1}(v_x/v_y)$) we finally obtain

$$\begin{aligned} \Pi_2(\mathbf{q}, \Omega) = & \frac{Q(v)}{N} (\mathbf{q}^2 + \gamma|\Omega|) \\ & \times \left[\log \frac{A\gamma}{\mathbf{q}^2 + \gamma|\Omega|} + \log \frac{q^2}{\mathbf{q}^2 + \gamma|\Omega|} \right] + \frac{1}{N} (A - 2|\Omega|). \end{aligned} \quad (186)$$

The constant contribution ($= A$) has to be neglected to avoid double counting as it comes from high energies and has already been absorbed into a bare $\chi_0(\mathbf{q}, \Omega)$. The

logarithmical terms, on the other hand, come from low energies and have to be kept.

We see that to a logarithmical accuracy \mathbf{q}^2 and $\gamma|\omega|$ are renormalized in exactly the same way, i.e., the diffusion coefficient does not diverge as the system approaches a QCP. It does acquire a nonsingular $1/N$ correction which is beyond the scope of our analysis. We however checked that the logarithmical divergence at $q = 0$ is fictitious and is eliminated when one included the self-energy of intermediate fermions.

Let's also check whether $\omega \log \omega$ term at $T = 0$ is collaborated by $T \log T$ term at a finite T , i.e., whether vertex corrections enforce ω/T scaling in the spin susceptibility. To address this issue we evaluate $\Pi_2(\mathbf{k}, \Omega)$ at finite T and $\Omega = q = 0$. The summation over Matsubara frequencies in (185) is straightforward. Performing the summation over ω' and substituting the explicit form of γ we obtain

$$\begin{aligned} \Pi_2(\mathbf{q}, \Omega) &= -\frac{2Q(v)\gamma}{N} \pi T \sum_{p=1}^{A/(2\pi T)} \frac{p-1}{p} \\ &= \frac{\gamma}{N} (-A + 2\pi T) \log \frac{A}{2\pi T} \end{aligned} \quad (187)$$

This result implies that finite T accounts for the shift of the bosonic frequency by $2\pi T$, i.e., it just shifts a bosonic $\Omega = 2\pi T n$ from $n = 0$ to $n = 1$. Obviously then, in real frequencies, $\Pi_2(\mathbf{q}, \Omega)$ *does not* contain a singular $T \log T$ term, i.e., there is no Ω/T scaling in the spin susceptibility at the QCP.

B. four-boson vertex

We next explicitly compute the four-boson vertex in Fig.16. In analytical form it is given by

$$\begin{aligned} b &= \frac{Ng^4}{(2\pi)^2} \int \frac{d\omega' d^2 q'}{i\omega' - \epsilon_{q'}} \frac{1}{i(\Omega + \omega_1 + \omega) - \epsilon_{Q+q'+q_1+q_2}} \\ &\times \frac{1}{i(\omega' + \omega_1 + \omega_2) - \epsilon_{q'+q_1+q_2}} \\ &\frac{1}{i(\omega' + \omega + \omega_2) - \epsilon_{Q+q'+q+q_2}} \end{aligned} \quad (188)$$

Linearizing, as before, the fermionic dispersion near hot spots as $\epsilon'_q = v_x q'_x + v_y q'_y$, $\epsilon_{q'+Q} = -v_x q'_x + v_y q'_y$, and performing the momentum integration, we obtain

$$\begin{aligned} b &= \frac{Ng^4}{16\pi v_x v_y} \int d\omega' \frac{\text{sign}(\omega') - \text{sign}(\omega' + \omega_1 + \omega_2)}{\epsilon_{q_1+q_2} - i(\omega_1 + \omega_2)} \\ &\times \frac{\text{sign}(\omega' + \omega_1 + \omega) - \text{sign}(\omega' + \omega + \omega_2)}{\epsilon_{Q+q_1-q_2} - i(\omega_1 - \omega_2)} \end{aligned}$$

The integration over ω' is also straightforward and yields

$$b = \frac{Ng^4}{8\pi v_x v_y} \frac{|\omega_2 + \omega| + |\omega_2 - \omega| - |\omega_1 + \omega| - |\omega_1 - \omega|}{[i(\omega_1 + \omega_2) - \epsilon_{q_1+q_2}][i(\omega_1 - \omega_2) - \epsilon_{Q+q_1-q_2}]} \quad (189)$$

This result is quoted in the main text.

C. First-order bosonic self-energy

We next explicitly compute the first order bosonic self-energy by contracting the external legs in the four-boson vertex and convoluting it with the spin susceptibility. The corresponding diagrams are presented in Fig. 16 b and c.

The first diagram is obtained by contracting the adjacent external legs of the four-fermion vertex. In this situation $\omega_1 = \omega_2$ and $\mathbf{q}_1 = \mathbf{q}_2$. Substituting this into Eq. (189) and then into the expression for the bosonic self-energy, we find that the self-energy vanishes due to still presence of double poles. This is consistent with our earlier result that the inclusion of the fermionic self-energy does not affect the form of the bosonic propagator.

The second diagram is obtained by contracting the external legs which are not adjacent to each other. In this situation, $\omega = q = 0$. Let's choose ω_1 to be an external frequency (which we label Ω for consistency of notations) and at first set the external $q_1 = 0$ (this corresponds to external momentum $\mathbf{q} = \mathbf{q}_1 + \mathbf{Q} = \mathbf{Q} = (\pi, \pi)$). The bosonic self-energy is then given by

$$\begin{aligned} \Pi_2(\mathbf{Q}, \Omega) &= -2 \int b(\Omega, \omega_2, \omega = 0) \chi(\mathbf{q}_2, \omega_2) \frac{d\omega_2 d^2 q_2}{(2\pi)^3} \\ &= \frac{-Ng^4 \chi_0}{(2\pi)^4 v_x v_y} \int \frac{|\omega_2| - |\Omega|}{[i(\Omega + \omega_2) - \epsilon_{q_2}][i(\Omega - \omega_2) - \epsilon_{Q-q_2}]} \\ &\times \frac{d\omega_2 d^2 q_2}{\gamma|\omega_2| + \mathbf{q}_2^2} \end{aligned} \quad (190)$$

(the combinatoric factor 2 accounts for two possibilities to choose the external frequency, the factor -1 comes from the summation over spin projections, which we re-installed here). One can easily make sure that to a logarithmical accuracy, we can neglect Ω in the denominator and set it as a lower cutoff in the integration over ω_2 . Subtracting the contribution from high energies we then obtain

$$\begin{aligned} \Pi_2(\mathbf{Q}, \Omega) &= \frac{-Ng^4 \chi_0}{16\pi^4 v_x v_y} |\Omega| \int \frac{1}{(i\omega_2 - \epsilon_{q_2})(i\omega_2 - \epsilon_{Q+q_2})} \\ &\times \frac{d\omega_2 d^2 q_2}{\gamma|\omega_2| + \mathbf{q}_2^2} \end{aligned}$$

This integrand is exactly the same as for $\Delta g/g$ in the Appendix A. Using the results from Appendix A we find

$$\Pi_2(\mathbf{Q}, \Omega) = \gamma|\Omega| \left| \frac{Q(v_x/v_y)}{2N\chi_0} \right| \log |\Omega| \quad (191)$$

We next evaluate the correction to the polarization operator when both Ω and $\mathbf{q}_1 = \mathbf{q} - \mathbf{Q}$ are nonzero. For simplicity we choose $v_x = v_y = v/\sqrt{2}$, and also set $q = q_x$. We will restore rotational symmetry at the end of computations. Rotating the coordinates such that $\epsilon_{q_2} = v_F q_{2x}$ and $\epsilon_{Q+q_2} = v_F q_{2y}$ we can express $\Pi_2(\mathbf{q}, \Omega)$ from (190) as

$$\Pi_2(\mathbf{q}, \Omega) = \frac{-2Ng^4\chi_0}{(2\pi)^4 v_F^2} \int \frac{|\omega_2| - |\Omega|}{i(\Omega + \omega_2) - v_F q_{2x}} \times \frac{1}{i(\Omega - \omega_2) + v_F q_{2y} - v_F q_y} \frac{d\omega_2 d^2 q_2}{\gamma|\omega_2| + q_{2x}^2 + q_{2y}^2} \quad (192)$$

As before, the dependence on Ω in the denominator can be eliminated by setting Ω as the lower limit on the integration over ω_2 . Furthermore, as typical ω_2 scale as q_2^2 and are obviously smaller than q_2 , the $i\omega_2$ term in the fermionic propagators can be reduced to $i\delta\text{sign}(\omega_2)$. With these simplifications, we obtain

$$\Pi_2(\mathbf{q}, \Omega) = \frac{4Ng^4\chi_0}{(2\pi)^4 v_F^2} Re \int_0^\infty d\omega_2 \int \frac{|\omega_2| - |\Omega|}{-i0_+ + v_F q_{2x}} \times \frac{1}{-i0_+ + v_F q_{2y} - v_F q_y} \frac{d^2 q_2}{\gamma|\omega_2| + q_{2x}^2 + q_{2y}^2} \quad (193)$$

Now one can easily evaluate first the integral over q_{2x} and then over q_{2y} and obtain

$$\Pi_2(\mathbf{q}, \Omega) = -\frac{Ng^4\chi_0}{4\pi^2 v^4} \int_0^\infty d\omega \frac{\omega_2 - |\Omega|}{\gamma\omega_2 + q_y^2} \quad (194)$$

Evaluating the frequency integral, subtracting the contribution from high frequencies, restoring the rotational symmetry, and expressing γ in terms of g and v_F we finally obtain

$$\Pi_2(\mathbf{q}, \Omega) = \frac{Q(v)}{N} (\mathbf{q}^2 + \gamma|\Omega|) |\log(\gamma|\Omega| + \mathbf{q}^2)| \quad (195)$$

To a logarithmical accuracy, this is indeed the same result as Eqn. (186).

XV. APPENDIX D

In this Appendix, we evaluate the fermionic self-energy at finite temperatures. We first consider the limit $N \rightarrow \infty$ at finite λ , and then discuss the modification of the results at finite N .

A. $N \rightarrow \infty$ limit

The sum we need to evaluate is given by Eq. (77). It reads

$$\Sigma(k_{hs}, \Omega_m) = i\pi T \lambda \sum_n \frac{\text{sign}\omega_n}{\sqrt{1 + \frac{|\omega_n - m|}{\omega_{sf}}}}. \quad (196)$$

Using Poisson summation formula

$$T \sum_n F(n) = \frac{1}{2\pi} \int_{-\infty}^{\infty} F(x) dx + \frac{1}{\pi} \sum_{p=1}^{\infty} \int_0^\infty (F(x) + F(-x)) \cos \frac{xp}{T} dx \quad (197)$$

to separate $T = 0$ and finite T contributions to the self-energy, we obtain after integrating over x in both terms in (197)

$$\Sigma(k_{hs}, \Omega_m) = 2i\lambda \left(\frac{\Omega_m}{1 + \sqrt{1 + \frac{|\Omega_m|}{\omega_{sf}}}} + P(\Omega_m, T) \text{sign}\Omega_m \right) \quad (198)$$

The T dependent term $P(\Omega_m, T)$ is expressed in terms of Fresnel integrals $S(x)$ and $C(x)$ as

$$P(\Omega_m, T) = \sum_{p=1}^{\infty} \left(\frac{2\pi T \omega_{sf}}{p} \right)^{1/2} \times \left[\cos \frac{p\omega_{sf}}{T} \left[S \left(\sqrt{\frac{p(\Omega_m + \omega_{sf})}{T}} \right) - S \left(\sqrt{\frac{p\omega_{sf}}{T}} \right) \right] + \sin \frac{p\omega_{sf}}{T} \left[C \left(\sqrt{\frac{p(\Omega_m + \omega_{sf})}{T}} \right) - C \left(\sqrt{\frac{p\omega_{sf}}{T}} \right) \right] \right] \quad (199)$$

The Fresnel integrals are defined as

$$S(\sqrt{x}) = \frac{1}{\sqrt{2\pi}} \int_0^x \frac{\sin t}{\sqrt{t}} dt \quad C(\sqrt{x}) = \frac{1}{\sqrt{2\pi}} \int_0^x \frac{\cos t}{\sqrt{t}} dt \quad (200)$$

At low $T \ll \omega_{sf}$, one can expand Fresnel integrals in powers of $1/\sqrt{x}$. In this limit, Eq (199) reduces to

$$P(\Omega_m, T) = \frac{(\pi T)^2}{12\omega_{sf}} \left(1 + 2 \left(\frac{\omega_{sf}}{|\Omega_m| + \omega_{sf}} \right)^{1/2} \right) - \frac{15}{8} \frac{T^4}{\omega_{sf}^3} \left(2.1 + 0.9f \left(\frac{\omega_{sf}}{|\Omega_m|} \right) \right) + O(T^6) \quad (201)$$

where $f(0) = 0$, $f(\infty) = 1$. At $\Omega_m \ll \omega_{sf}$, one recovers a conventional Fermi liquid result $P(\Omega_m, T) \approx (\pi T)^2 / (4\omega_{sf})$. At $\Omega_m \gg \omega_{sf}$, but still $T \ll \omega_{sf}$ (i.e., for large m), the leading functional dependence is still T^2 , but the prefactor is reduced by $1/3$. Also notice that the subleading, T^4 corrections become comparable with T^2 terms starting from relatively small $T \sim 0.5 \omega_{sf}$.

In the opposite limit $T \gg \omega_{sf}$, the contributions to the sum (196) from all $n \neq m$ can be simplified by approximating

$$\left(1 + \frac{|\omega_{n-m}|}{\omega_{sf}}\right)^{-1/2} \rightarrow \left(\frac{\omega_{sf}}{|\omega_{n-m}|}\right)^{1/2}. \quad (202)$$

With this approximation, one can sum over n explicitly:

$$\begin{aligned} \Sigma(\Omega_m) &= i\frac{\pi}{2} T\bar{\omega}^{1/2} \sum_{n \neq m} \frac{\text{sign}(2n+1)}{|\omega_{n-m}|^{1/2}} \\ &= i \left(\frac{\pi T\bar{\omega}}{2}\right)^{1/2} \left(\zeta\left(\frac{1}{2}\right) - \zeta\left(\frac{1}{2}, 1+m\right)\right) \end{aligned} \quad (203)$$

where ζ is a Zeta function. The absence of the correlation length in this expression is a consequence of the fact that the product $\lambda\sqrt{\omega_{sf}} = 0.5\sqrt{\bar{\omega}}$ is independent of ξ . One indeed would expect this independence in the quantum-critical regime.

In real frequencies, the imaginary part of the self-energy at finite T can be obtained using the spectral representation. We have at $\mathbf{k} = \mathbf{k}_{hs}$ and $v_s \rightarrow \infty$,

$$\begin{aligned} \Sigma''(\Omega) &= \frac{\lambda v_F \xi}{2\pi^2} \int_{-\infty}^{\infty} \text{Im} \frac{d\omega d^2k}{1 + (\mathbf{k}\xi)^2 - i\frac{\omega}{\omega_{sf}}} \\ &\times \text{Im} \frac{1}{v_F k_x - \Sigma^R(\Omega - \omega)} f(\Omega/2T, \omega/2T) \end{aligned} \quad (204)$$

where

$$f(x, y) = \tanh(x - y) + 1/\tanh(y). \quad (205)$$

At $N \rightarrow \infty$ and finite ξ , the momentum integration can be factorized and we obtain:

$$\Sigma''(\Omega) = \frac{\lambda}{2} \text{Im} \int_{-\infty}^{\infty} \frac{d\omega}{\sqrt{1 - i\frac{\omega}{\omega_{sf}}}} f(\Omega/2T, \omega/2T) \quad (206)$$

Note that the presence of Σ^R in the integrand is irrelevant as when momentum integration is factorized, the integral over k_x just gives a constant density of states, independent on Σ^R . It is convenient to separate the contributions to $\Sigma''(\Omega)$ from static and dynamical spin fluctuations. This can be done in a standard way by replacing $f(x, y)$ by

$$f(x, y) = \frac{1}{y} + f_1(x, y) \quad (207)$$

where

$$f_1(x, y) = \tanh(x - y) + 1/\tanh(y) - 1/y, \quad (208)$$

Substituting the form of $f(x, y)$ into (206) we obtain

$$\Sigma''(\Omega) = \Sigma''_{st}(\Omega) + \Sigma_{dyn}(\Omega), \quad (209)$$

where

$$\Sigma''_{st}(\Omega) = T\lambda\pi \quad (210)$$

and

$$\Sigma_{dyn}(\Omega) \approx \frac{\lambda}{2} \text{Im} \int_{-\infty}^{\infty} \frac{d\omega}{\sqrt{1 - i\frac{\omega}{\omega_{sf}}}} f_1(\Omega/2T, \omega/2T) \quad (211)$$

At $\Omega \gg \omega_{sf}$, typical $\omega \gg \omega_{sf}$, and $\Sigma_{dyn}(\Omega)$ can be approximated by

$$\Sigma_{dyn}(\Omega) \approx \frac{\sqrt{\bar{\omega}}}{4\sqrt{2}} \int_{-\infty}^{\infty} \frac{d\omega}{\sqrt{\omega}} f_1(\Omega/2T, \omega/2T) \quad (212)$$

This result can be rewritten in the scaling form

$$\Sigma_{dyn}(\Omega) = \left(\frac{T\bar{\omega}}{2}\right)^{1/2} D\left(\frac{\Omega}{T}\right) \quad (213)$$

where $D(x)$ is given by

$$\begin{aligned} D(x) &= \int_0^{\infty} \frac{dy}{\sqrt{y}} \\ &\times \left(\frac{1}{e^y - 1} - \frac{1}{y} + \frac{1}{2} \left(\frac{1}{e^{y+x} + 1} + \frac{1}{e^{y-x} + 1}\right)\right) \end{aligned} \quad (214)$$

In the two limits, $D(x)$ behaves as $D(x \gg 1) = \sqrt{x} - 2.58 - 0.822/x^{3/2} + \dots$, and $D(x \ll 1) = -1.516 + 0.105x^2 + \dots$

The real part of $\Sigma_{dyn}(\Omega)$ is obtained from (213) by Kramers-Kronig transformation. It contains the same \sqrt{T} dependence as (213) but a different scaling function of Ω/T .

B. finite N

We recall that the need to study a finite N is related to the fact that at a nonzero temperature, some of $1/N$ terms also scale with ξ and therefore become relevant for physical $N = 8$. Here we single out and explicitly evaluate these terms. We, however, still will be neglecting regular $1/N$ contributions.

Our point of departure is Eqn (204). At finite N , the momentum integration in (204) cannot be factorized. Let's use (207) and consider the static and dynamical contributions to $\Sigma''(\Omega)$ separately. This separation requires care as to single out the truly static contribution (the one from a boson with zero Matsubara frequency) we not only have to replace $f(x, y)$ by $1/y$ but also set $\omega = 0$ in the fermionic propagator. The static contribution is given by

$$\begin{aligned} \Sigma''_{st}(\Omega) &= \frac{\lambda v_F \xi^2}{2\pi^2} \int_{-\infty}^{\infty} \text{Im} \frac{d\omega d^2k}{1 + (\mathbf{k}\xi)^2 - i\frac{\omega}{\omega_{sf}}} \frac{2T}{\omega} \\ &\times \text{Im} \frac{1}{v_F k_x - \Sigma^R(\Omega)} \end{aligned} \quad (215)$$

The integration over ω is straightforward. Also, since $\text{Im}\Sigma^R > 0$, we can integrate over k_x by close the integration contour over the lower half plane. Introducing then $\tilde{\Sigma} = \Sigma^R(\Omega)/v_F\xi^{-1}$, we obtain

$$\begin{aligned}\Sigma''_{st}(\Omega) &= T\lambda Im \int_{-\infty}^{\infty} \frac{dx}{\sqrt{x^2+1+\tilde{\Sigma}} \sqrt{x^2+1}} \\ &= 2T\lambda Im \frac{\log \left[\tilde{\Sigma} + \sqrt{1+\tilde{\Sigma}^2} \right]}{\sqrt{1+\tilde{\Sigma}^2}}\end{aligned}\quad (216)$$

As we discuss in the main text, at $T \ll N\omega_{sf}$, the fermionic self-energy in the integrand can be approximated by its $T = 0$ value, Eqn (38). The latter, however, can be neglected only if $\tilde{\Omega} \ll 1$ or $\Omega \ll \tilde{\Omega} = N^2\omega_{sf}/9$. For infinite N , this scale is above $\bar{\omega}$ and is irrelevant for our study. For finite N , however, $\tilde{\Omega}$ scales with ω_{sf} and definitely become smaller than $\bar{\omega}$ if $\xi \rightarrow \infty$ at a finite N . Obviously, in this situation, $\tilde{\Sigma}$ cannot be neglected, and the $N = \infty$ result for Σ''_{st} , Eq. (210) is invalid.

In the quantum critical regime, $\Sigma^2 = i\Omega/\tilde{\Omega}$. Substituting this into (216) we obtain the result cited in (92).

The dynamical contribution to $\Sigma''(\Omega)$ consists of two parts $\Sigma_{dyn}(\Omega) = \Sigma_{dyn}^1(\Omega) + \Sigma_{dyn}^2(\Omega)$. The first contribution accounts for the difference between $\Sigma^R(\Omega - \omega)$ and $\Sigma^R(\Omega)$:

$$\begin{aligned}\Sigma_{dyn}^1(\Omega) &= \frac{\lambda v_F \xi}{2\pi^2} \int_{-\infty}^{\infty} Im \frac{d\omega d^2k}{1 + (\mathbf{k}\xi)^2 - i\frac{\omega}{\omega_{sf}}} \frac{2T}{\omega + i0} \\ &\times Im \left[\frac{1}{v_F k_x - \Sigma^R(\Omega - \omega)} - \frac{1}{v_F k_x - \Sigma^R(\Omega)} \right]\end{aligned}\quad (217)$$

This integral is nonsingular when $\xi \rightarrow \infty$. We can then use a conventional $N \rightarrow \infty$ approach and factorize the momentum integration. Performing it, we immediately find that $\Sigma_{dyn}^1(\Omega)$ vanishes to leading order in $1/N$.

The second contribution to the dynamical part is given by (204) with f_1 instead of f . As $f_1(x, y)$ is non-singular at $y \rightarrow 0$ (i.e., at $\omega \rightarrow 0$), the leading (in $1/N$) piece in Σ_{dyn}^2 can again be obtained by factorizing the momentum integration. This piece is then the same as in (213).

Finally, we found that the momentum integration in (204) can be performed explicitly at arbitrary N by, e.g., transforming to polar coordinates. Furthermore, by explicitly evaluating $ImG(k, \Omega)$ and pulling the Im symbol for bosonic propagator out of frequency integral, we can obtain the full expression for $\Sigma(\Omega, T)$, not only its imaginary part. Performing the momentum integration, we found

$$\begin{aligned}\Sigma(\Omega, T) &= \frac{\lambda}{4\pi i} \int_{-\infty}^{\infty} d\omega f(\Omega/2T, \omega/2T) \\ &(S_R(\Omega, \omega) - S_A(\Omega, \omega)) \text{sign}(\Omega - \omega)\end{aligned}\quad (218)$$

where

$$\begin{aligned}S_{R,A}(\Omega, \omega) &= \frac{1}{\sqrt{\tilde{\Sigma}_{R,A}^2 + \Pi_R}} \\ &\times \log \frac{\sqrt{\tilde{\Sigma}_{R,A}^2} - \sqrt{\tilde{\Sigma}_{R,A}^2 + \Pi_R}}{\sqrt{\tilde{\Sigma}_{R,A}^2} + \sqrt{\tilde{\Sigma}_{R,A}^2 + \Pi_R}}\end{aligned}\quad (219)$$

and $\Pi_R = \Pi_R(\omega) = 1 - i\omega/\omega_{sf}$ and $\tilde{\Sigma}_{R,A}^2 = \Sigma_{R,A}(\Omega - \omega)/(v_F \xi^{-1})$.

This expression is of limited use as it contains regular $1/N$ terms which are beyond our accuracy as we neglected $1/N$ vertex corrections. Nevertheless, it is useful for the understanding how small are regular $1/N$ terms. The Σ'' from Eq. (218) is plotted in Fig. 20.

-
- [1] J.G. Bednortz and K.A. Muller, Rev. Mod. Phys. **60**, 585 (1988).
 - [2] S. Chakravarty, B. I. Halperin, and D.R. Nelson, Phys. Rev. B **39**, 2311 (1989); S.M. Hayden *et al*, Phys. Rev. Lett. **66**, 821 (1991); T. Imai *et al*, Phys. Rev. Lett. **70**, 10002 (1993); D. C. Johnson, Phys. Rev. Lett. **62**, 957 (1989); B. Keimer *et al*, Phys. Rev. Lett. **67**, 1930 (1991).
 - [3] K. Gofron *et al*, Phys. Rev. Lett. **73**, 3302 (1994); D.S. Dessau *et al* Phys. Rev. Lett. **71**, 2781 (1993); Jian Ma *et al*, Phys. Rev. B **51**, 3832 (1995); J. C. Campuzano *et al.*, Phys. Rev. B **53**, R 14 737 (1996).
 - [4] M. R. Norman *et al.*, Phys. Rev. Lett. **79**, 3506 (1997); J. C. Campuzano *et al.*, Phys. Rev. Lett. **83**, 3709 (1999); Z. X. Shen *et al.*, Science **280**, 259 (1998);
 - [5] Ch. Renner *et al*, Phys. Rev. Lett. **80**, 149 (1998); Y. DeWilde *et al*, *ibid* **80**, 153 (1998); V.M. Krasnov *et al*, Phys. Rev. Lett. **84**, 5860 (2000); J. F. Zasadzinski *et al*, Phys. Rev. Lett. to appear.
 - [6] G. Blumberg *et al*, Science, **278**, 1427 (1997).
 - [7] D. A. Wollmann, D. J. Van Harlingen, W. C. Lee, D. M. Ginsberg, and A. J. Leggett, Phys. Rev. Lett. **71**, 2134 (1993); C.C. Tsuei and J.R. Kirtley, Rev. Mod. Phys. **72**, 969 (2000).
 - [8] T. Valla *et al*, Science **285**, 2110 (1999).
 - [9] A. Kaminski *et al*, Phys. Rev. Lett. **84**, 1788 (2000).
 - [10] e.g. A. Puchkov, D. Basov, and T. Timusk, J. Phys.: Cond. Matter **8**, 10049 (1996).
 - [11] R. C. Yu *et al*, Phys. Rev. Lett. **69**, 1431 (1992); S.J. Hagen, Z.Z. Wang, and N.P. Ong, Phys. Rev. B **40**, 9389 (1989).
 - [12] see e.g. Z. Yusof *et al*, cond-mat/0104367
 - [13] P.W. Anderson, *The Theory of Superconductivity in the High T_c Cuprates* (Princeton University Press, Princeton, New Jersey, 1997).
 - [14] T. Senthil and M.P.A. Fisher, Phys. Rev. B **63**, 4521 (2001); N. Nagaosa and P.A. Lee, Phys. Rev. B **61**, 9166 (2000); P.A. Lee and X-G Wen, cond-mat/0008419, D.A. Ivanov, P.A. Lee, and X-G Wen, cond-mat/990931.
 - [15] C. Varma *et al.*, Phys. Rev. Lett. **63**, 1996 (1989), *ibid* **64**, 497 (1990); P. Littlewood and C. Varma, Phys. Rev. B **46**, 405 (1992); G. Kotliar *et al*, Europhys. Lett. **15**, 655 (1991).
 - [16] C. Castellani, C. DiCastro, and M. Grilli, Phys. Rev. Lett. **75**, 4650 (1995); J. Phys. Chem. Solids **59**, 1694 (1998).

- [17] D. Pines, *Z. Phys. B* **103**, 129 (1997) and references therein.
- [18] S. Sachdev, *Science*, **288**, 475 (2000); M. Vojta and S. Sachdev, *Phys. Rev. Lett.* **83**, 3916 (1999); see also N. Read and S. Sachdev, *Phys. Rev. Lett.* **66**, 1773 (1991).
- [19] S. Sachdev, A.V. Chubukov, and A. Sokol, *Phys. Rev. B* **51**, 14874 (1995).
- [20] A. Chubukov, *Europhys. Lett.* **44**, 655 (1997).
- [21] S. Sachdev, *Quantum Phase Transitions*, Cambridge University Press (Cambridge, 1999).
- [22] A. Chubukov, S. Sachdev, and J. Ye, *Phys. Rev. B* **49**, 11919 (1994).
- [23] C.M. Varma, *Phys. Rev. B* **55**, 14554 (1997).
- [24] S. Chakravarty, R. Laughlin, D. Morr, and C. Nayak, *cond-mat/0005443*.
- [25] D.J. Scalapino, *Phys. Rep.* **250**, 329 (1995).
- [26] G. Aeppli *et al.*, *Science* **278**, 1432 (1997) and references therein.
- [27] A. Millis, H. Monien, and D. Pines, *Phys. Rev. B* **42**, 197 (1990),
- [28] P. Bourges in *The gap Symmetry and Fluctuations in High Temperature Superconductors*, J. Bok, G. Deutscher, D. Pavuna, and S.A. Wolf eds. (Plenum Press, 1998), pp. 349-371 and references therein.
- [29] P. Monthoux and D. Pines, *Phys. Rev. B* **47**, 6069 (1993); *ibid* **50**, 16015 (1994).
- [30] E.M. Lifshitz and L.P. Pitaevskii, *Statistical Physics, p.2* (Butterworth-Heinemann, 1995, Oxford)
- [31] see, e.g., J. Annett, N. Goldenfeld, and S. Renn in *Physical properties of high temperature superconductors*, ed. by D. Ginsberg (World Scientific, NJ 1990).
- [32] B. I. Shraiman and E. D. Siggia, *Phys. Rev. Lett.* **62**, 1564 (1989).
- [33] E. Dagotto, A. Nazarenko, and M. Boninsegni, *Phys. Rev. Lett.* **73**, 728 (1994); E. Dagotto, A. Nazarenko, and A. Moreo, *Phys. Rev. Lett.* **74**, 310 (1995); S. Haas, E. Dagotto, and A. Moreo, *Phys. Rev. Lett.*, to appear; A. Nazarenko, K.J.E. Vos, S. Haas, E. Dagotto, and R.J. Gooding, *Phys. Rev. B*, **51**, 8676 (1995).
- [34] J.R.Schrieffer, X.G.Wen, and S.C.Zhang, *Phys. Rev. B* **39**, 11663 (1989); A.V.Chubukov and D.M.Frenkel, *ibid* **46**, 11884 (1992).
- [35] A. H. Castro-Neto, *cond-mat/0102281*.
- [36] S-C Zhang, *Science*, **275**, 1089 (1997); E. Arigoni, M.G. Zacher, and W. Hanke, *cond-mat/01051125* and references therein.
- [37] O.P. Sushkov, *cond-mat/0002421* and references therein.
- [38] P. Aebi *et al*, *Phys. Rev. Lett.* **72**, 2757 (1994); *ibid* **74**, 1886 (1995).
- [39] Ar Abanov, A. V. Chubukov, and J. Schmalian, *cond-mat/0005163*.
- [40] Ar. Abanov, A. Chubukov, and A.M. Finkel'stein, *cond-mat/9911445*, *Europhys. Lett.*, **54**, 488 (2001)
- [41] C. Stemmann, C. Pépin, and M. Lavagna, *Phys. Rev. B* **50**, 4075 (1994); D. Z. Liu, Y. Zha, and K. Levin, *Phys. Rev. Lett.* **75**, 4130 (1995); I. Mazin and V. Yakovenko, *ibid.* **75**, 4134 (1995); A. Millis and H. Monien, *Phys. Rev. B* **54**, 16172 (1996); N. Bulut and D. Scalapino, *Phys. Rev. B* **53**, 5149 (1996); D. K. Morr and D. Pines, *Phys. Rev. Lett.* **81**, 1086 (1998); S. Sachdev and M. Vojta, *Physica B* **280**, 333 (2000); Y.-J. Kao *et al.*, *Phys. Rev. B* **61**, R11898 (2000); F. Onufrieva and P. Pfeuty, *cond-mat/9903097*; O. Tchernyshyov *et al.*, *cond-mat/0009072*; J. Brinckmann and P.A. Lee, *Phys. Rev. Lett.* **82**, 2915 (1999); M. R. Norman and H. Ding, *Phys. Rev. B* **57**, R11089 (1998); M. R. Norman, *Phys. Rev. B* **61**, 14751 (2000); Ar. Abanov and A. Chubukov, *Phys. Rev. Lett.* **83**, 1652 (1999);
- [42] D. J. Scalapino, *The electron-phonon interaction and strong coupling superconductors*, in *Superconductivity*, in *Superconductivity*, Vol. 1, p. 449, Ed. R. D. Parks, Dekker Inc. N.Y. 1969; J. R. Schrieffer, *Theory of Superconductivity* (Benjamin, Reading, Mass., 1966).
- [43] H. von Lohneysen *et al*, *Phys. Rev. Lett.* **72**, 3262 (1994); D. Bitko, T. Rosenbaum and G. Aeppli, *Phys. Rev. Lett.* **77**, 940 (1966); S. Raymond *et al*, *J. Low Temp. Phys.* **107**, 295 (1997); F. Steglich *et al*, *Z. Phys. B* **103**, 235 (1997); Y. Aoki *et al*, *J. Phys. Soc. Jpn*, **66**, 2993 (1997).
- [44] N. Mathur *et al*, *Nature* **394**, 39 (1998).
- [45] D. Vollhardt, *Rev. Mod. Phys.*, **56**, 99 (1984); T Morya and J. Kawabata, *J. Phys. Soc. Jpn.*, **34**, 639 (1973); K.B. Blagoev *et al*, *Phys. Rev. Lett.* **82**, 133 (1999).
- [46] see e.g., P. Coleman, *Nature* **406**, 508 (2000); P. Coleman, C. Pépin, Q. Si, and R. Ramazashvili, *cond-mat/0105006*; A. Rosh, *Phys. Rev. Lett.* **82**, 4280 (1999); A. Rosh, *cond-mat/0103446* and references therein; Q. Si *et al*, *cond-mat/0011477*.
- [47] O. Stockert *et al*, *Phys. Rev. Lett.* **80**, 5627 (1998); A. Schröder *et al*, *ibid*, **80**, 5623 (1988); A. Schröder *et al*, *Nature* **407**, 351 (2000).
- [48] B.P. Stojkovic and D. Pines, *Phys. Rev. B* **55**, 8576 (1997); *ibid* **56**, 11931 (1997).
- [49] L.B. Ioffe, A.I. Larkin, A.J. Millis, and B.L. Altshuler, *JETP Lett.*, **59**, 65 (1994); B. L. Altshuler, L.B. Ioffe, and A. J. Millis, *Phys. Rev. B* **52**, 5563 (1995).
- [50] L.B. Ioffe and A. J. Millis, *Phys. Rev. B* **51**, 16151 (1995); see also A.M. Tsvetlik and M. Reizer, *Phys. Rev. B* **48**, 9887 (1993).
- [51] D. Manske, I. Eremin, and K.H. Bennemann, *Phys. Rev. B* **63**, 054517 (2001) and references therein.
- [52] T. Dahm and L. Tewordt, *Phys. Rev. Lett.* **74**, 793 (1995); T. Dahm, D. Manske and L. Tewordt, *Phys. Rev. B* **58**, 12454 (1998).
- [53] M.L. Lercher and J.M. Wheatley, *JMMM* **185**, 384 (1998), *Phys. Rev. B* **63**, 012403 (2000).
- [54] A. Georges *et al*, *Rev. Mod. Phys.*, **68**, 13 (1996).
- [55] J.A. Hertz, *Phys. Rev. B* **14**, 1165 (1976).
- [56] A.J. Millis, *Phys. Rev. B* **48**, 7183 (1993).
- [57] A. Chubukov, *Phys. Rev. B* **52**, R3840 (1995). The expression for the vertex correction in this paper should contain $0.5 \log \sin \phi/2$ instead of $\log \cos \phi/2$.
- [58] A. Chubukov and J. Schmalian, *Phys. Rev. B* **57**, R11085 (1998).
- [59] A.Chubukov and D. Morr, *Phys. Rev. Lett.* **81**, 4716 (1998). Ar. Abanov and A. Chubukov, *Phys. Rev. Lett.*, **83**, 1652 (1999).
- [60] A. Chubukov, D. Morr, and P. Monthoux, *Phys. Rev. B* **56**, 7789 (1997).
- [61] Ar. Abanov and A. Chubukov, *Phys. Rev. Lett.* **84**, 5608 (2000).

- [62] R. Haslinger, Ar. Abanov, and A. Chubukov, Phys. Rev. B **63**, 020503(R) (2001).
- [63] C. H. Pao and N. E. Bickers, Phys. Rev. Lett. **72**, 1870 (1994); Ph. Monthoux and D.J. Scalapino, Phys. Rev. Lett. **72**, 1874 (1994); S. Grabowski, M. Langer, J. Schmalian, and K. H. Bennemann, Europhys. Lett. **34**, 219 (1996); J. Schmalian, S. Grabowski, and K. H. Bennemann, Phys. Rev. B **56**, R509 (1997); N. Bulut and D. Scalapino, Phys. Rev. B **53**, 5149 (1996); D. J. Scalapino and S.R. White, Phys. Rev. B **58**, 1347 (1998); S. Trugman, Phys. Rev. B **37**, 1597 (1988).
- [64] H.J. Schulz, Phys. Rev. Lett. **64**, 1445 (1990); I. Dzyaloshinskii and V. Yakovenko, JETP **94**, 344 (1988)
- [65] A. Chubukov and K.A. Musaelian, Phys. Rev. B **50**, 6238 (1994); A. Singh and Z. Tesanovic, Phys. Rev. B **41**, 614 (1990).
- [66] L. Ioffe and A. I. Larkin, Phys. Rev. B **39**, 8988 (1989).
- [67] Th. Dombre, J. Physique, **51**, 847 (1990).
- [68] A. Chubukov and K.A. Musaelian, Phys. Rev. B **5**, 12605 (1995).
- [69] S. A. Kivelson, E. Fradkin, and V. J. Emery, Nature **393**, 550 (1998); J. Zaanen, Nature **404**, 714 (2000) and references therein.
- [70] R. Hlubina and T.M. Rice, Phys. Rev. B , **52**, 13043 (1995).
- [71] M. R. Norman *et al.*, Phys. Rev. Lett. **79**, 3506 (1997); Z-X. Shen *et al.*, Science **280**, 259 (1998); T. Sato *et al.*, Phys. Rev. B to appear.
- [72] J.M. Luttinger and J.C. Ward, Phys. Rev. **118**, 1417 (1960); J.M. Luttinger, Phys. Rev. **119**, 1153 (1960).
- [73] P.D. Johnson *et al.*, cond-mat/0102260
- [74] P.V. Bogdanov *et al.*, cond-mat/0004349
- [75] P. Bourges *et al.*, Science **288**, 1234 (2000) and references therein.
- [76] V. Barzykin *et al.*, *ibid* **49**, 1544 (1994)
- [77] S.B. Treiman, R. Jackiw, and D.J. Gross, in *Lectures on Current Algebra and its Applications* (Princeton University Press, Princeton, 1972).
- [78] G.M. Eliashberg, Sov. Phys. JETP **11**, 696 (1960). On recent discussion on the applicability of the Eliashberg approach to phonons see A.S. Alexandrov, cond-mat/0102189 and references therein.
- [79] A.B. Migdal, Sov. Phys. JETP, **7**, 996 (1958).
- [80] G.D. Mahan, Many-Particle Physics, Plenum Press, 1990.
- [81] A.J. Millis, Phys. Rev. B **45**, 13047 (1992).
- [82] S. Sachdev and A. Georges, preprint, cond-mat/9503158.
- [83] L. Kadanoff, Phys. Rev. **132**, 2073 (1963).
- [84] A. Chubukov and D. Morr, Phys. Rep., **288**, 355 (1997).
- [85] A.P. Kampf and J.R. Schrieffer, Phys. Rev B **42**, 7967 (1990). J.R. Schrieffer, J. Low Temp. Phys. **99**, 397 (1995).
- [86] J.R. Schrieffer, J. Low Temp. Phys. **99**, 397 (1995).
- [87] I. Vilks and A. M. S. Tremblay, J. Phys. I **7**, 1309 (1997).
- [88] J. Schmalian, D. Pines, and B. Stojkovic, Phys. Rev. Lett. **80**, 3839 (1998).
- [89] M.V. Sadovskii, cond-mat/0102111.
- [90] A. Chubukov, D. Morr, and K. Shakhnovich, Philos. Mag. B **74**, 563 (1996).
- [91] M. Lavagna, cond-mat/0102119; M. Lavagna and C. Pépin, Phys. Rev. B **62**, 6450 (2000).
- [92] L. B. Ioffe and A. J. Millis, private communication
- [93] L. B. Ioffe and A. J. Millis, Phys. Rev B **58**, 11631 (1998), see also A. T. Zheleznyak, V. Yakovenko, H. D. Drew, and I. I. Mazin, Phys. Rev. B **57**, 3089 (1998).
- [94] see e.g. S.V. Shulga, in *Proceedings of the Albena Workshop, 1998*, Kluwer Publishers, Dordrecht, p.323 (2001) and references therein.
- [95] D. B. Tanner and T. Timusk, *Optical Properties of High-Temperature Superconductors in Physical Properties of High-Temperature Superconductors* D.M. Ginsberg, ed (World Scientific, Singapore, 1992).
- [96] C.C. Homes *et al.*, Phys. Rev. Lett. **71**, 1645 (1993).
- [97] D. N. Basov *et al.* Phys. Rev. Lett. **77**, 4090 (1996).
- [98] J.J. Tu *et al.*, cond-mat/01004208.
- [99] M.A. Quijada *et al.*, Phys. Rev. B **60**, 14917 (1999).
- [100] A.A. Abrikosov and V.M. Genkin, Sov. Phys. JETP **38**, 417 (1974).
- [101] M.V. Klein and S.B. Dierker, Phys. Rev. B **29**, 4976 (1984).
- [102] T.P. Devereaux *et al.*, Phys. Rev. Lett. **72**, 396 (1994); Phys. Rev. B **54**, 12523 (1996); T.P. Devereaux and A.P. Kampf, Int. J. Mod. Phys. B **11**, 2093 (1997).
- [103] H. Monien and A. Zavadowski, Phys. Rev. B **41**, 8798 (1990); W.C. Wu and A. Griffin, Phys. Rev. B **51**, 1190 (1995); T. Devereaux and D. Einzel, *ibid* **51**, 15357 (1995).
- [104] A. Chubukov and D. Frenkel, Phys. Rev. B **52**, 9760 (1995) and references therein.
- [105] W.L. McMillan, Phys. Rev. **167**, 331 (1968).
- [106] Ph. Monthoux and G.G. Lonzarich, Phys. Rev. B **59**, 14598 (1999).
- [107] R. Roussev and A. Millis, cond-mat/0005449Z; Wang *et al.*, cond-mat/0104097
- [108] F. Bouis *et al.*, cond-mat/9906369.
- [109] V. Yu Irkhin, A.A. Katanin and M.I Katsnelson, cond-mat/0102381 and references therein.
- [110] E. Abrahams and C. Varma, Proc. Natl. Acad. of Sciences **97**, 5714 (2000).
- [111] S. Spielman *et al.*, Phys. Rev. Lett. **73**, 1537 (1994).